THESIS

EXPERIMENTAL AND CFD INVESTIGATION OF RE-AGENT MIXING IN AN SCR SYSTEM

Submitted by

KRISHNA IVATURI

Mechanical Engineering

In partial fulfillment of the requirements

For the Degree of Master of Science

Colorado State University

Fall 2007

COLORADO STATE UNIVERSITY

November 2, 2007

WE HEREBY RECOMMEND THAT THE THESIS PREPARED UNDER OUR SUPERVISION BY KRISHNA IVATURI ENTITLED "EXPERIMENTAL AND CFD INVESTIGATION OF RE-AGENT MIXING IN AN SCR SYSTEM" BE ACCEPTED AS FULFILLING IN PART REQUIREMENTS FOR THE DEGREE OF MASTER OF SCIENCE.

Committee on Graduate Work

Dr Daniel B. Olsen, Advisor

Dr. Charles E. Mitchell

Dr. Robert Meroney

Dr. Allan T. Kirkpatrick, Department Head

ABSTRACT OF THESIS

EXPERIMENTAL AND CFD INVESTIGATION OF RE-AGENT MIXING IN AN SCR SYSTEM

Nitrogen oxides (NO_x) cause a gamut of problems such as harmful particulate matter, ground level ozone (smog) and acid rain. Currently, a significant capital is being invested researching new techniques to control NO_x emissions. One of the best ways to break down NO_x is the Selective Catalytic Reduction (SCR) after-treatment method. A reducing agent (re-agent) is injected into exhaust gases and passed through a catalyst that facilitates NO_x breakdown into Nitrogen and Water. To ensure effective NO_x conversion, there must be uniform mixing between re-agent and exhaust gas upstream of the catalyst blocks. The current thesis focuses on investigating the mixing quality for an SCR test system employed for a 2-stroke lean-burn natural gas engine. CFD investigations were conducted to simulate the physical flow process. The mixing quality for different injector locations and the effect of utilizing a downstream in-line mixer was investigated. The CFD simulations were compared to experimental results. To measure ammonia concentrations experimentally, a traversing probe was designed and built. Re-agent concentrations were measured at various locations on a plane slightly upstream of the catalyst substrate. Detailed discussion is presented on different cases of CFD analysis. Experiments were conducted for the best and worst case of mixing based on CFD computation. Results suggest that a mixer plays a vital role in improving the mixing.

Krishna Ivaturi
Mechanical Engineering Department
Colorado State University
Fort Collins, CO 80523
Fall 2007

Acknowledgements

I would like to offer my sincere thankfulness to Dr. Daniel Olsen on providing me the opportunity and guidance to work on the current thesis. I am grateful to Dr. Robert Meroney for his constant reassurance and invaluable help that drove me in the right direction. I appreciate Dr. Charles Mitchell for serving as a thesis committee member, who was instrumental in helping me in heat transfer and CFD analysis.

Also, I thank the Engines and Energy Conversion Laboratory for providing me with excellent test facilities that were utilized for the experimental work.

I take this opportunity to thank Colorado State University and the Mechanical Engineering Department on providing me admission into one the country's best research institutes.

Finally, I am forever indebted to my family for their continuous support and love without whom this success would not be possible.

TABLE OF CONTENTS

List of Figures

List of Tables

List of Abbreviations

SCR	- Selective Catalytic Reduction
NO_x	- Nitrogen Oxides
EPA	- Environmental Protection Agency
NO	- Nitrogen Oxide
NO_2	- Nitrogen Dioxide
ΔH	- Change in enthalpy
CH_4	- Methane
NH_3	- Ammonia
HCN	- Hydrogen Cyanide
O_2	- Oxygen
HNCO	- Isocyanic acid
$(NH_2)_2CO$	- Urea
ppm	- Parts per million
2-D	- Two dimension
3-D	- Three dimension
CFD	- Computational Fluid Dynamics
SAE	- Society of Automotive Engineers
α	- Degree of Heterogeneity
Pro/E	- Pro Engineer
THC	- Total Hydrocarbons
VOC	- Volatile Organic Compounds

Chapter 1: INTRODUCTION

1.1 Oxides of Nitrogen (NO_x):

Oxides of Nitrogen include various nitrogen compounds like Nitrogen dioxide (NO_2) and Nitric Oxide (NO). These compounds play an important role in the atmospheric reactions that create harmful particulate matter, ground-level ozone (smog) and acid rain. NO_x forms when fuels are burned at high temperatures. The two major emissions sources are transportation vehicles and stationary combustion sources such as electric utility and industrial boilers. Power plants account for 21% of the NO_x that is emitted nationwide in the USA. Since the advent of the Clean Air Act in 1970, NO_x emissions have increased by nearly 19%[1] due to increased fossil fuel usage.

NO_x emissions contribute to the formation of fine particles and ozone smog that cost society billions of dollars annually from illness and deaths[1]. Finally, NO_x emissions contribute to a suite of year-round environmental problems from acid rain to eutrophication, a process where a water body is deprived of oxygen leading to degradation in water and harm to aquatic life. NO_x emissions also contribute to haze air pollution in national parks and wilderness areas.

The Environmental Protection Agency (EPA) has taken steps to control NO_x emissions. One significant step to combat summer-time ozone problems was the introduction of a program in May 2002 that required eastern states to reduce NO_x levels from power plants and other sources. Some states like North Carolina, New Hampshire, Massachusetts and Texas have adopted policies that control NO_x and other pollutants year round[1].

1.2 Lean NO_x traps (LNTs):

The successful commercialization of lean burn gasoline engines is dependant upon development of an effective emission after treatment system, which can provide HC, CO, and NO_x control under not only lean operating conditions, but also when the engine operates at the stoichiometric point under conditions of high engine speed and/or load. NO_x adsorber catalysts (NO_x) are capable of storing NO_x under lean conditions and subsequently releasing and catalyzing its reduction under rich conditions with respect to the stoichiometric point during a regeneration cycle[2]. After-treatment systems based on these types of catalysts show great potential for reaching current and future emission standards. Key to the successful application of NO_x adsorber catalysts is the development of engine control strategies, which maximize NO_x conversion while minimizing fuel economy penalty associated with adsorber regeneration.

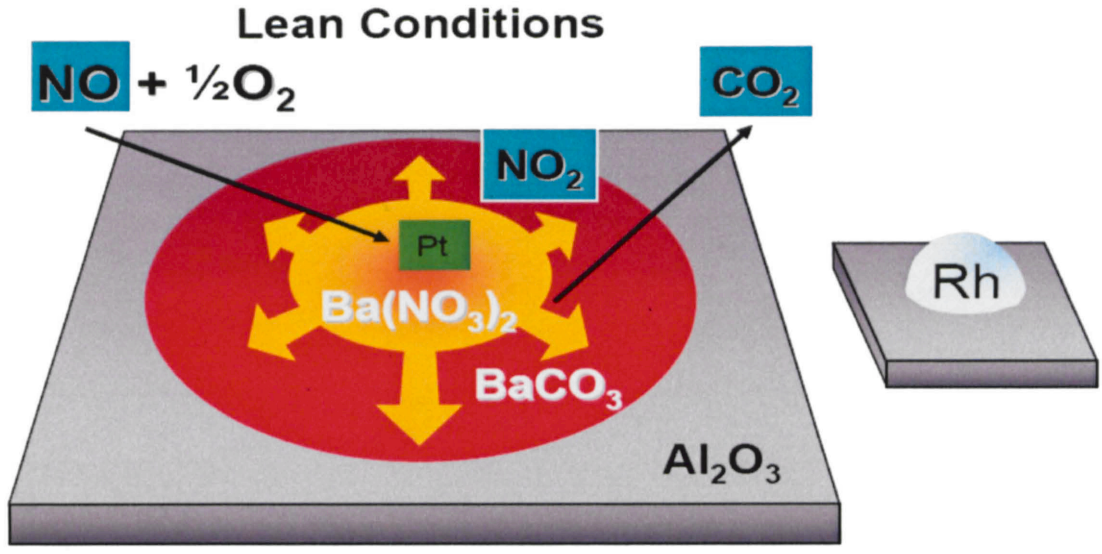

$$2NO_2 + BaO + 1/2O_2 = Ba(NO_3)_2$$

Figure 1.1: LNT during lean conditions[3]

Figures 1.1 and 1.2 show the schematic representation of how an LNT works. NO_x is trapped on alkaline earth metal such as Barium (Ba) until the regeneration is performed. Ba holds NO_x as Barium Nitrate $Ba(NO_3)_2$ and then precious metals such as Platinum (Pt) or Rhodium (Rh) are used for oxidation, reforming and reduction purposes.

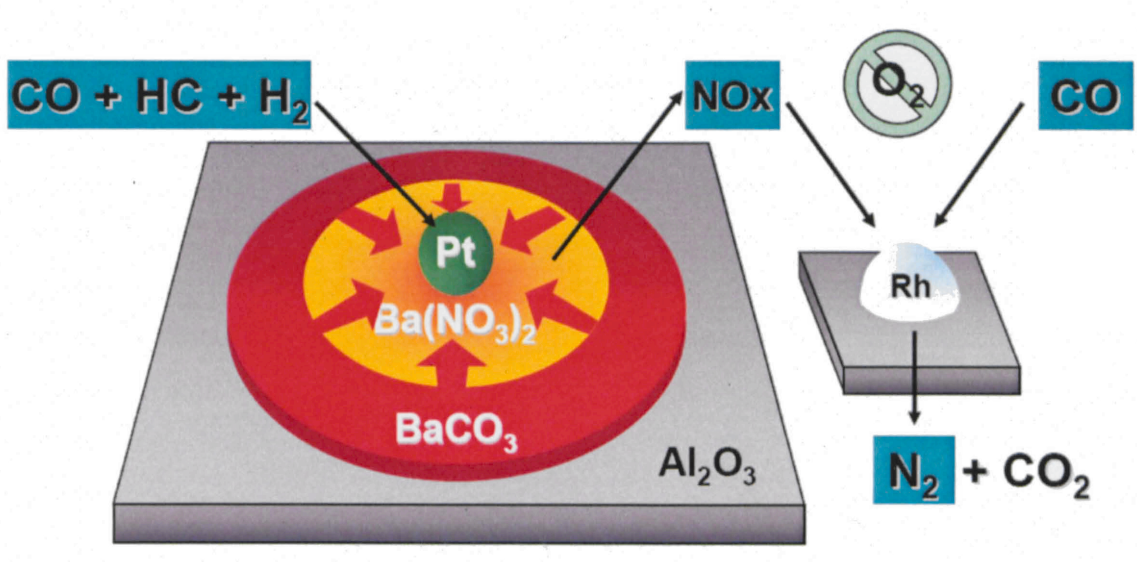

Figure 1.2: LNT during rich conditions[3]

1.3 Selective Catalytic Reduction (SCR):

Perhaps, the best after-treatment technology for NO_x reduction in lean-burn natural gas engines is SCR. In SCR, a re-agent is injected into the exhaust upstream of a catalyst. A major disadvantage of SCR is the requirement that the re-agent must be stored at the engine site. Typically, one of three different re-agents is used: Isocyanic acid (HNCO), Urea (NH_2CONH_2) or Ammonia (NH_3). In addition to being flammable and corrosive, ammonia is hazardous and can damage lungs, central nervous system, liver and kidneys. Isocyanic acid and urea are, therefore, preferred from a safety standpoint. Urea is used most commonly in catalysts as a 32% by weight solution in water. Urea is readily

available due to its use in a wide range of industrial applications including chemical, water, food processing and agriculture.

In SCR systems, NO_x destruction occurs through a series of chemical reactions involving the reducing agent, catalyst and various species in the exhaust. Urea decomposes into isocyanic acid and ammonia. Cyanuric acid reacts with free radicals to produce NH_3, which subsequently reacts with NO. The end products, in theory, are nitrogen, carbon dioxide and water (refer Figure 1.3 for equations). Ideally, a stoichiometric amount of urea is supplied, the urea is well mixed with the exhaust and the reactions proceed to completion across the catalyst. In reality, the process is not ideal. First, it is possible that the mixture of urea and exhaust is non-uniform. This results in regions of high or low urea concentrations. The former produces excess ammonia that is emitted into the atmosphere. Ammonia is likely to be regulated as a pollutant emission in the future because of this effect and its production in 3-way catalysts under rich conditions. In regions of low urea concentrations, the NO_x reduction suffers.

Another potential problem with SCR catalysts is the formation of toxic emissions across the catalyst that would not otherwise be present. In fact, the constituents used in the manufacturing of Hydrogen Cyanide (HCN) are present within an SCR catalyst on a lean burn natural gas engine. The required constituents for the production of HCN are methane, ammonia and oxygen, according to the reaction

$$CH_4 + NH_3 + 1.5\ O_2 \rightarrow HCN + 3\ H_2O \qquad \Delta H = +481.9\ kJ/mol$$

Figure 1.3 represents a schematic drawing of a complete SCR system. It includes an upstream oxidation catalyst (V) to oxidize NO, which is the dominant species in NO_x present in the exhaust gas. Just downstream of this section is the re-agent injection. Then a hydrolysis catalyst (H) is present to break down urea into ammonia, which is the main species involved in the NO_x destruction. The SCR catalyst (S) follows which breaks down NO_x into nitrogen and water. Further downstream, there is a second oxidation catalyst (O), whose function is regulate the excess ammonia that is present at this stage. It breaks down ammonia in to nitrogen and water.

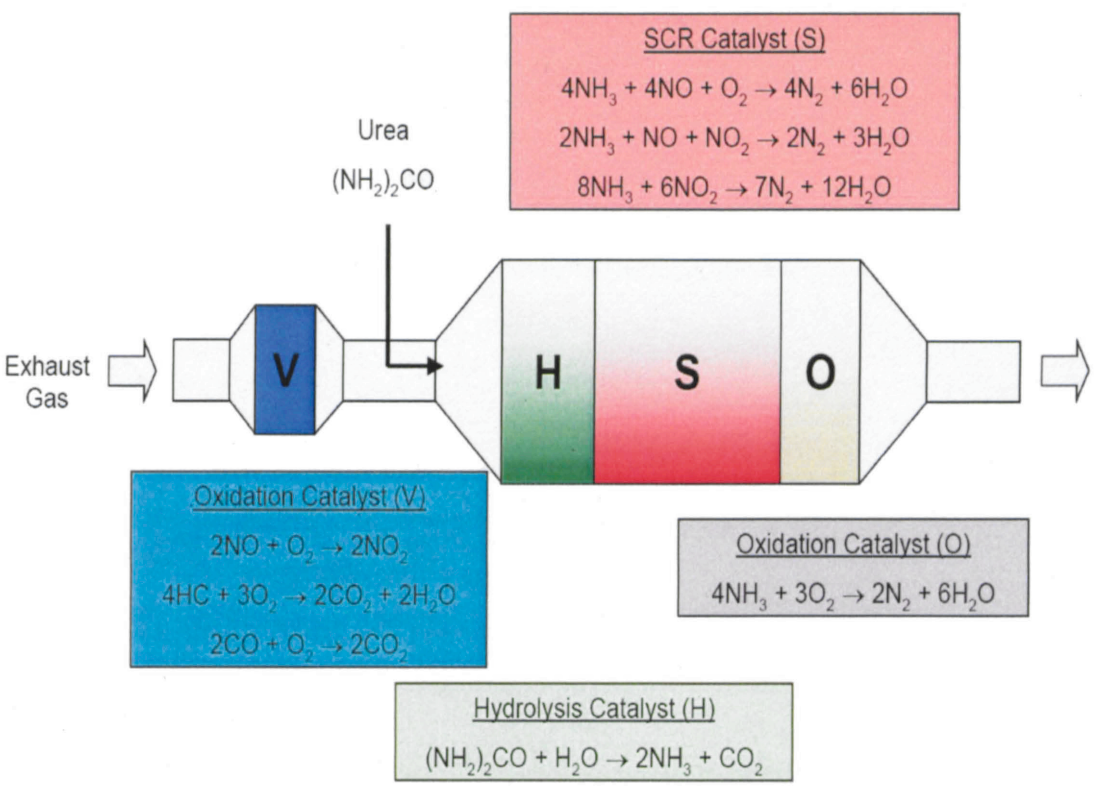

Figure 1.3: Schematic of an SCR system[3]

1.3.1 Oxidation Catalyst upstream of SCR catalyst (S):

The major purpose of utilizing an oxidation catalyst upstream of the SCR catalysts is to achieve a more optimal NO_2/NO_x ratio. In typical diesel exhausts, which have small NO_2/NO_x ratios (~10%), the oxidation catalyst converts NO to NO_2 to increase the NO_2/NO_x ratio. Fastest NO_x conversion rates are seen when the NO_2/NO_x ratio is approximately 50% and is known as the "fast" SCR reaction. Depending on the NO_2/NO_x ratio different reactions can dominate the NO_x reduction process. Three main reactions and the corresponding NO_2/NO_x ratios where the reaction are dominant are,[4]

$4NH_3 + 4NO + O_2 \rightarrow 4N_2 + 6H_2O$ {Low NO_2NO_x ratios}

$4NH_3 + 2NO + 2NO_2 \rightarrow 4N_2 + 6H_2O$ {"Fast SCR"; $NO_2/NO_x \sim 0.5$}

$4NH_3 + 3NO_2 \rightarrow 3.5N_2 + 6H_2O$ {Proceeds slowly; Large NO_2/NO_x ratios}

The presence of NO_2 has a dramatic effect on the activity of an SCR catalyst at low temperatures in particular. It is more pronounced at low temperatures and vanishes at high temperatures. At temperatures above 400°C, the effect of the NO_2/NOx is negligible[4]. Figure 1.4 shows the effect of NO_2/NO_x ratios at 200°C on NO_x reduction efficiency[4]. Temperature, residence time (inverse of the space velocity, which expresses how fast something moves through a system in equilibrium) inlet NO_x concentration and ammonia slip are held constant. The ammonia injection rate is varied to maintain constant ammonia slip. It is evident from the plot that the NO_2/NO_x has a large impact at this temperature.

It is often assumed that the oxidation catalyst will always oxidize NO to NO_2, thereby increasing NO_2/NO_x ratios. However, if thermodynamic equilibrium favors a lower NO_2/NO_x ratio, the reaction can proceed in the direction of dissociating NO_2 to

create more NO. The composition thermodynamically favored depends on the temperature, pressure and mole fractions of NO, NO_2 and O_2 in the exhaust. The temperature dependency of NO_2/NO_x ratio for a partial pressure of O_2 at 0.1 bar can be understood from Figure 1.5. Note that at about 750°F equilibrium concentration results in a favorable NO_2/NO_x ratio of roughly 50%. The addition of an upstream oxidation catalyst to shift the NO_2/NO_x ratio toward equilibrium will most likely improve performance, unless the NO_2/NO_x ratio happens to be very close to 50% in the engine-out exhaust.

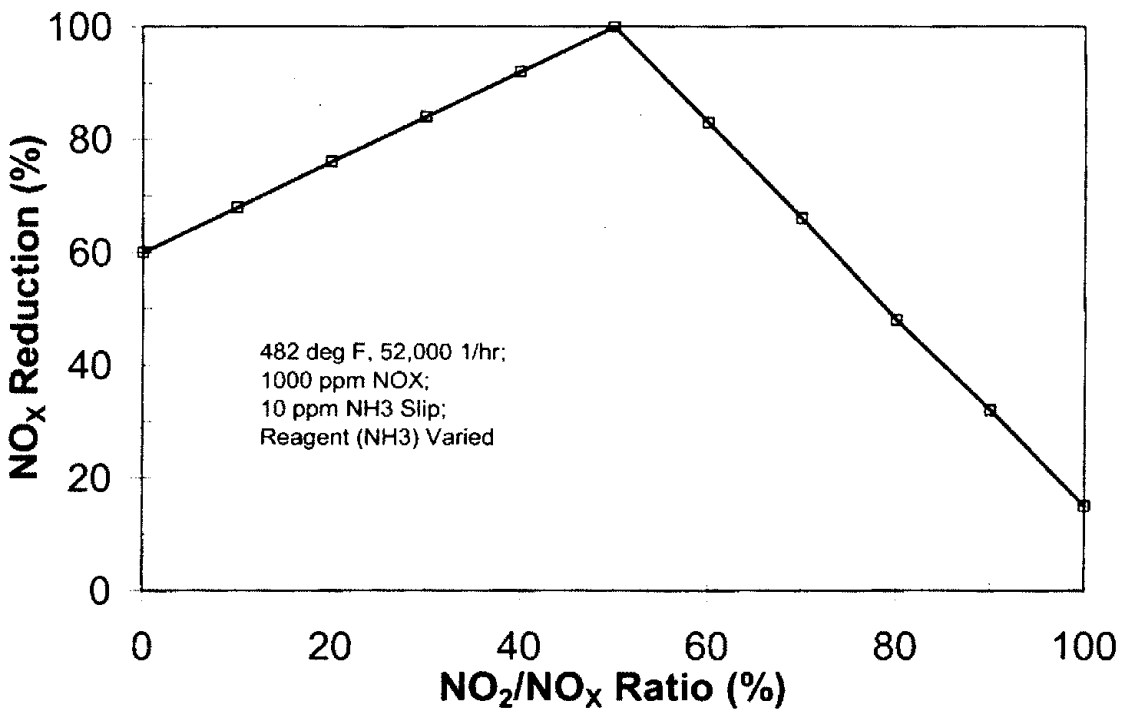

Figure 1.4: NO_X reduction efficiency vs. NO_2/NO_X ratio[4]

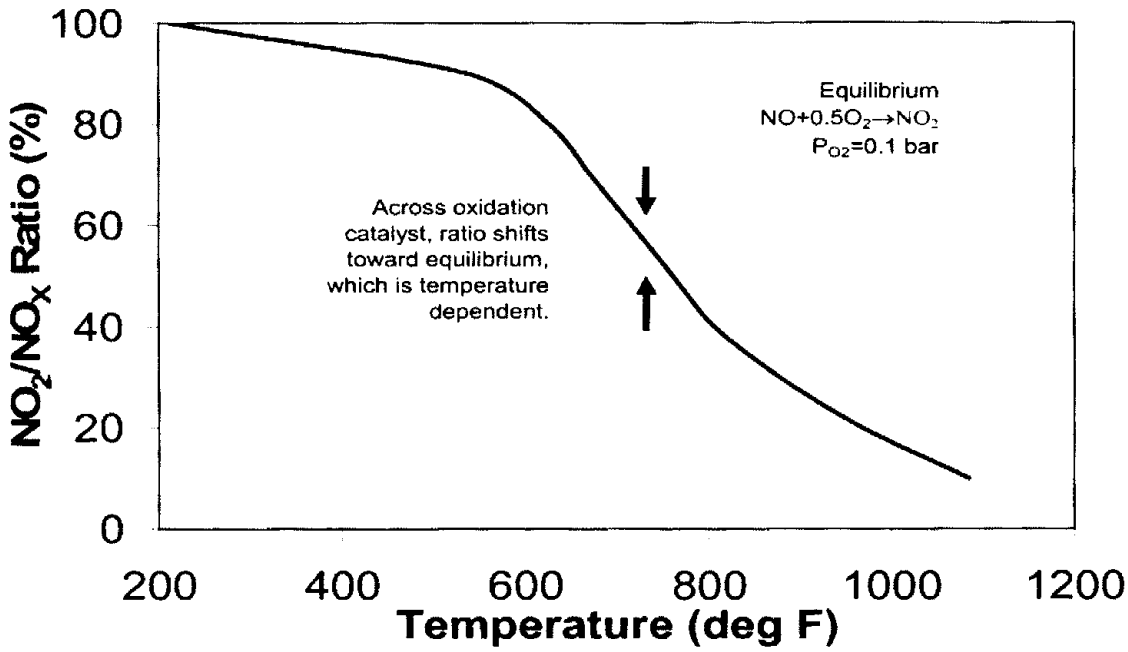

Figure 1.5: Thermodynamic equilibrium analysis determines which way NO_2/NO_X ratio will shift across oxidation catalyst[4]

Oxidation catalysts are also used for NO_2/NO_x ratio augmentation in mobile applications[5, 6] . In the work by Gieshoff, et al. a performance comparison is made on an SCR system between NO_2/NO_x ratios of 0 and 0.5. At 350°C, when the ratio is altered from 0 to 0.5 with synthetic exhaust gas, NO_x reduction efficiency improves from about 78% to 98%. The performance advantage significantly increases at lower temperatures and is maintained at high temperatures (up to 500°C). This is in contrast to the work by Koebel, et al.[4], where the advantage of the optimal NO_2/NO_x ratio diminishes above 400°C.

1.3.2 Reducing Agent:

Urea is commercially produced from carbon dioxide and ammonia at high temperatures and pressures and may be considered as a storage compound for ammonia. Although it is generally accepted that ammonia is ultimately the active reducing compound in the catalyst, pure ammonia is normally not injected into the exhaust stream for most applications. Urea is the re-agent most commonly used owing to its transportability and non-hazardous nature as compared with ammonia. Typically, urea is thermally decomposed to ammonia in the hot exhaust prior to entering the SCR catalyst.

$$(NH_2)_2\,CO \rightarrow NH_3 + HNCO$$

$$HNCO + H_2O \rightarrow NH_3 + CO_2$$

Isocyanic acid (HNCO) is included in the "ammonia slip". This is appropriate since Isocyanic acid is partially reacted urea and, if give more time, would form more ammonia. The second reaction can be accelerated with a hydrolysis catalyst[7].

Solid urea has a melting point of 133°C. As it is slowly heated, decomposition begins at about 80°C and is fully evident at 133°C. The slow heating process produces ammonia, biuret, triuret and ammonium cyanate. Beyond 180°C, isocyanic acid and other heavy compounds are formed. In contrast, faster heating leads to just ammonia and HNCO, which is the preferred reaction[8]. The reaction is exothermic and the heat required per mole of urea decomposed will be reduced considerably if hydrolysis (another exothermic reaction) can be carried out simultaneously. Additional heat at about 200°C-400°C must then be supplied to heat the products.

Although, Urea has advantages in terms of safety, transportability and storage, Ammonia was selected as Re-agent. Two major reasons were higher capital and

operational costs in case of urea and possibility of unwanted intermediate compounds such as Hydrogen Cyanide (HCN).

Anhydrous Ammonia was selected as re-agent instead of urea to eliminate the thermal decomposition as a variable. However, for field implementation of SCR on natural gas engines, aqueous NH_3 may be used. The compound urea, available in liquid or solid form, produces ammonia when heated. Owing to its advantages mentioned above, urea deserves consideration as a replacement for anhydrous or aqueous ammonia in SCR systems. Current research is being conducted to use urea as a replacement for ammonia. Research includes establishing optimum operating parameters, evaluating undesirable by-products from urea decomposition and studying the mechanics of transporting urea to the control skid and the injection point[17] .

1.3.3 Oxidation Catalyst to Reduce Ammonia Slip:

In practical SCR systems, it is common to inject a slight excess of re-agent to maximize conversion efficiencies[9]. Permitted ammonia slip is normally less than 5 ppm-10 ppm. An oxidation catalyst can be used downstream of the SCR catalyst to reduce ammonia slip without impacting NO_x reduction efficiencies. Ideally, the oxidation catalyst converts the ammonia into nitrogen and water[4]. The global reaction mechanism is,

$$4NH_3 + 3O_2 \rightarrow 2N_2 + 6H_2O$$

This approach has been successfully employed in mobile applications[5,6]. In these applications the usefulness of ammonia slip oxidation catalysts is generally accepted. They are implemented without any quantification of their benefits.

1.3.4 SCR Catalyst Composition:

The catalysts most used in investigations found in the literature were Vanadium-Titanium based catalysts[10, 11, 12]. There were a few investigations where Fe-Cr [13, 14] based and Pt-Cu based catalysts[14] were implemented.

Ammonia adsorption in the presence of water (5%) and O_2 (10%) was investigated in various catalyst samples[15]. Two monolithic cordierite honeycombs designated K50 and K64 were immersed into a suspension of TiO_2, whereas catalyst K50 was coated with TiO_2 and 9% WO_3. Both samples were dried and calcined for 3 hrs at 500°C. Subsequently, both samples were impregnated with NH_4VO_3. Another sample used was an extruded monolithic honeycomb consisting of V_2O_5-WO_3/TiO_2 for comparison. Results show the addition of WO_3 is essential to achieve low ammonia slip under practical conditions[15].

Koebel, et al.[4] write about the possible role of NO_2 catalysts that are based on TiO_2-WO_3-V_2O_5. Two monolithic catalysts, one extruded and the other coated, were used for the experiments. Investigations were performed to study the re-oxidation of vanadium species in the catalyst. Experiments suggest that the V^{+4} species forming during reduction of NO with NH_3 are re-oxidized faster to NO_2 than by O_2, resulting in increased rate of NO reduction[4]. The kinetics of the Selective Catalytic Reduction of NO by NH_3 has been investigated over a Vanadia based commercial catalyst[12]. The catalyst contained TiO_2 (>70%), V_2O_5, WO_3 and MoO_3. NO_x conversion by varying water and oxygen concentrations was studied.

In the paper by Bauerle, et al.[13], Fe-Cr based catalysts were used for parametric and durability studies. The catalyst was prepared by impregnating carrier pellets with

aqueous solutions of $Fe(NO_3)_3.9H_2O$ and CrO_3. The moist pellets were dried at 160^0C and then calcined at 500°C. A catalyst was prepared with American Cyanamide Aeroban ZW-1470 Al_2O_3-SiO_2 spheres (3/16 in. diameter) at optimum Fe_2O_3 concentrations. Varying concentrations of Fe were used. The reduction of NO_x with NH_3 on these catalysts was studied in flow reactors using simulated gas temperatures from 200°C-500°C. The optimum catalyst contained 10% active metal oxides at a weight ratio of 9:1 Fe:Cr. Conversion of NO_x, which was maximized at 400°C, was not affected by CO_2 or H_2O but, showed a sharp increase with increase in O_2 from 0-0.5%[13].

Investigations on the effect of SO_2 and space velocity on catalysts based on Pt and Cu were carried out as well[14]. The former was observed to be more active at lower temperatures (190°C-250°C), while the latter was observed to be more active at higher temperatures (usually 350°C). Results suggest that higher NO_x activity was achieved without SO_2 on Pt-based catalysts; Cu zeolite catalysis may be practical for Diesels if sulfur is eliminated from Diesel fuel. In addition, decreasing space velocity by increasing catalyst volume will help NO_x removal by Pt and Cu.

1.4 Laboratory SCR test Setup:

The layout design of the slipstream SCR system was based on a number of considerations. One of these considerations was having the capability to test the reactor at high temperatures. Given the inherent low temperatures of a 2-stroke natural gas engine exhaust, the reactor must be located as close to the cylinders as possible to avoid losses due to heat transfer. The GMV-4TF has a cooled exhaust manifold, so it was important to extract the exhaust upstream of the exhaust manifold. As such, the exhaust was

extracted from ports in the exhaust elbows that connect the cylinders to the exhaust manifold. The sizing of the slip stream system was based on a 3 g/bhp-hr NO_x engine. The GMV engine has a volumetric flow rate of 1600 SCFM within a 12 inch pipe. In order to divert approximately 6% of the GMV flow for the slip stream, a minimum of 3 inch pipe was necessary to run to the catalyst to maintain similar flow velocities.

As described earlier, to minimize temperature drop, the exhaust for the slip stream was extracted from the exhaust elbows allowing the slip stream exhaust to bypass the cooled exhaust manifold. A concern with flow stratification arose because the slip stream exhaust comes from independent cylinder exhaust elbows. A slip stream mixing device was designed to address this concern. The exhaust mixer has four 1.5 inch inlets which come from each of the four sample ports on the engine exhaust elbows. Each end of the mixing device has two inlet flows. The inlet flows are opposing and offset to promote mixing. After the inlet flows swirl and mix, the gas exits out the 4 inch port on top of the device. Two 1.5 inch holes were drilled and tapped into long opposite faces of a square tube. Finally a 4 inch thread-O-Let was welded to the 4 inch hole on top of the square tube.

1.4.1 Motivation:

A critical aspect of an efficient Selective Catalytic Reduction (SCR) setup is the mixing of the reducing agent (re-agent) with the exhaust gas stream upstream of the catalyst. To ensure uniform Nitrogen Oxide (NO_x) conversion downstream of the catalyst, uniform mixing must be ensured between the re-agent and the exhaust gas upstream of the catalyst. A well-mixed reactor will result in a well-distributed NO_x

conversion than one that is poorly or under mixed. The exhaust flow from an internal combustion engine is inherently unsteady. Temperature, pressure and composition all vary axially in the exhaust due to variation between cylinders, mixture non-uniformity in the cylinder, intake mixture short circuiting (4-strokes), the blow-down event (2-strokes) and other scavenging effects (2-strokes). The injection of re-agent is steady in nature and is not tailored to match variations in exhaust composition. Factors such as re-agent injector design, flow rate of injection, position relative to the reactor and exhaust flow rates are key parameters that influence mixing uniformity. Hence, a major challenge is to ensure there is best possible mixing of the re-agent with the exhaust gases.

1.5 SCR System Selection and Final Layout:

Figures 1.6 and 1.7 show the drawing of the test skid that was used for the laboratory test and a view of the re-agent injection and the SCR catalyst housing are shown. Figure 1.7 is representative of the model built in *GAMBIT*, a Computational Fluid Dynamics (CFD) modeling tool.

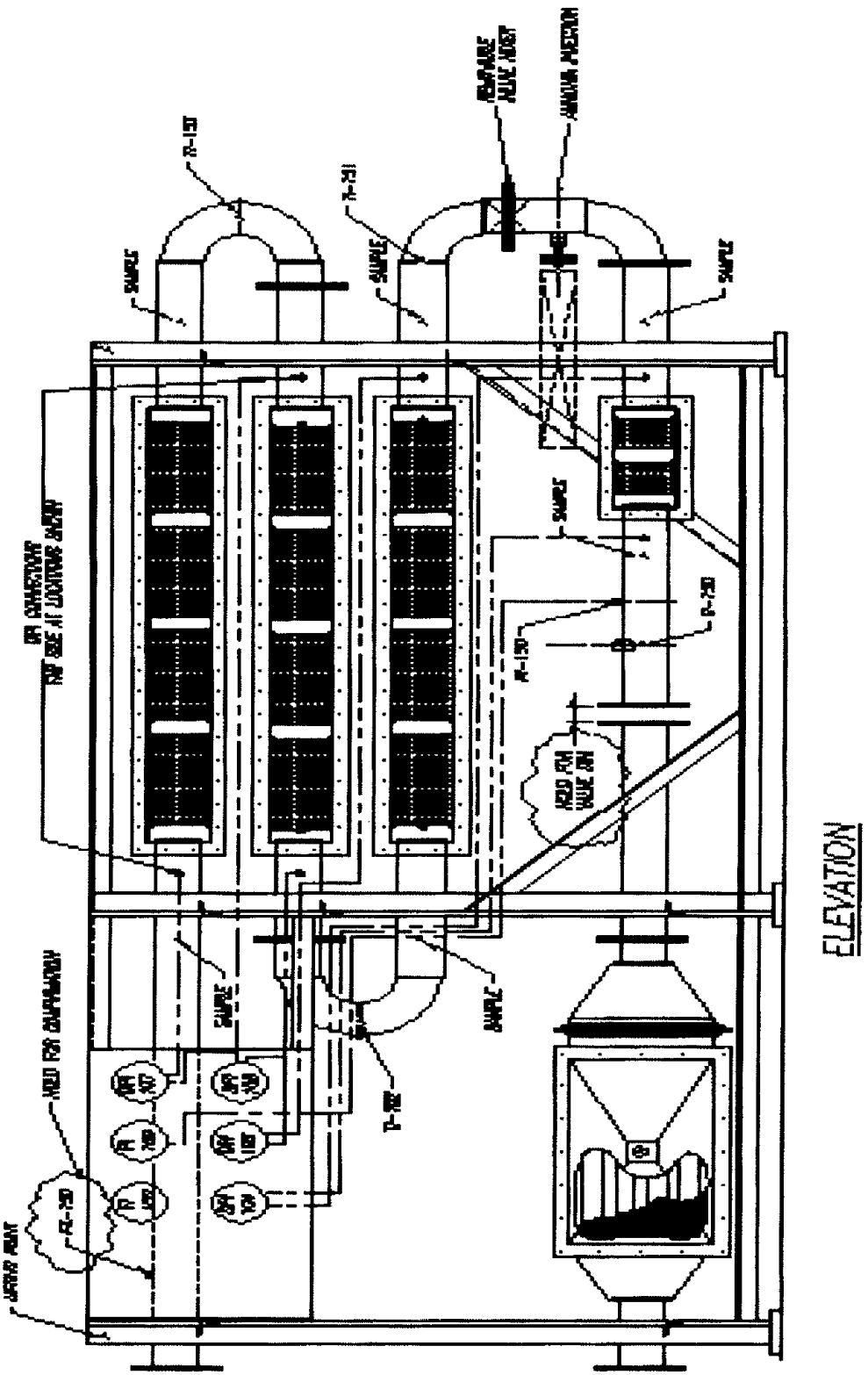

Figure 1.6: EKI skid drawing (elevation)

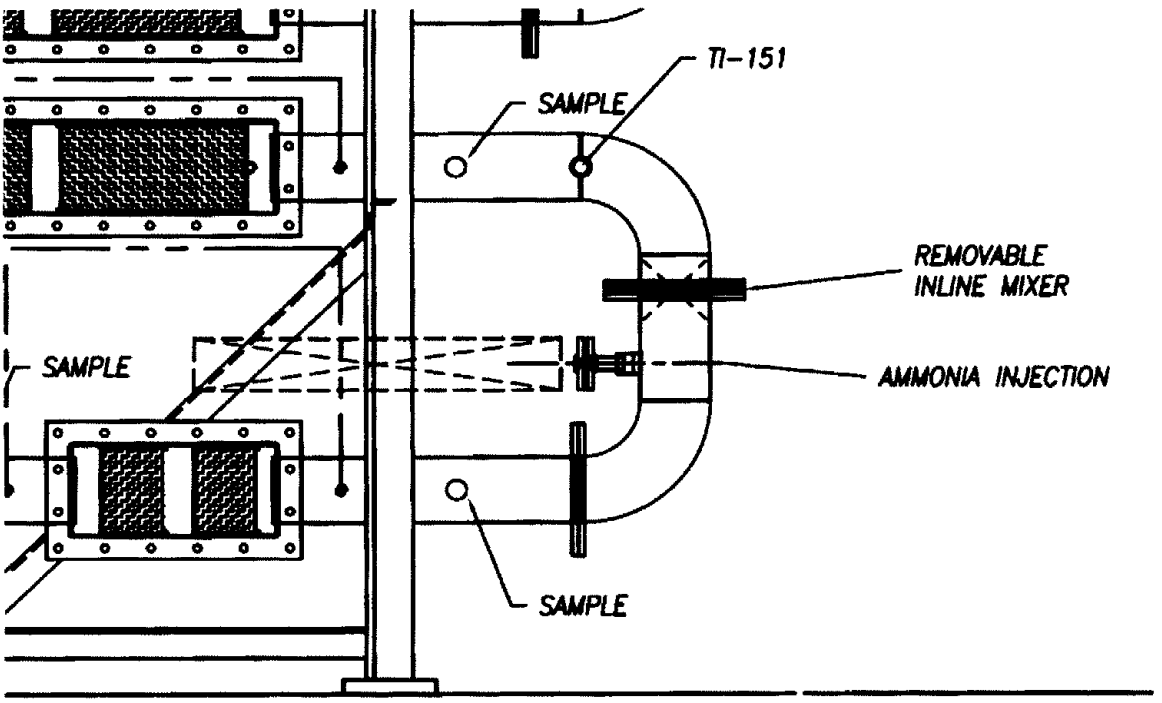

Figure 1.7: Mixing reactor drawing

1.5.1 Reducing Agent Selection:

Reagent Type	Total Capital Cost ($)	Operating cost ($/month)	Atomization Steam requirement cost ($/month)	Reagent Cost ($/month)	Power Cost ($/month)
Urea	9,146,000	77,760	34,560	34,560	8640
Aqueous ammonia	8,442,000	49,824	17,280	26,784	5760
Anhydrous ammonia	8,277,000	19,728	-	19,008	720

Table 1.1: cost comparison between different re-agents[16]

Table 1.1shows a cost comparison between different re-agents that can be used for industrial purposes. Compounds with the superscript '1' in Figure 1.8 are only attributed to SCR systems with urea as the Re-agent and only likely when excess urea is

supplied. However, in the study by Koebel and Elsener[17] on a urea SCR system, biuret, ammeline and melamine, often attributed to the use of urea, were not detected.

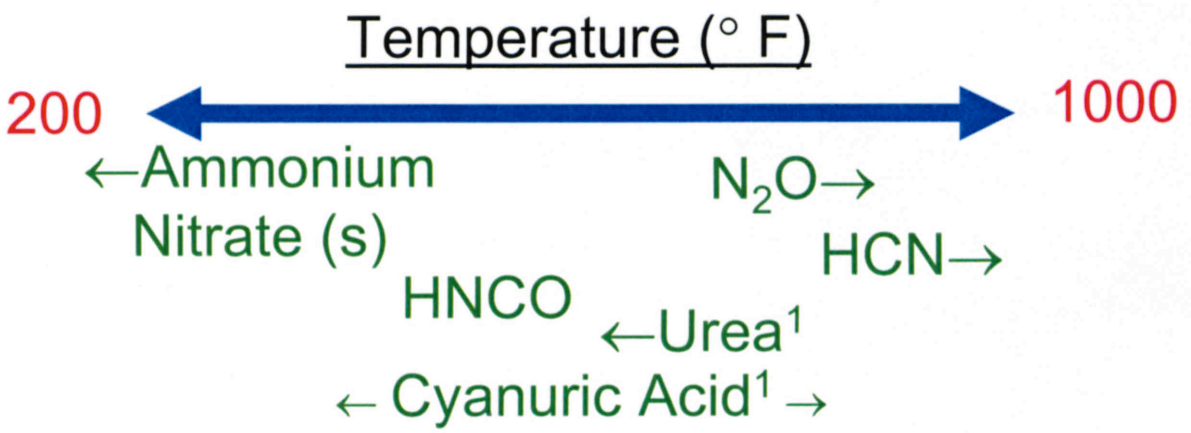

Figure 1.8: Possible formation of unwanted compounds with approximate temperature[17]

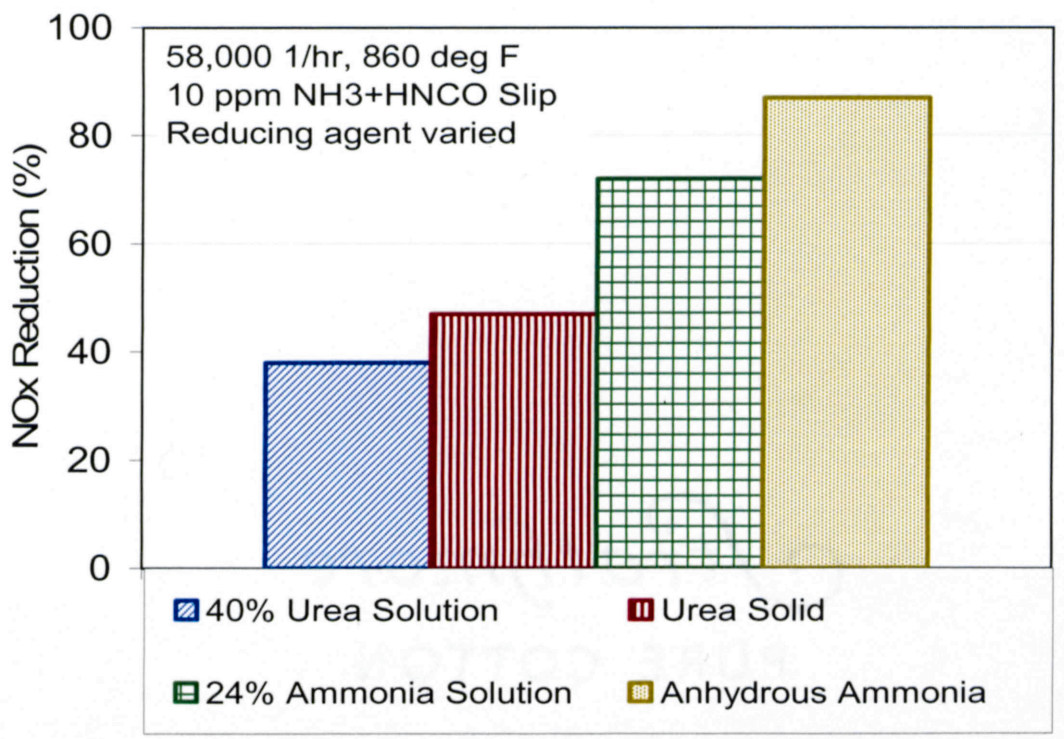

Figure 1.9: Comparison of NO_x conversion rates of various Re-agents[8]

From Figure 1.9 (above), we can see clearly that Anhydrous Ammonia has maximum NO_x conversion rates for the same amount of Re-agent used. It was observed that anhydrous ammonia has almost two times the rate as 40% Urea Solution.

1.6 Problem Statement:

3-dimensional (3-D) numerical solution of re-agent mixing was simulated using *GAMBIT & FLUENT.* These results were compared with the experimental values obtained at the laboratory test centre. Numerical simulations were obtained by injecting re-agent at different locations radially. First, the re-agent was injected axially at the centre through an orifice in the direction of the flow, while the end was plugged. Next, the injector tube was terminated at the wall of the pipe and was injected radially. In addition, the effect of using an in-line mixer (two 'D' shaped metal plates at right angles to each other) was tested in both the cases numerically and experimentally.

Endnotes:

[1] http://www.google.com/search?q=nox+effects&ie=utf-8&oe=utf-8&aq=t&rls=org.mozilla:en-US:official&client=firefox-a

[2] Owen Balley, Dannan Dou, Gregory W. Denison, "Regenration strategies for NO_x Adsorber Catalysts", SAE Technical paper series, 972845, 1997

[3] Tim Johnson, "*Diesel – The environmental benchmark for heavy duty applications*", *CORNING*, August 2002.

[4] Koebel, M., Madia, G., and Elsener, M. "Selective Catalytic Reduction of NO and NO_2 at low temperatures", *Catalysis Today*, Vol. 73, pp. 239-247, 2002.

[5] Gieshoff, J., et al., "Advanced Urea SCR Catalysts for Automotive Applications", SAE Technical Paper Series, Paper No. 2001-01-0514, Warrendale, PA, 2001.

[6] Walker, A.P., Allansson, R., Blakweman, P.G., et al., "The Development and Performance of the Compact SCR-Trap System: 4-Way Diesel Emission Control System, SAE Technical Paper Series, Paper No. 2003-01-0778, Warrendale, PA, 2003.

[7] Fang, H.L., and DaCosta, H.F., "Thermolysis Characteristics of Urea_SCR", 8th Diesel Engine Emissions Reduction Conference, San Diego, CA, August 25-29, 2002.

[8] Koebel, M. and Strutz, E.O., "Thermal and Hydrolytic Decomposition of Urea for Automotive Selective Catalytic Reduction Systems: Thermochemical and Practical Aspects", *Ind. Eng. Chem. Res.*, Vol 42, pp. 2093-2100, 2003.

[9] Chen, M. and Williams, S., "Modelling and Optimization of SCR-Exhaust Aftertreatment Systems", SAE Technical Paper Series, Paper No. 2005-0-0969, Warrendale, PA, 2001.

[10] Madia, G., Koebel, M., Elsener, M. and Wokaun, A., "Side Reactions in the Selective Catalytic Reduction of NO_x with various NO_2 fractions", *Ind. Eng. Chem. Res.*, Vol. 41, pp. 4008-4015, 2002.

[11] Koebel, M., Madia, G., Raimondi, F. and Wokaun, A., "Enhanced Reoxidation of Vanadia by NO_2 in the Fast SCR Reaction", *Journal of Catalysis*, Vol. 209, pp. 159-165, 2002.

[12] Willi, R., Roduit, B., Koeppel, R.A., Wokaun, A. and Baiker, A., "Selective Reduction of NO by NH_3 over Vanadia based Commercial Catalyst: Parametric Sensitivity and Kinetic Modeling", *Chemical Engineering Science*, Vol. 51, No. 11, pp. 2897-2902, 1996.

[13] Bauerle, G.L., Wu, S.C. and Nobe, K., "Parametric and Durability Studies of NO_x Reduction with NH_3 on Fe-Cr Oxide Catalysts", *Ind. Eng. Chem. Prod. Res. Dev.*, Vol. 17, No. 2, 1978.

[14] Adams, K.M., Cavataio, J.V. and Hammerle, R.H., "Lean NO_x Catalysis for Diesel Passenger Cars: Investigating Effects of Sulfur Dioxide and Space Velocity", *Applied Catalysis B: Environmental*, Vol. 10, pp. 157-181, 1996.

[15] Kleemann, M., Elsener, M., Koebel, M. and Wokaun, A., "Investigation of the Ammonia Adsorption on Monolithic SCR Catalysts by Transient Response Analysis", *Applied Catalysis B: Environmental*, Vol. 27, pp. 231-242, 2000.

[16] Noroozi, S. and Daniel, F., "Urea Enhances Safety in SCR Applications", *Power Engineering*, December, 1993.

[17] Koebel, M and Elsener, M., "Determination of Urea and its Thermal Decomposition Products by High-Performance Liquid Chromatography", *Journal of Chromatography A*, Vol. 689, pp. 164-169, 1995.

Chapter 2: LITERATURE REVIEW

Although numerous published papers and reports were available on SCR systems, only a few that incorporated CFD studies were found. Two papers by by Zhang et al and one by Soo-Jin Jeong et al that deal with mixing characteristics of NH_3 upstream of the SCR catalyst using CFD were published in the Society of Automotive Engineers (SAE).

Zhang et al[18] in their 2006 publication have addressed the geometrical effects on flow mixing by using three dimensional CFD. Mixing enhancement was achieved by adding a flow mixer. The shapes and locations of flow mixers, as well as the number of blades inside the mixer were investigated to show the effect on fluid mixing downstream along the flow direction. Results showed great improvement of mixing by adding a delta wing mixer. Turbulent flow generated by delta wings proved to be very useful for a significant mixing enhancement within a short distance. It was found that a flow mixer in front of injector resulted in higher mixing flow indexes just downstream of the mixer. The effect of a swirl flow was also studied by utilizing twisted delta wing mixer. It was found that the turbulent flow had a dominant effect on the flow mixing index in the short distance right behind the flow mixer while the swirling flow dominated through a longer distance.

Geometries used in CFD simulations include a round straight pipe with or without flow mixers. The diameter and length of the pipe are 55mm and 450mm respectively. For numerical accuracy, the additional pipe length (twice the pipe diameter) was added in front of the flow mixer for flow development. Inside the pipe, fine meshes were generated towards the pipe wall as well as to both sides of flow mixer. In the vicinities of

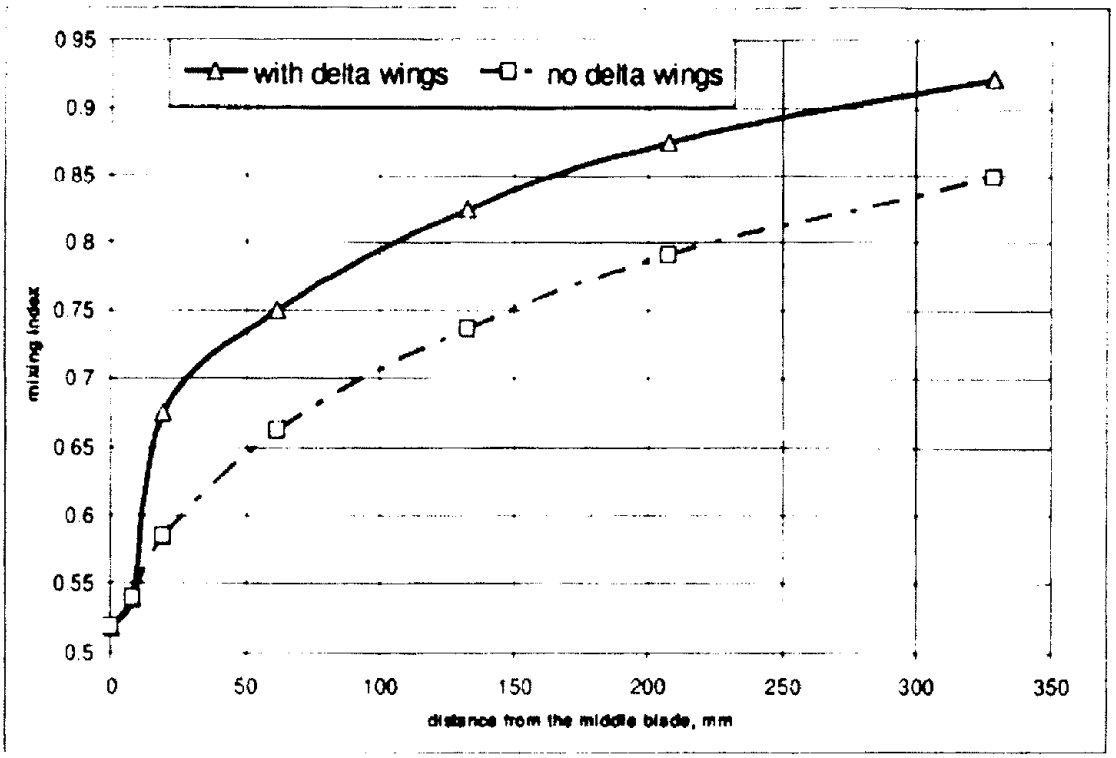

Figure 2.1: comparison of flow mixing indexes in the flow direction for cases with and without flow mixer[18]

the mixer blades, very fine meshes were constructed to ensure the capture of local small scale vortices.

From Figure 2.1, a significant improvement just downstream of the flow mixer can be evidenced by the comparison of indexes between both geometries. Flow mixing index was calculated based on the formula,

$$\Gamma = 1.0 - (\int|C-C_o|\, dA) / 2A_oC_o$$

Where, $C_o = \int CdA/A_o$ and C is the NH_3 mass concentration across plane A

The flow mixing index increased from 0.58 to 0.67 20mm away from the centre of flow mixer. The percentage improvement decreases as the location moves further downstream and goes down to less than 10% at the fluid exit. Majority of the enhancement is seen in very short distances downstream of the flow mixer.

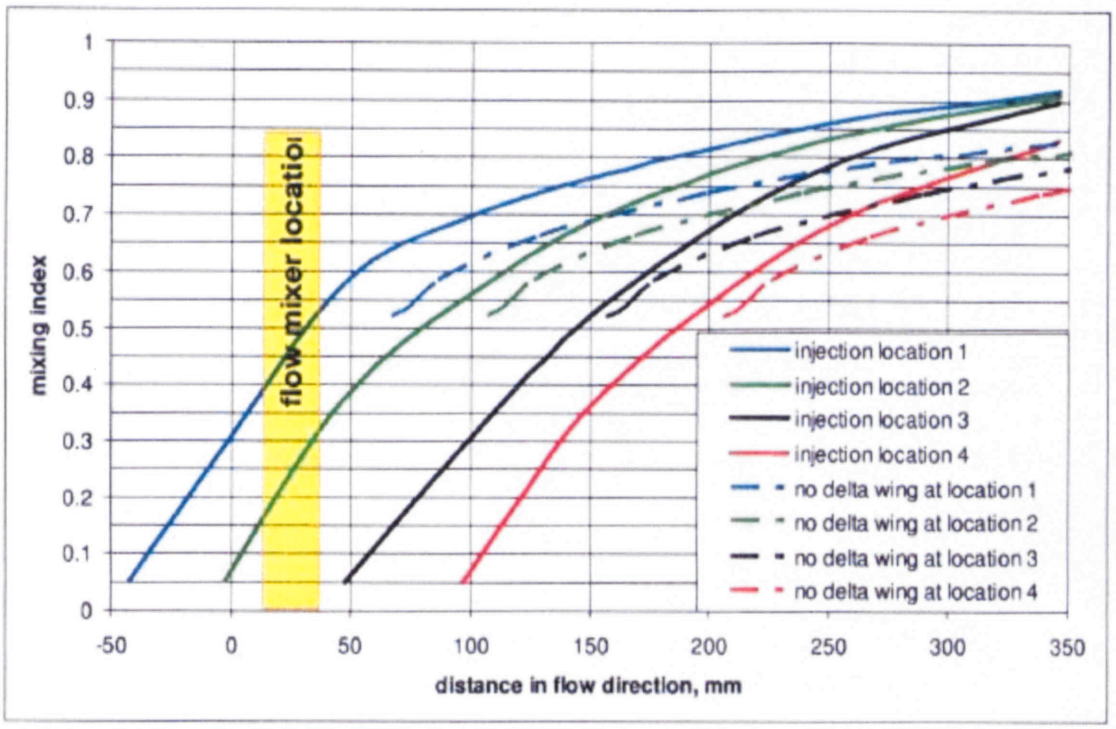

Figure 2.2: comparison of flow mixing indexes among geometries of four locations of NH_3 injection with and without delta flow mixer presented[18]

Figure 2.2 plots mixing indexes change along the flow direction for four NH_3 injector locations. Solid lines represent mixing indexes with a flow mixer while dotted lines represent those without a flow mixer. The delta wing mixer is located in front of the pipe between 0 and 50mm as specified in the yellow region in Figure 2.2. A jump of flow mixing index is evidenced right after flow mixer for injector location 1 and 2, while for locations 3 and 4, a more smooth increase is found. Much lower mixing index is found when NH_3 injector is installed downstream 60mm away from flow mixer.

The comparison of flow mixing index along the pipe is shown in figure 2.3 for three geometries with different number of blades. Lowest mixing index was found for the flow mixer with only two blades. However, no significant effect was found within 100mm behind flow mixer when compared with that of six blades. It was noticed that

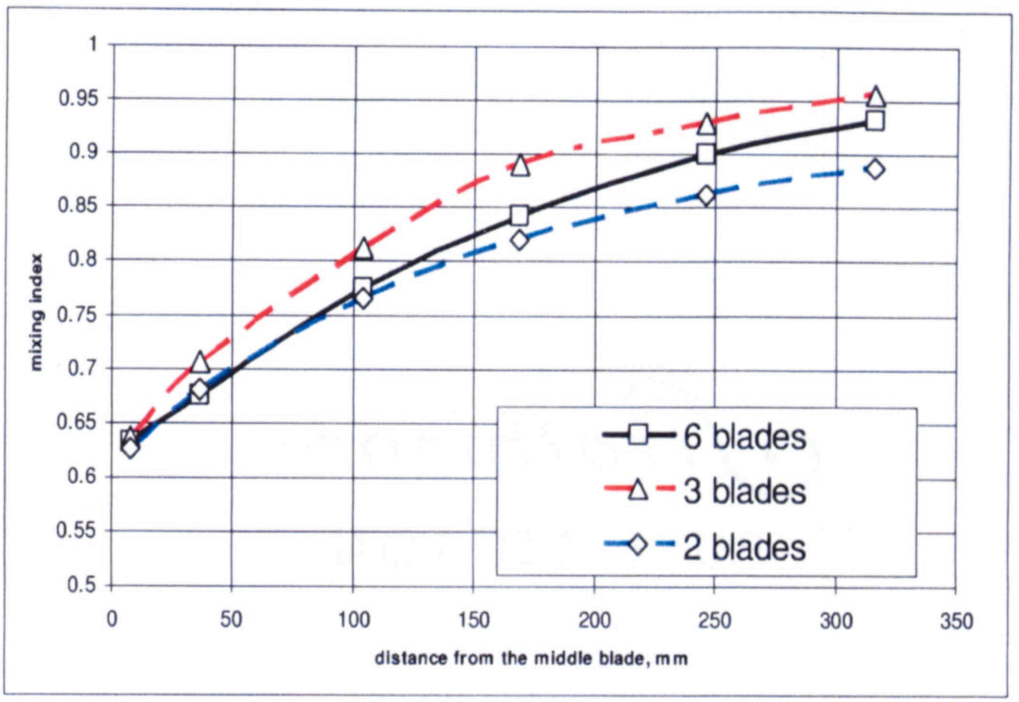

Figure 2.3: flow mixing index comparison along flow direction among the geometries with different number of twisted blades[18]

highest mixing index was along the flow direction all the way to the flow exit in the geometry with three twisted blades. Almost 8% higher flow mixing index was found right behind the flow mixer for the geometry with three blades. The percentage of increment keeps its strength all the way downstream to the location 170mm away from the mixer.

In summary, flow mixing could be greatly improved by using a delta wing shape mixer. The study of the locations of flow mixer indicated a rapid enhancement of flow mixing by placing a flow mixer downstream of NH_3 injection, whereas for a better mixing performance in a longer pipe, a flow mixer should be located upstream of NH_3 injection.

Zhang et al[19], in their more recent publication, have investigated flow mixing phenomenon in an SCR system. First, the effect of mass flow rates of injected NH3 and exhaust gas on flow mixing and pressure loss was investigated for a traditional tube injector with single or multiple nozzles. Then, a concept of ring shaped injector with multiple nozzles was built for 3-D CFD simulations. Comparisons of flow mixing index and injection pressure were made between the two types of injectors. Next, the locations of nozzles in the ring injector were studied and the effect on flow mixing index and NH_3 injection pressure were addressed. Finally, the effect of a swirling flow, which can be generated by a span element or flow mixer in front of the substrate, was studied and the enhancement on flow mixing index was discussed.

Two gaseous species, hot air and cold NH_3, were used to simulate the species transportation. The pipe length was approximately 360mm for evaluating the degree of fluid mixing. A straight exhaust pipe with a diameter of 59mm was used throughout the paper. The diameter of the circular pipe was the same as the tube injector pipe, which was approximately 10mm. Very fine meshes were built in the vicinities of the injector pipe wall and nozzle locations.

Mixing index depends not only NH_3 injection rate, but on exhaust gas flow rate as well. First, the exhaust gas mass flow rate was set to 282g/s. The effect of NH_3 injection rate on flowing mixing index and injection pressure were studied for a tube injector with single nozzle. The area of the nozzle was 2.59 square millimeter and NH_3 mass flow rate ranged from 0.1255 to 0.7847 g/s.

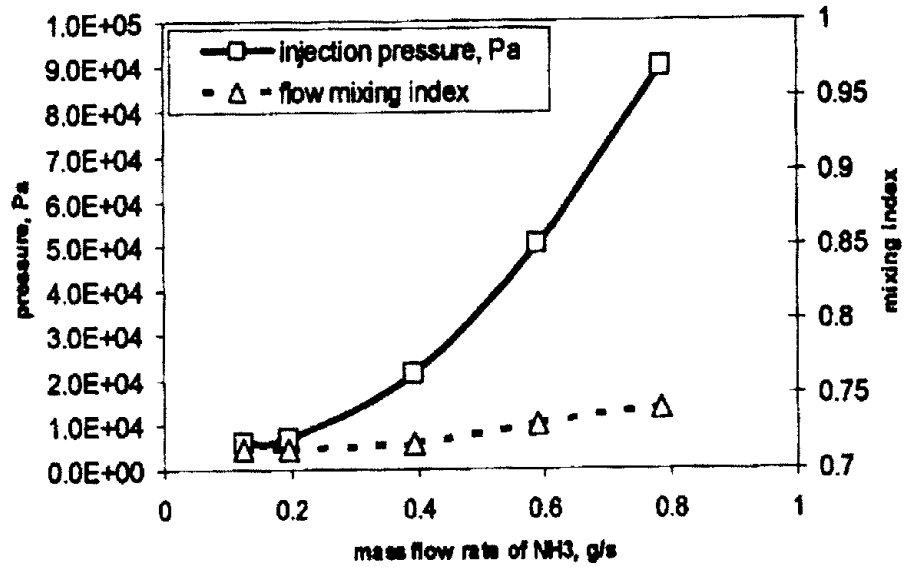

Figure 2.4: fluid mixing index and NH_3 injection pressure versus NH_3 mass flow rate[19]

In Figure 2.4, the solid line with square markers represents injector inlet static pressure with the vertical axis on the left and dotted line with triangle markers stands for flow mixing index with the vertical axis on the right. As expected, injection pressure increased exponentially with the increase of injection mass flow rate. Flow mixing index was also found to increase with the mass flow rate, but in a slower and a more linear manner. About 4% improvement was found when NH_3 mass flow rate increases from 0.1255 to 0.7847 g/s.

The effect of exhaust gas flow rate on flow mixing index and NH_3 injection pressure was also investigated next. The results are shown below in Figure 2.5. Exhaust mass flow rates ranged from 84.6 g/s to 564 g/s corresponding to different engine operating conditions. Mass flow rate of NH_3 was set constant at 0.3923 g/s. Single injection system was used and all boundary conditions remained the same.

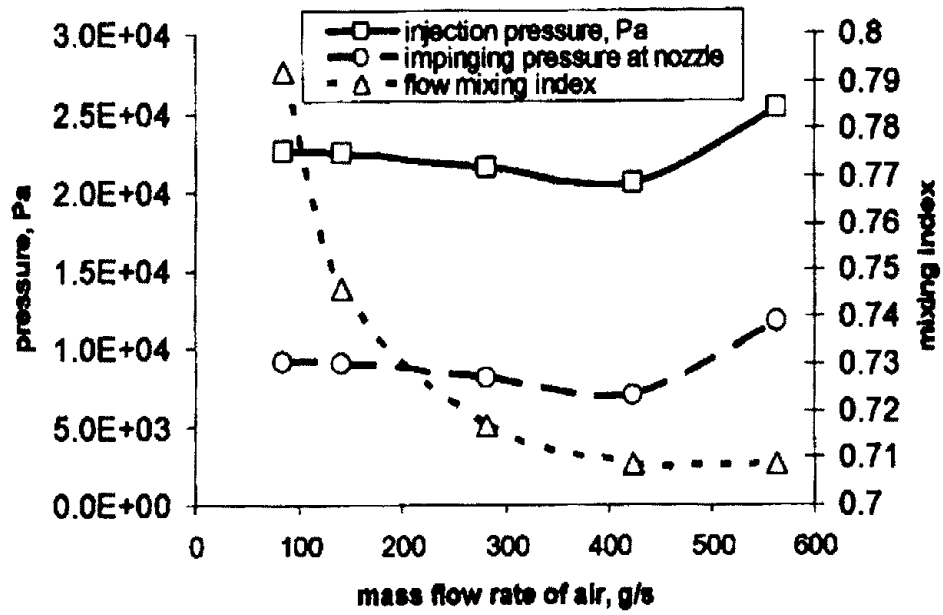

Figure 2.5: fluid mixing index, static pressures at injector outlets and injector inlet versus exhaust gas mass flow rate[19]

Flow mixing index decreases with increase in exhaust gas mass flow rate. Rapid decrease of mixing index was evidenced at lower exhaust mass flow rate and the speed of decrement slowed down as exhaust gas flow rate increased further. More than 10% drop of flow mixing index was found when mass flow rate increased from 85 g/s to 564 g/s. Based on the trend, as mass flow rate increased beyond 570 g/s, flow mixing index was expected to increase.

Injection pressure for the ring injector was 11445 Pascal (Pa) higher than the tube injector, which was 6867 Pa. This is due to the smaller total nozzle area which leads to higher velocity at the throat of nozzles for the ring injector. As expected, the total pressure loss through the exhaust pipe was also higher for the ring injector. The pressure

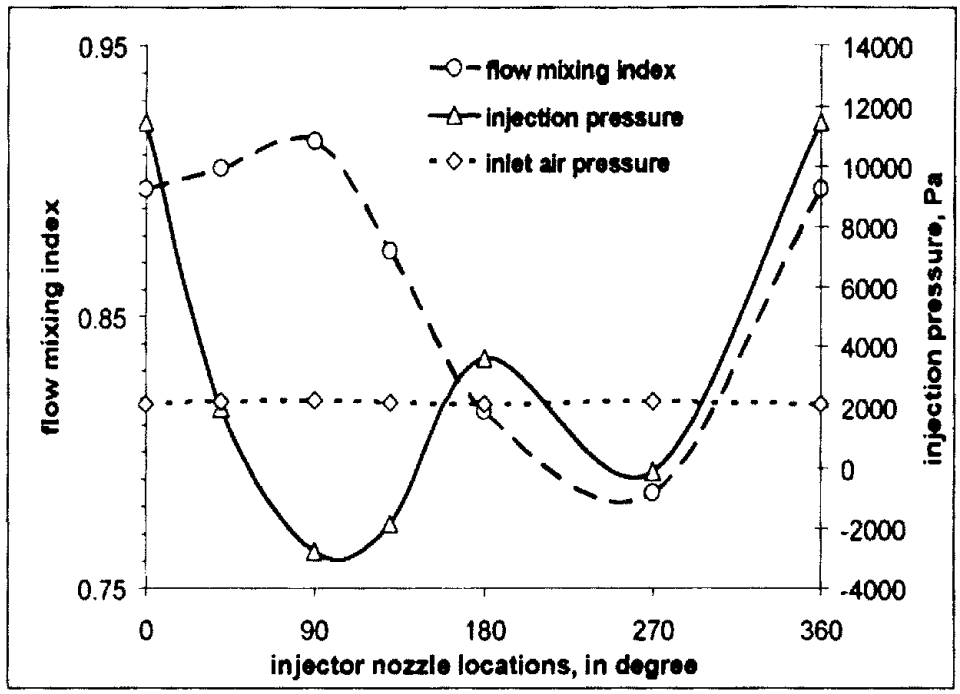

Figure 2.6: flow mixing index, static injection pressure and system pressure loss versus the locations of nozzles[19]

loss for the system with a tube injector was around 663 Pa while with the ring injector was 2095 Pa.

Figure 2.6 depicts the flow mixing index, static injection pressure and system pressure loss at various locations of nozzles. Flow mixing increased as the nozzle location moves from front side (0 degree) to outer side (90 degrees) and reached a maximum value roughly at the location where the lowest injection pressure is found. As the nozzle moves further to 180 degrees, a sharp loss of flow mixing index was observed. The flow mixing index dropped from 0.915 to 0.815. As the location moves from 180 to 270 degrees, the mixing index dropped continually and reached its lowest value at the location where the second lowest injection pressure was found. A rapid increase of flow

mixing index was seen when location moves from 270 degrees to 0 degree. Mixing index can be varied from 0.785 to 0.915 based on different nozzle locations.

In summary, for a traditional tube injector the flow mixing index, as well as injection pressure, increased with the increase of NH_3 injection rate. Flow mixing index decreased with increase of exhaust gas flow rate. In general, the ring injector achieved higher mixing index than the tube injector. Swirling flow was proved to be very helpful to improve flow mixing index for a tube injector system. More than 100% increment in enhancement was found right after the NH_3 injector. Only slight mixing index improvement was observed for a ring injector.

Jeong et al[20] in this paper have studied three dimensional numerical simulation of urea injection of heavy-duty diesel engine under various injection pressure, injector locations and number of injection holes. The effect of location and number of holes of urea injector on the uniformity of ammonia concentration distribution and the amount of water at the entrance of SCR monolith has been examined in detail under various injection pressures.

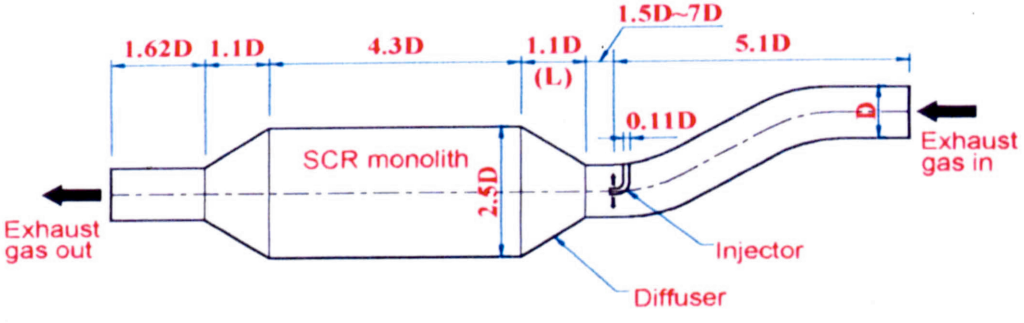

Figure 2.7 Geometry of Urea-SCR[20]

The geometry of urea-SCR system for a 7.2 liter diesel engine used in this work was modeled and is shown in Figure 2.7. It was assumed that the exhaust gas consisted of 77% Nitrogen (N_2) and 23% Oxygen (O_2) in mass fraction. The cell density of the monolith, open frontal area and geometric surface area were 200 cells per square inch (cpsi), 69% and 18.5 square centimeter / cubic centimeter (cm^2/cm^3). The wall thickness of the monolith was about 0.3 millimeter (mm). Urea solution of 32.5% concentration was used.

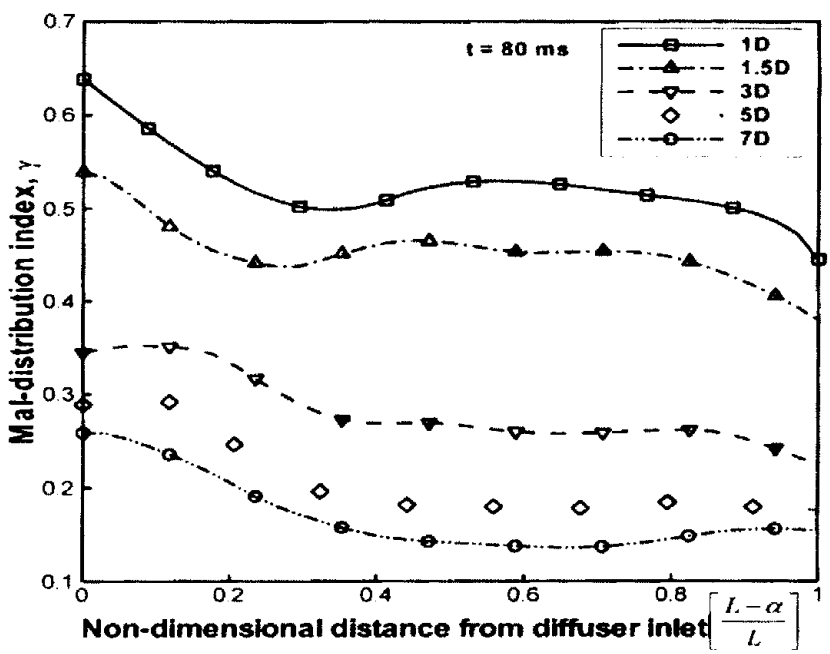

Figure 2.8: comparison of mal-distribution index in diffuser as function of injection nozzle location[20]

Figure 2.8 shows axial mal-distribution index of ammonia from inlet expansion to SCR monolith face at the end of injection (t=80 milliseconds) for various injector locations of 6 hole urea injector at 1 bar pressure. Mal-distribution index (γ) was calculated using the formula,

$$\gamma = 1/(2n) * \sum \sqrt{(C_i - C_{average})} \,\hat{}\, 2 / C_{average}$$

Where, n = number of points; Ci = concentration of ammonia at location 'i' &

$C_{average}$ = average surface concentration of ammonia

It can be observed that when injector was located at 1D (one times the diameter of the exhaust pipe, D) upstream of the monolith, the mal-distribution index decreases linearly ranging from inlet expansion to 30% of total diffuser length. There is not a significant variation between 30% and 85% of the total diffuser length. But, a sharp decrease is observed from 85% to the monolith face. 1,5D, 3D, 5D and 7D represent the injector location that is 1.5, 3,5 and 7 times the diameter of the exhaust pipe. Mal-distribution index of ammonia concentration on the monolith face decreased by 13%, 47%, 58% and 61% when the injectors were placed at 1.5D, 3D, 5D and 7D respectively.

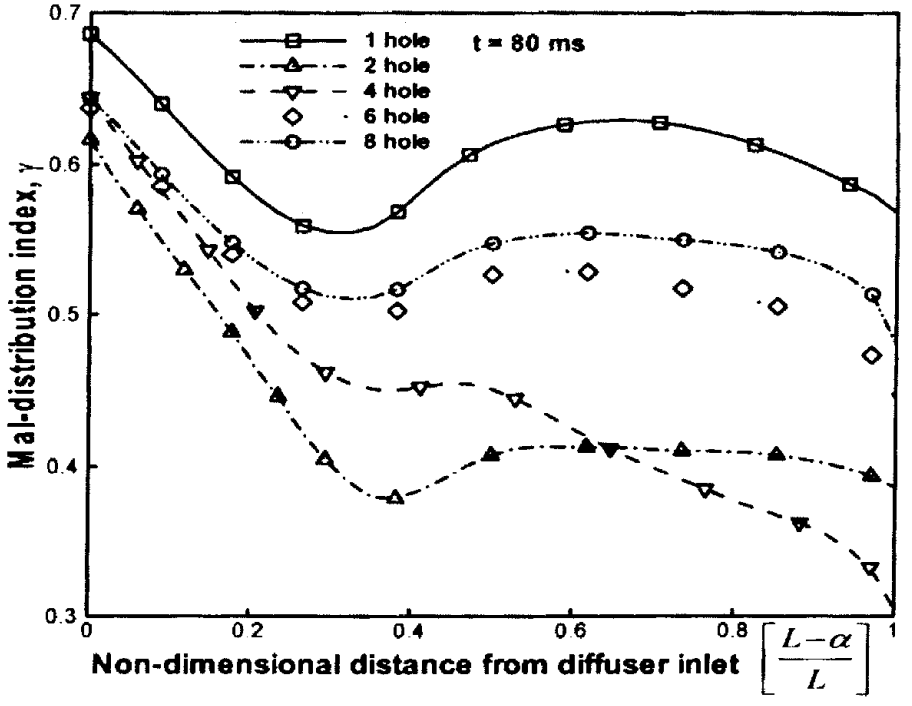

Figure 2.9: comparison of mal-distribution index in diffuser as function of injection nozzle hole[20]

Figure 2.9 suggests the mal-distribution index in the diffuser for different number of injector nozzle holes when the injector is located at 1D upstream of the monolith and at 1 bar pressure.

Where L = diffuser length

α = fractional diffuser length

It can be observed that highest mal-distribution index on the monolith face occurs for a 1 hole injector. The non-uniformity of a 2 hole injector is lower than that of a 6 hole and an 8 hole. In all cases, uniformity increased linearly until about 30% of the total diffuser length. There was an increase in non-uniformity from 30% to 60% in each of the case, which was followed by a gradual decrease. Best mixing was seen in a 4 hole injector, with the mal-distribution index being close to 0.3 on the monolith face.

In summary, the location of injector and the number of injector holes should be considered as an important design factor as they have a strong influence on NH_3 slip and NO_x conversion.

Endnotes:

[18] Xiaogang Z. , Martin R., "3-D Numerical Study of Mixing Characteristics of NH_3 in front of SCR", SAE Technical paper series, 2006-01-3444

[19] Xiaogang Z. , Martin R., "3-D Numerical Study of Flow Mixing in front o f SCR for different injection systems", SAE Technical paper series, 2007-01-1578

[20] Soo-Jin Jeong, Sang-Jin Lee, Woo-Seung Kim and Chun Beom Lee, "Simulation on the optimum shape and location of urea injector for urea-SCR system of heavy duty diesel engine to prevent NH_3 slip", SAE Technical paper series, 2005-01-3886

Chapter 3: NUMERICAL SOLUTION (2-d MODEL)

3.1 Motivation:

Although the actual solution for a mixing model of this kind requires a complete three dimensional model that takes into account the precise replication of the physical hardware, to gain an understanding of the flow structures and other contours a two dimensional model was first made and analyzed. The study of a 2-d model was quite helpful in making certain assumptions for the 3-d model and thus reducing unnecessary complications.

3.2 Modeling:

The dimensions of the experimental setup were first recorded from an *AUTOCAD* file that was provided by the hardware manufacturer, *ENVIROkinetics*, and then *GAMBIT* was used to build the model and create the mesh. Only a part, the section of interest, of the complete SCR system utilized at the EECL was modeled. The section of interest covers the point downstream of the first oxidation catalyst (not utilized in the experiment) position to the point just upstream of the SCR catalyst. The re-agent injection system is about 2.5 inches downstream of the first 90° bend. The injector tube is an ordinary 0.5 inch diameter transport tube that is operated at Standard Liters per Minute (SLM) from the ammonia storage tank to injection point. The injector tube is about 12-15 feet long with a number of turns in its course before reaching the injection point. Three cases of ammonia injection at the wall with no down-stream mixer, an angled down-stream mixer and a central mixer are discussed in this chapter. Due to the diversion of flow of the exhaust around the injector in a 2-dimensional case, the injector was modeled to inject

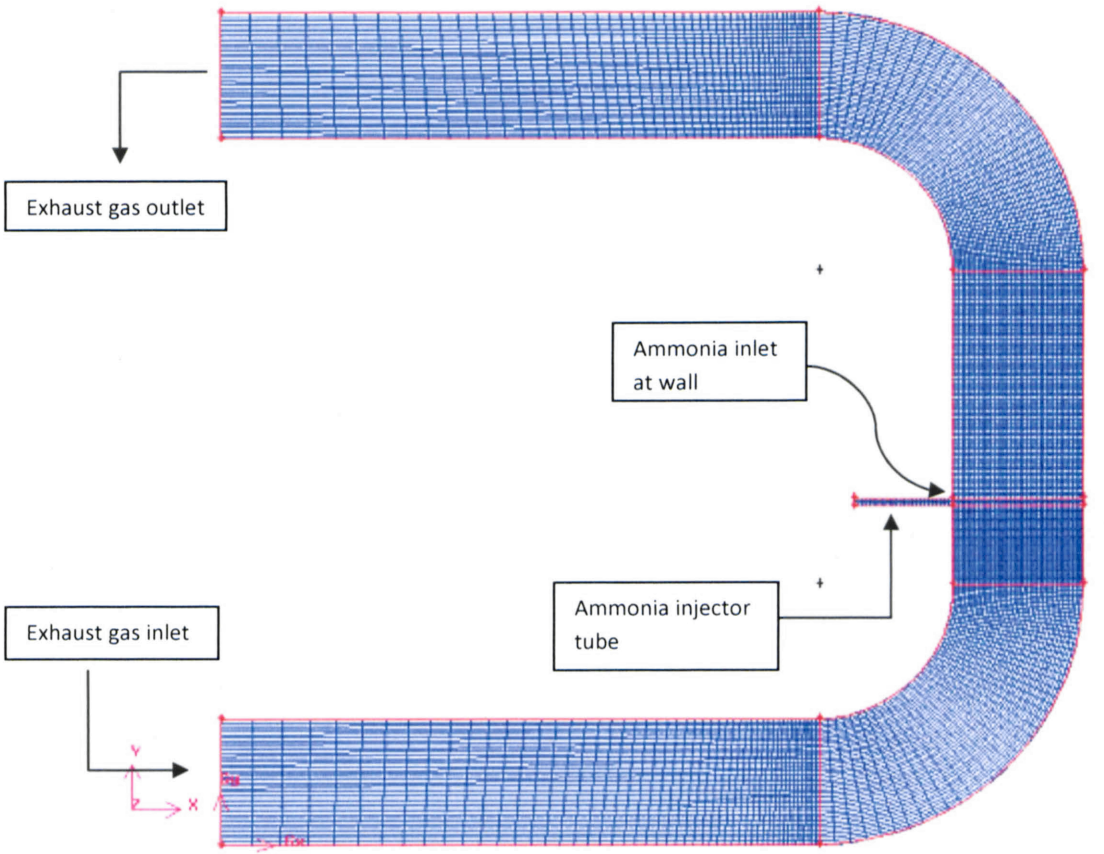

Figure3.1: Mesh in case (a)

ammonia from the wall end of the reactor (the part of the model to which the injector is attached). The three cases – their meshes and boundary conditions – are shown in Figure 3.1.

As can be seen in Figure 3.1, a 2-d model was created using the actual hardware dimensions for the pipe section and the injector tube. Only 3 inches of the injector was modeled as the flow is fully developed. The Quad map scheme of mesh was applied to the entire model. A quad-map scheme generates a regular, structured quadrilateral grid of mesh elements. Approximately 13,000 elements were created with the mesh. The two bends seen in the Figure 3.1 were meshed using a sizing function. A sizing function

allows the user to define the mesh for a face or volume as a function of growth rate and the maximum size of the mesh element. It can be observed that the mesh is fine inside and just outside the injector tube so as to compute the parameters of interest accurately in that vicinity. Figure 3.2 and 3.3 show the boundary conditions that were imposed on the model for case (a). Figure 3.3 shows the magnified area of the re-agent injector tube. Since the actual flow values of velocity inlet (exhaust), pressure outlet (exhaust and re-agent), and mass flow rate of re-agent were known, they were utilized as the boundary conditions. 'Interior' simply means that flow can pass through it and does not obstruct flow. 'Wall' means that that particular edge/face acts as a wall (obstruction).

Figure 3.2: boundary conditions in case (a)

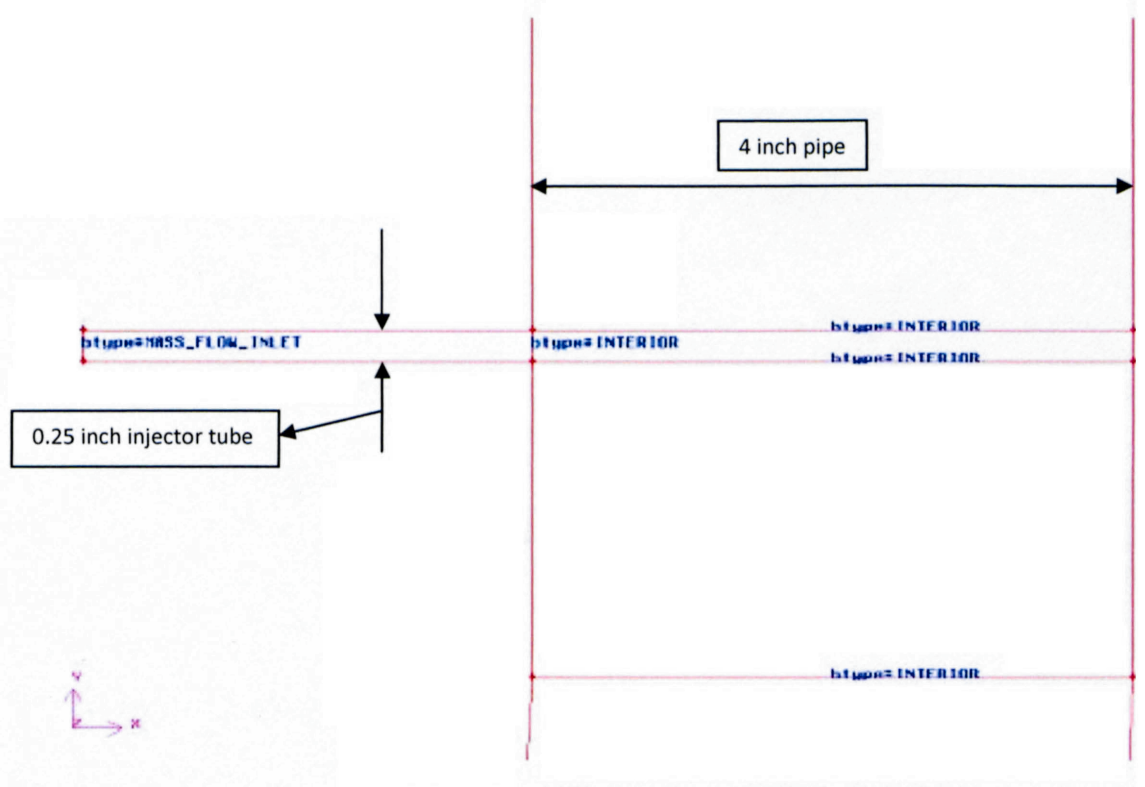

Figure 3.3: boundary conditions (zoom) in case (a)

In the second case – ammonia injection at wall and an included down-stream angled wall mixer – an angled wall at approximately 4 inches downstream of the injector and 45° to the horizontal was modeled to induce some amount of turbulence in the flow. Although this is not the actual shape of mixer utilized in the laboratory experiment, it has been done so to replicate the use of a mixer. A tri pave scheme was used for the reactor part and quad map scheme for the rest of the geometry. A tri pave scheme generates an unstructured grid of only triangular elements. Again, approximately 13,000 elements were created with the mesh and a sizing function was used to mesh the two 90° bends. Images of the mesh and the boundary conditions are shown in Figures 3.4 and 3.5.

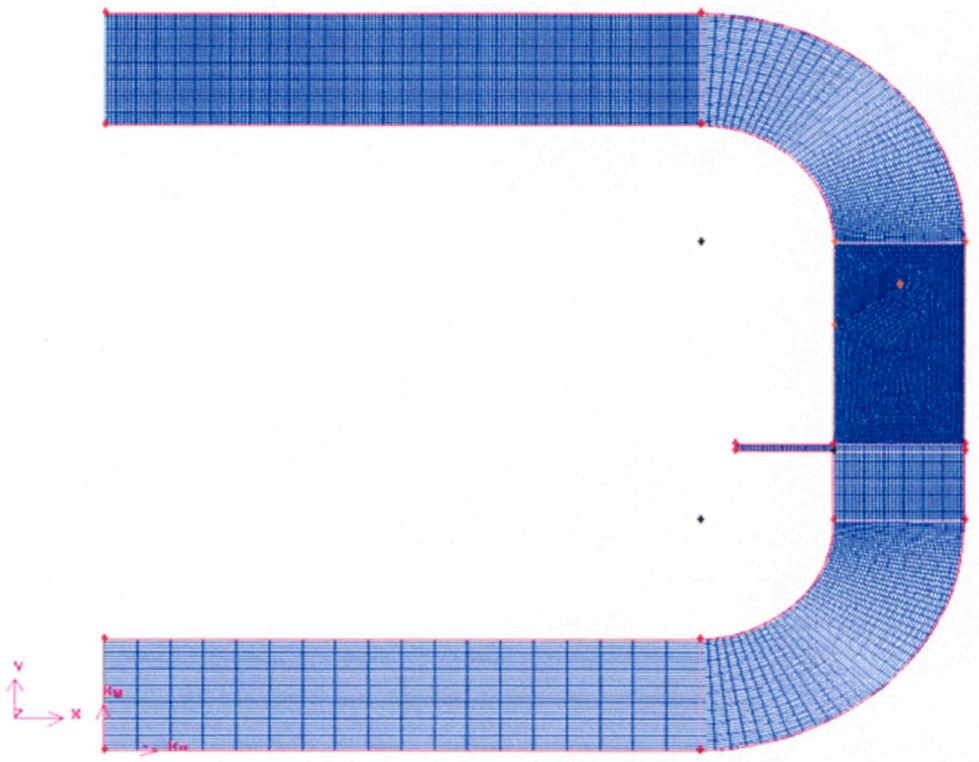

Figure3.4: mesh in case (b)

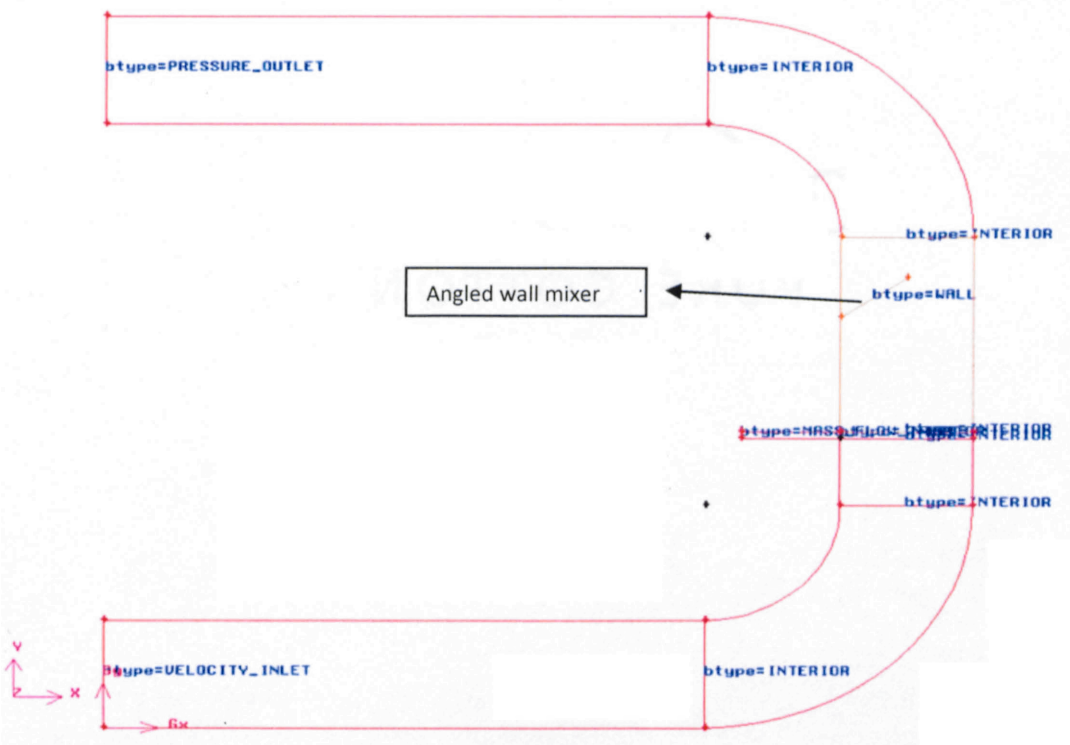

Figure 3.5: boundary condition in case (b)

A third case incorporates a one inch horizontal wall located five inches down-stream of the ammonia injector and equally spaced from both the ends of the wall of the reactor. A quad map scheme was used throughout the model for meshing. The total number of elements is approximately 14,000. Images of the mesh and the boundary conditions are shown Figures 3.6 and 3.7. A sizing function was used to mesh the two 90° bends.

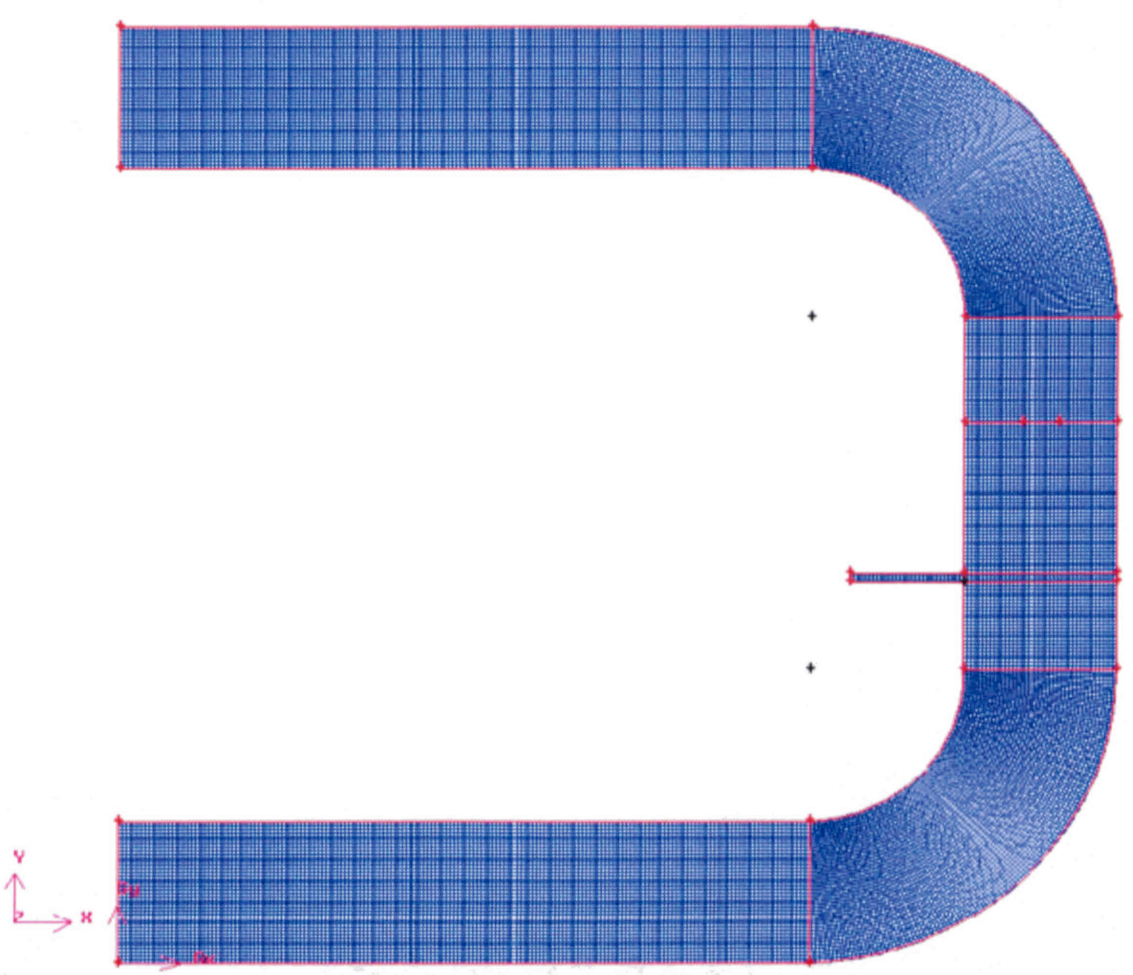

Figure 3.6: mesh in case (c)

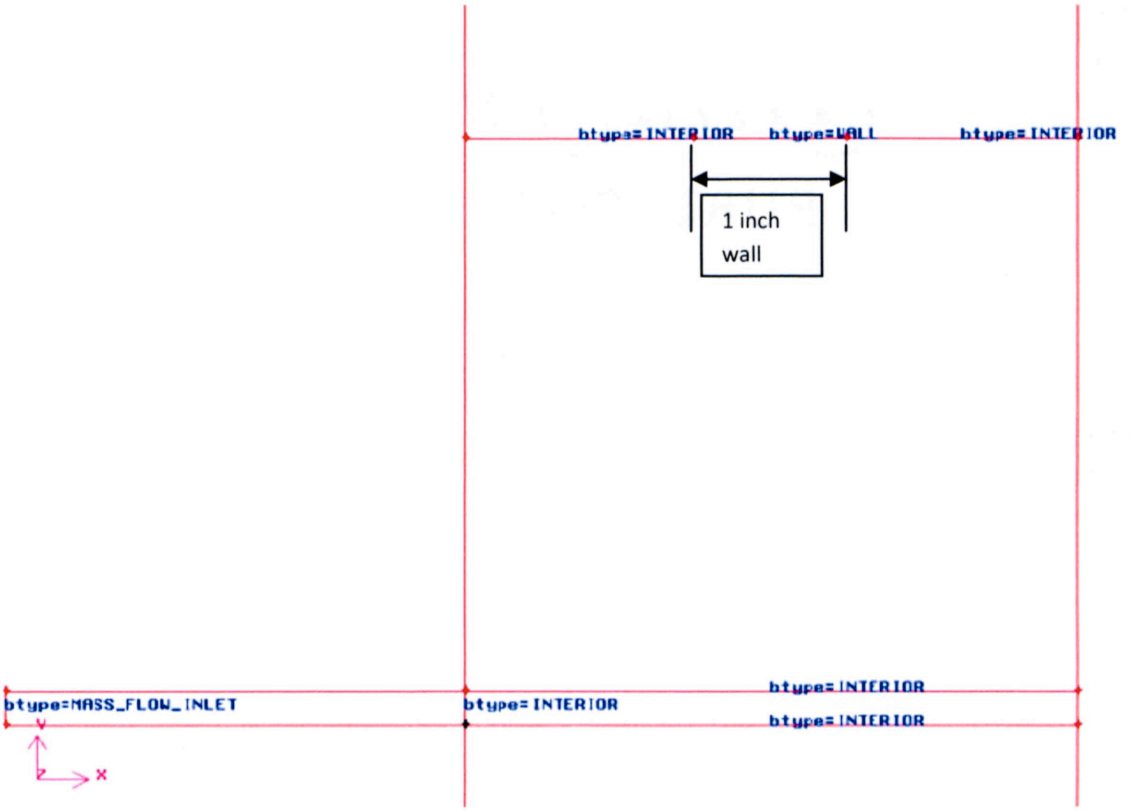

Figure 3.7: boundary conditions in case (c)

The models were imposed to be analyzed under a set of boundary conditions, which were chosen based experimental data. A velocity inlet for the exhaust gas flow, a mass flow rate for the ammonia (re-agent) and a pressure outlet for the overall flow was selected for the *FLUENT* analysis. For *FLUENT* analysis, in case of all other 2-d models, the same constraints were imposed. Baseline data (various parameters such as volumetric flow rates, mass flow rates, pressures and temperatures) was collected for the SCR system using five different catalysts (based on the donor) tested through a range of operating conditions. Data measured for a typical case was taken for *FLUENT* analysis.

3.3 *FLUENT* Analysis:

In conducting *FLUENT* analysis, certain assumptions necessary for the simplification of problem solving, while maintaining a consistency with test data and actual hardware, were made. The exhaust gas composition was assumed to have Nitrogen (N_2), Oxygen (O_2), Carbon dioxide (CO_2) and Water (H_2O). Concentrations of the assumed gases in the exhaust were extracted from the baseline data that was recorded using different catalysts in the SCR catalyst housing separately. The exhaust gas from the engine was passed through a 5-gas analyzer (O_2, CO_2, NO_x, THC and CO) and a Fourier Transform Infrared Spectrometer (FTIR). This data was used to estimate the exhaust gas concentrations. O_2 was analyzed by a 5-gas rack analyzer, while CO_2 and H_2O were analyzed by an FTIR system. N_2 was calculated assuming the remaining gas was N_2 (N_2 balance). The 5-gas rack analyzer measures the concentration in dry and hence needed to be converted to wet in order to calculate the mole fractions and thereby mass fractions, which *FLUENT* utilizes. The FTIR measures concentrations in raw (wet) parts per million (ppm). This can be converted into mole fraction, thereby mass fraction. Other information such as density, specific heat, thermal conductivity and kinematic viscosity were taken from the *FLUENT* library. Additionally, outlet mass fractions of the exhaust gases were calculated based on the ammonia mass flow rate.

If $m_{dot\text{-}exit}$ = mass flow rate at the exit

$m_{dot\text{-}inlet}$= mass flow rate at the inlet

$m_{dot\text{-}NH3}$= mass flow rate of ammonia

$m_{dot\text{-}exit(i)}$=mass flow rate of species 'i' at exit

$m_{dot\text{-}inlet(i)}$=mass flow rate of species 'i' at inlet

$Y_{(i)\text{-}inlet}$=mass fraction of species 'i' at inlet

$Y_{(i)\text{-}exit}$=mass fraction of species 'i' at exit

- $m_{dot\text{-}exit} = m_{dot\text{-}inlet} + m_{dot\text{-}NH3}$
- $m_{dot\text{-}exit(i)} = Y_{(i)\text{-}inlet} * m_{dot\text{-}inlet(i)}$
- $m_{dot\text{-}exit(i)} = m_{dot\text{-}inlet(i)} = (Y_{(i)\text{-}exit}) * m_{dot\text{-}exit}$
- $m_{dot\text{-}inlet(i)} = Y_{(i)\text{-}inlet} * m_{dot\text{-}NH3}$

From the above,

- $Y_{(i)\text{-}exit} = (m_{dot\text{-}inlet(i)} / m_{dot\text{-}exhaust})$

From the baseline testing data in the laboratory, the following was extracted:

- Inlet conditions:

  Average velocity of exhaust gas = 14.29 m/s

  Mass Flow rate = 0.094 kg/s

  Average temperature = 572 K

- Outlet conditions:

  Average exhaust gauge pressure = 0.99 psig = 6825.8 Pag

  Average temperature = 572 K

- Re-agent (Ammonia) Injection:

  Average ammonia flow = 595 ml/min ~ 6.743E-6 kg/s

  Injected @ Standard Temperature and Pressure (STP)

Case (a): Ammonia injection with no down-stream mixer

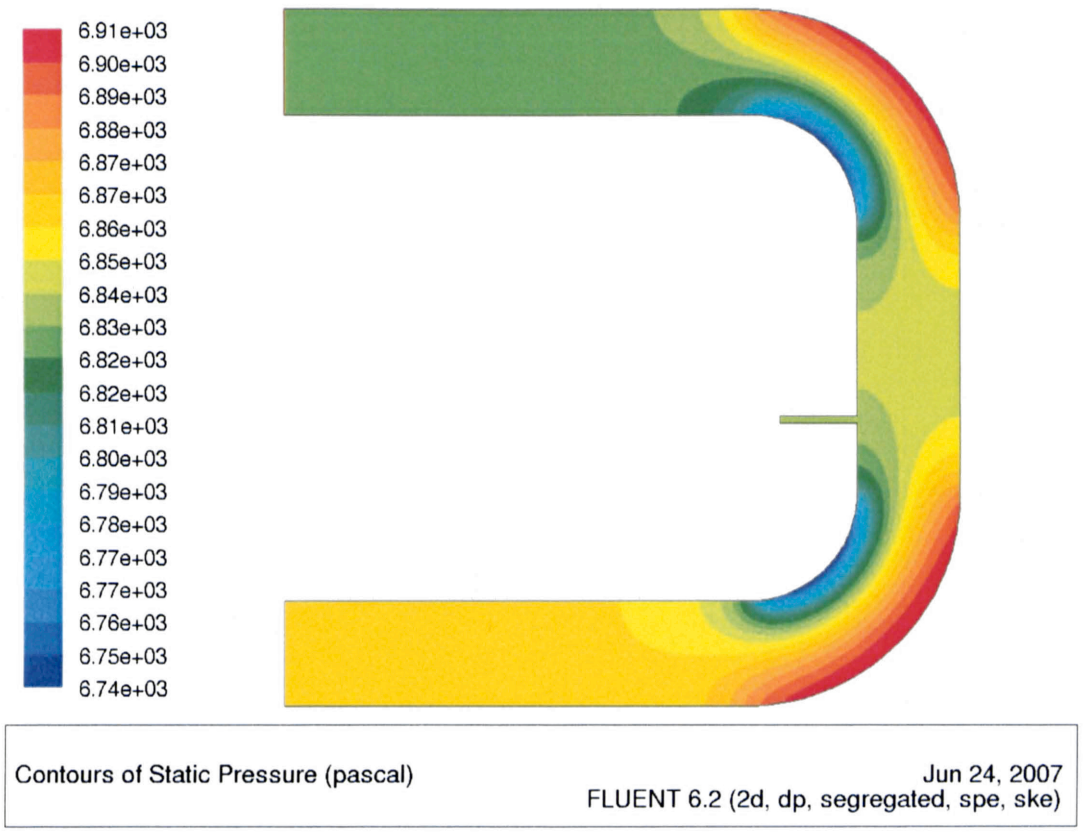

Figure 3.8: contours of static pressure in case (a)

Figure 3.8 depicts the static pressure contours for case (a). The average exhaust gauge pressure was determined from experimental data. This pressure was applied as the outlet pressure and was approximately 0.99 pounds per square inch gage (psig), or 6830 Pascals gage (Pag). *FLUENT* automatically calculated the inlet pressure for the given exhaust flow velocity and ammonia mass inflow rate. An inlet pressure of about 6740 Pag is evidenced. As expected, regions of high pressure can be observed at the outer walls of the two 90° bends, while regions of low pressure can be observed close to the inner walls of the bends.

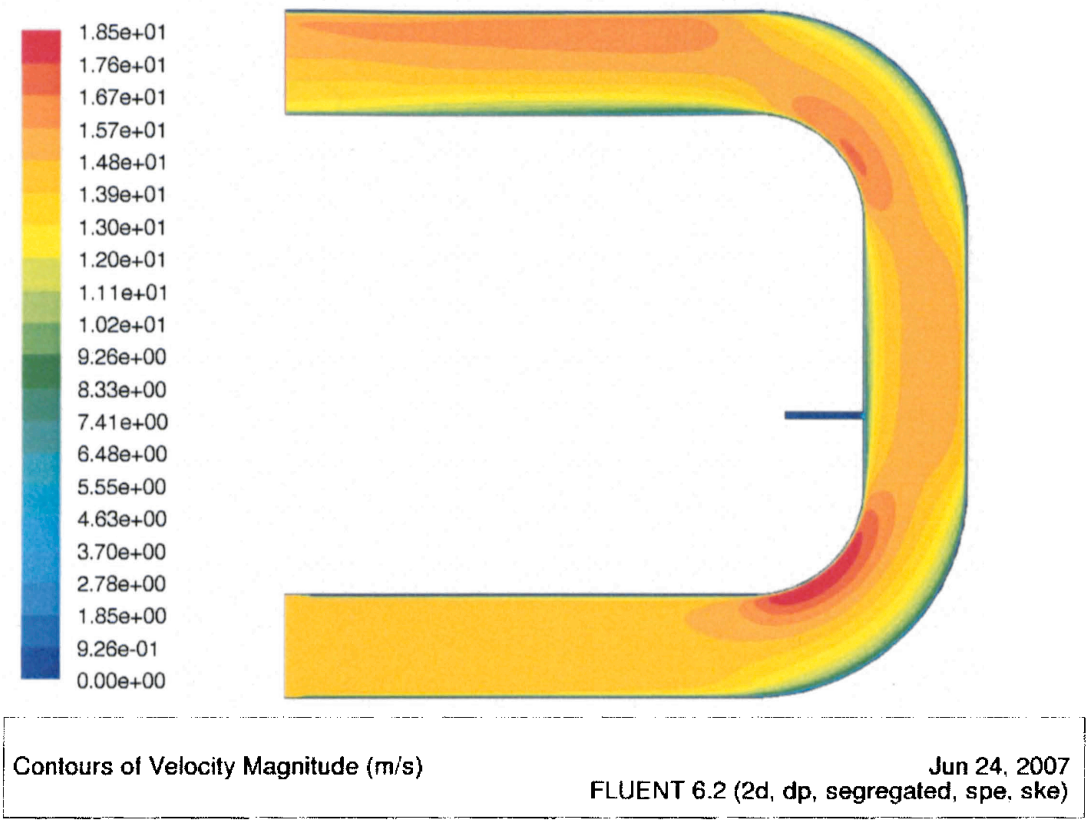

Figure 3.9: contours of velocity magnitude in case (a)

Contours of velocity magnitude can be seen in Figure 3.9. Normally, we would expect velocity to maximize at regions where pressure is lowest. However, it can be observed that the velocity is highest near the first 90° bend but is different at the second bend. This is due to the difference in total pressure before and after the first bend. There is a slight loss due to the wall friction and also the boundary layer separation after the first bend. The same can be expected after the second bend. The velocity inside the ammonia injector cannot be seen in this range as it is injected at very low speeds when compared with the exhaust gas. It can also be observed that there is a thickening in

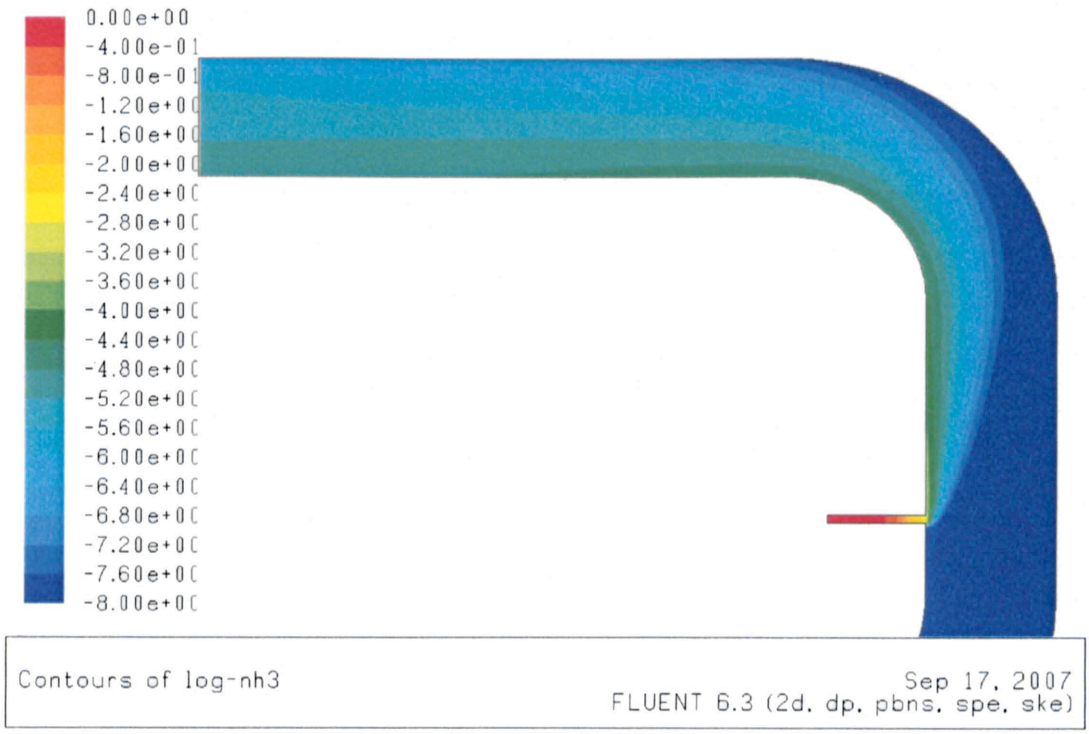

Figure 3.10: contours of $\log_{10}$ mass fractions of NH_3 in case (a)

boundary layer attached to the inner wall of the reactor, which quickly thins down. This is due to the injection of ammonia.

Figure 3.10 depicts contours of the logarithmic plots of the mass fractions of ammonia. Logarithmic plots have been chosen to show the entire contour in one single range. *FLUENT* also produces indistinguishable color artifacts when plotting different ranges for the mass fractions of ammonia. It is seen that the ammonia sticks to the inner wall of the pipe. This happens due to the very low velocity injection of ammonia in comparison with the exhaust gases. The flow, almost completely, sticks to the wall. Figure 3.10 shows that the stratification of ammonia across the outlet wall ranges from $10^{-6.2}$ to $10^{-5.2}$ mass fractions. There is a ten factor difference seen in the stratification.

Case (b): Ammonia injection with angled down-stream mixer

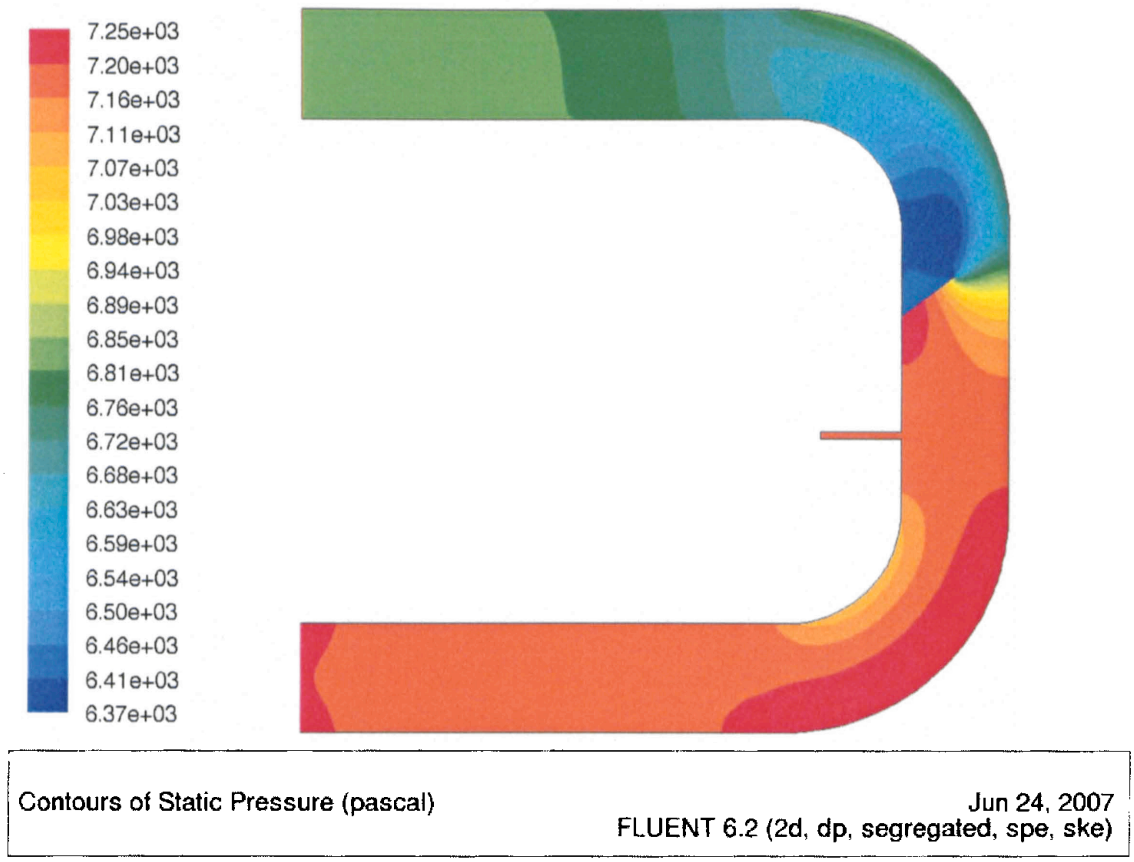

Figure 3.11: contours of static pressure in case (b)

The motivation to run this case is to compute the flow stream at the introduction of a wall downstream of the ammonia injector. It is obvious from Figure 3.11 that there is a definite change in the flow stream. High pressures are seen all the way up until the flow is obstructed by the angled wall (mixer) and then a region of low pressure can be seen right behind the mixer. As with case (a), highest pressure is observed at the first 90° bend's outer wall. However, no low pressure is seen at the inner wall of the first bend. This is due to the shape and location of the mixer, which is attached to the inner wall of the reactor. Pressure increases in regions towards the inner wall.

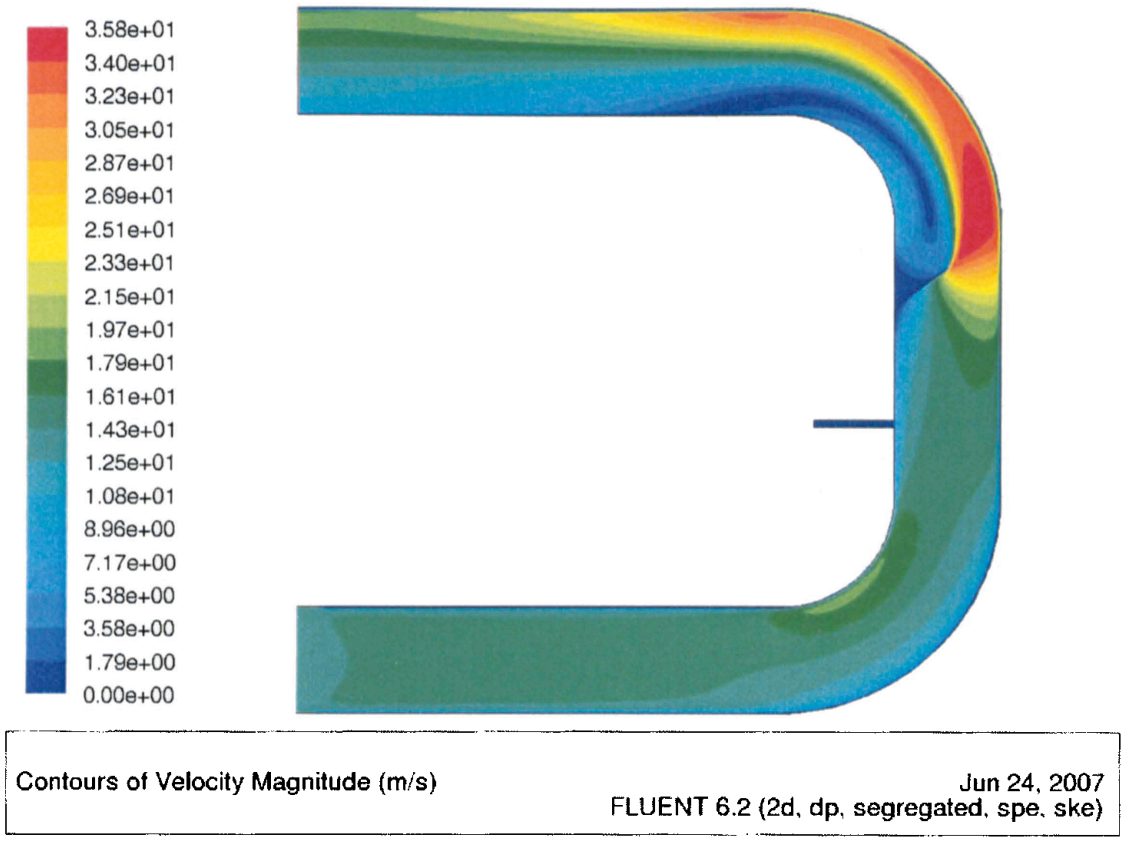

Figure 3.12: contours of velocity magnitude in case (b)

Figure 3.12 shows velocity contours colored by velocity magnitude. It can be observed that the flow moves with greater velocity at the inner wall of first bend than the outer layers due the pressure increase at the first bend outward from the inner wall. The inclusion of the angled wall downstream of the ammonia injector induces the flow to go around it and induces mixing. The exhaust gas and ammonia mixture is forced around the end of the angled wall, creating a high velocity region. The region in red, in Figure 3.12, shows areas of maximum velocity reaching approximately 35 m/s. The flow then flows along the outer wall after being diverted by the mixer and slowly disperses downstream.

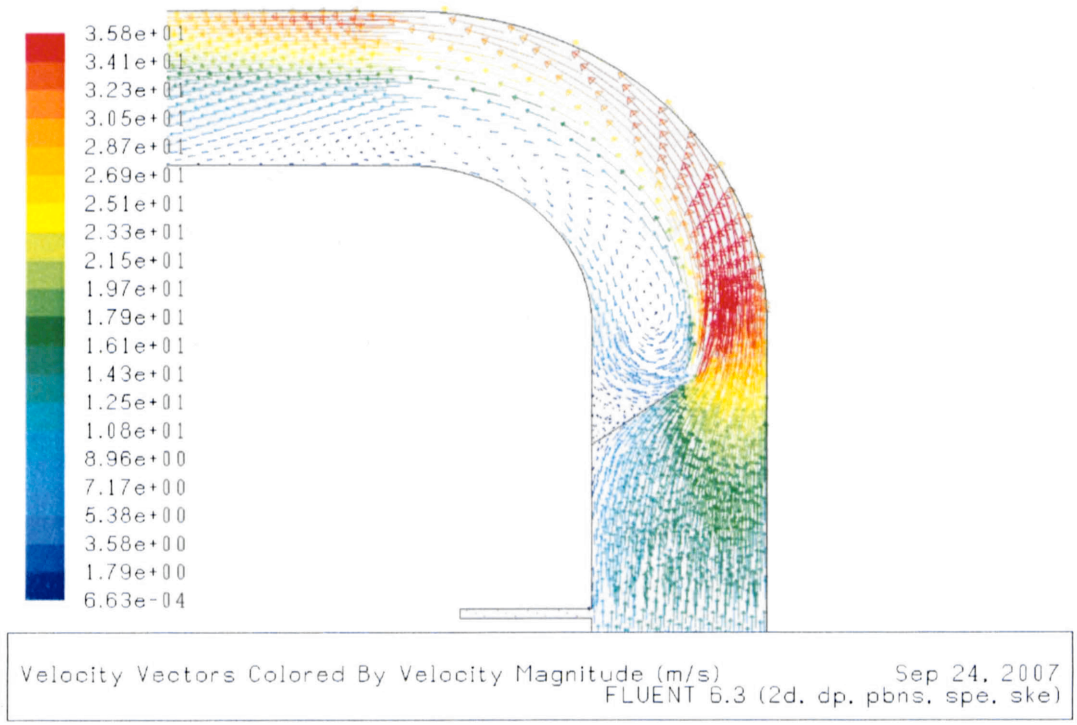

Figure 3.13: contours of velocity vectors in case (b)

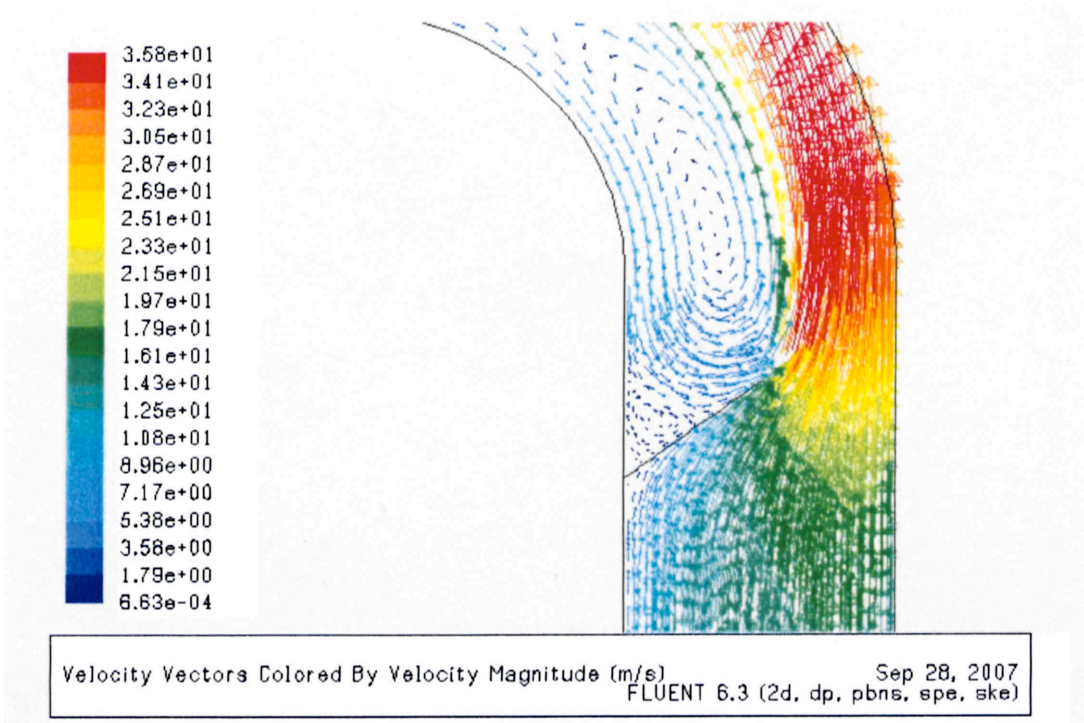

Figure 3.14: contours of velocity vectors (zoomed) in case (b)

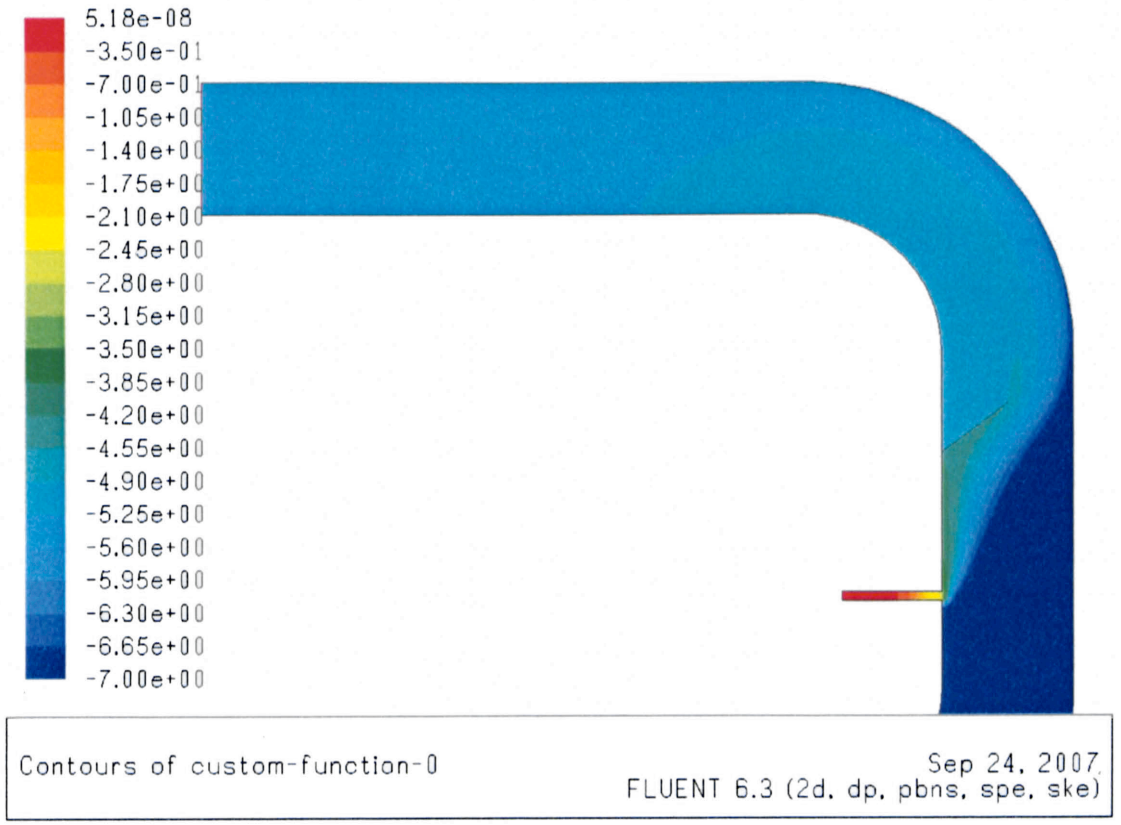

Figure 3.15: contours of $\log_{10}$ mass fractions of NH_3 in case (b)

Figures 3.13 and 3.14 show the velocity vectors colored by the velocity magnitude of the flow. Localized eddies can be seen behind the mixer. This suggests that there is a significant amount of turbulence introduced by the mixer

Figure 3.15 shows contours of the mass fractions of ammonia on a logarithmic basis. The plot suggests that there is a very effective mixing at the outlet. We can attribute this to the presence of the mixer. The concentrations at the outlet were computed in the range of $10^{-5.3}$ to 10^{-5}. This strengthens the argument of the use of a mixer downstream of re-agent injection.

Case (c): Ammonia injection with central wall down-stream mixer

In this case, a variation in the orientation of the mixer was modeled to examine the effect on flow and mixing. A central wall that is about one inch in length and equidistant from both the walls of the pipe was created downstream of the ammonia injector. The mixer is about five inches downstream of the ammonia injector.

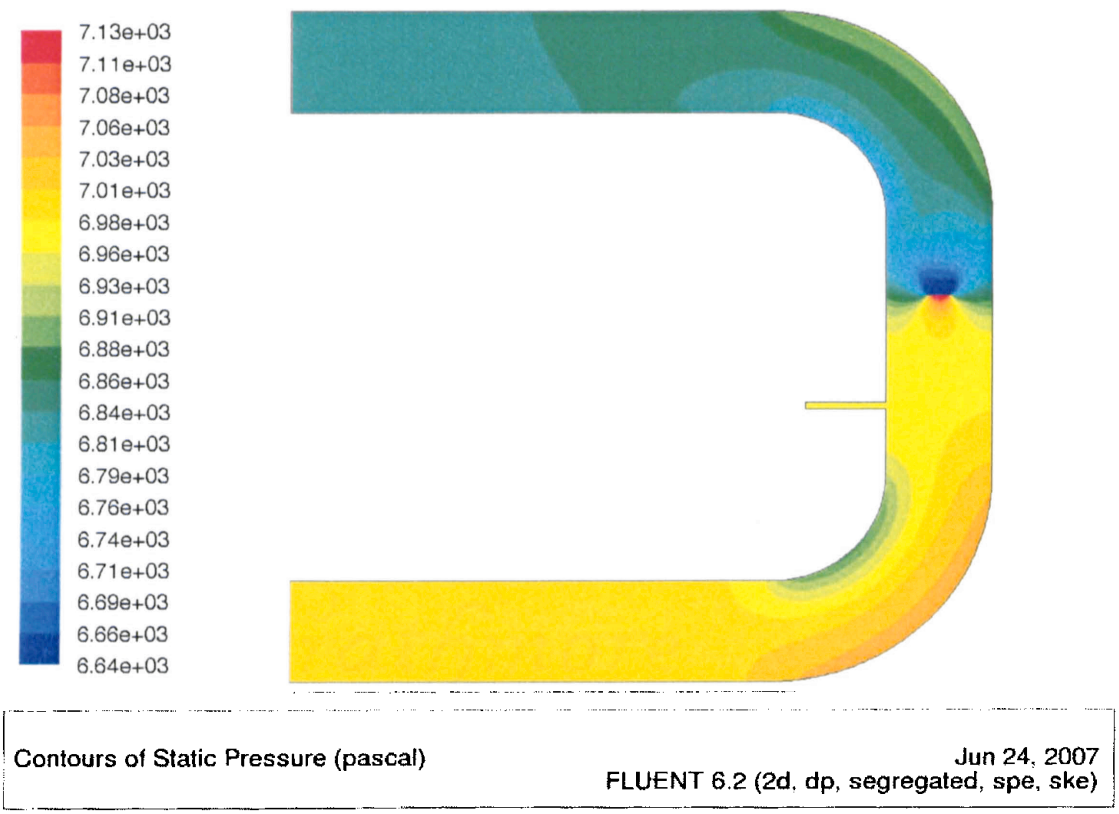

Figure 3.16: contours of static pressure in case (c)

Figure 3.16 represents pressure contours of the case in discussion. Higher pressures are noted just upstream of central wall mixer. The flow passes through the first bend with lower pressures at the inner wall and greater pressures at the outer bend. Just downstream of the mixer is a region of low pressure, which increases by about 20 Pa

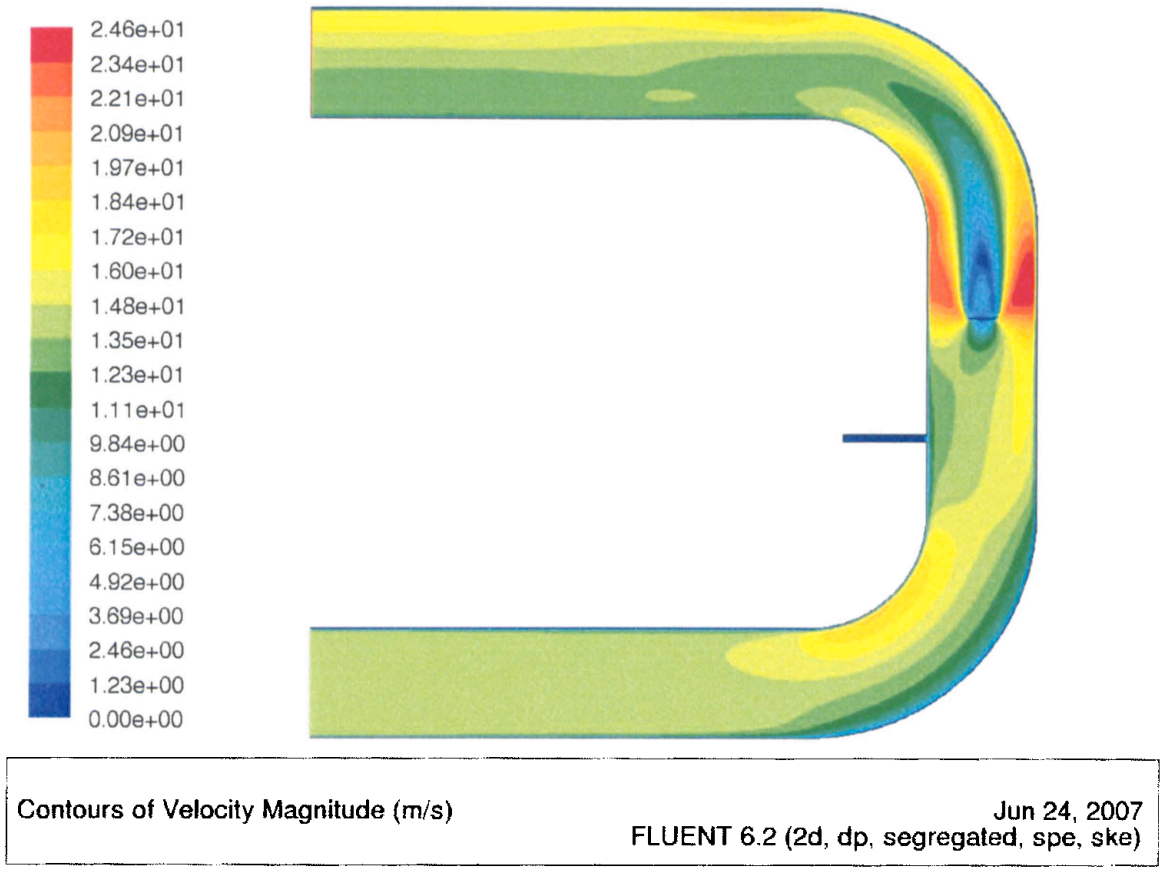

Figure 3.17: contours of velocity magnitude in case (c)

radially outward. This is due to the flow of the exhaust and ammonia mixture around the central wall that is concentrated towards the walls of the reactor.

The velocity contours suggest that there is a maximum velocity on either side of the central wall slightly downstream of the mixer. It is observed that velocities are very low just behind (downstream) the mixer. Due to the immediate bend in the pipe downstream of the mixer, there is a higher velocity observed towards the outer wall close to the outlet. The flow is pushed towards the outer wall as it tends to separate slightly from the inner wall of the second bend. The contours for velocity vectors are shown in Fig 3.18. Flow recirculation can be observed just downstream of the mixer. Two eddies

can be seen on either side of the mixer after deviating from the mixer. This causes turbulence in the flow. The eddies develop elliptically and their velocities add to the neighboring layers, thereby increasing the velocity magnitudes of the layers of flow on either side of the mixer.

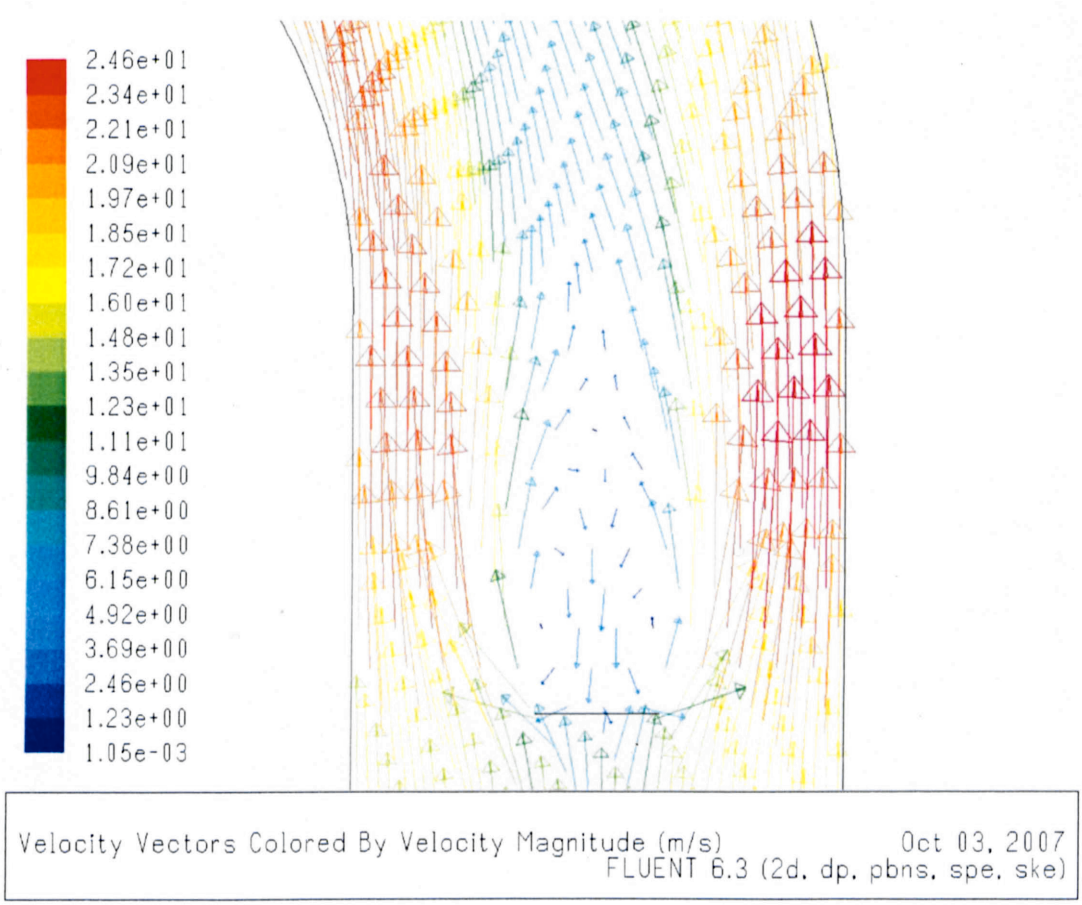

Figure 3.18: contours of velocity vectors in case (c)

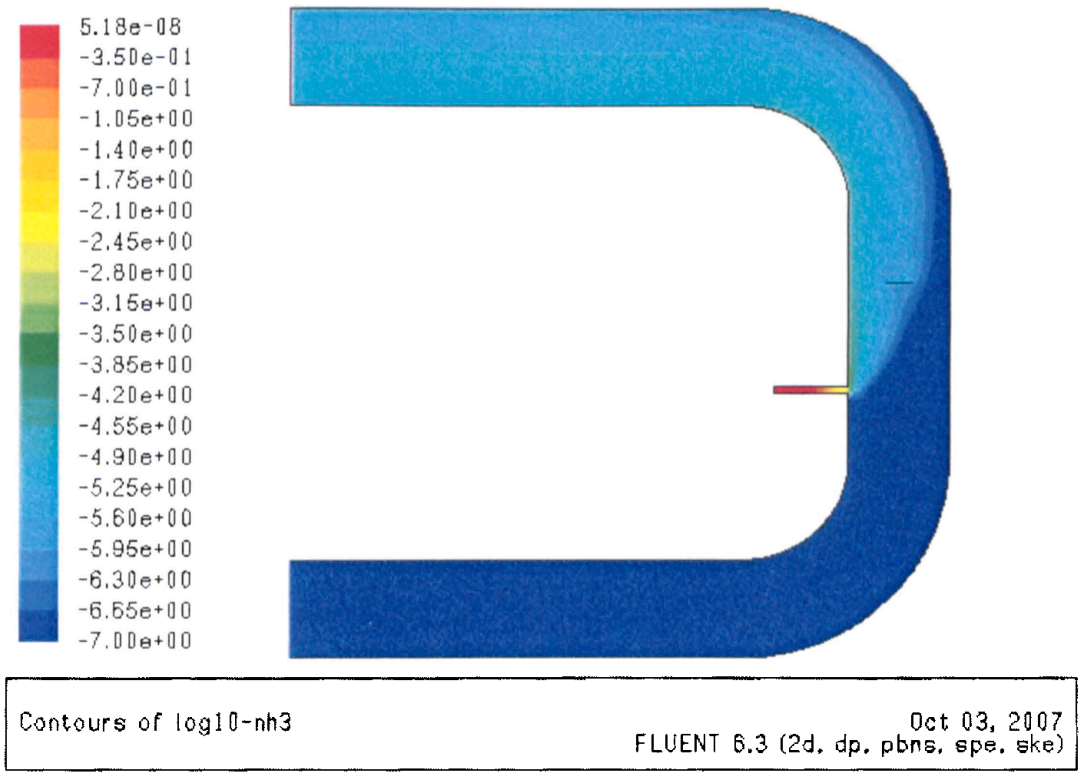

Figure 3.19: contours of $\log_{10}$ mass fractions of NH_3 in case (c)

Figure 3.19 shows us the contours of the ammonia mass fraction on a logarithmic basis. The results show there is effective mixing induced by the central mixer. The mass fractions range from about $10^{-5.6}$ to 10^{-5} at the exit section. Therefore, there is effective mixing at the outlet and the ammonia distribution is relatively uniform. Perhaps, mixing could be improved by increasing the length of the central mixer. However, the analysis of 2-D cases has been stopped at this point. The analysis of 3-dimensional cases began as it replicated the system more accurately.

Chapter 4: NUMERICAL SOLUTION (3-D MODEL)

4.1 Motivation:

The three different models analyzed in 2-D shows us the flow characteristics without and with different shapes of mixers downstream of the reagent injection. The 2-D analysis suggests that turbulence can be induced using a flow obstruction to see a uniformity in the reagent at catalyst inlet using *FLUENT*. Hence, a 3-D model was constructed to analyze the flow. Some simplifications to the fluent analysis were implemented based on the 2-D analysis. For example, the pressure outlet condition was changed to outflow, the density was set to volume-weighted-mixing law to eliminate the usage of energy equation, thereby reducing the iteration time.

4.2 Modeling:

A 3-d model was created in *GAMBIT*. An expansion in the model towards the outlet was created. The expansion from the circular pipe of four inches diameter to the square pipe six inches in diameter was modeled to include more hardware features. The mixing uniformity will be measured by utilizing a traversing probe in the square piping just upstream of the SCR catalyst bricks. The ammonia injection system is about 2.5 inches downstream of the first 90° bend. The injection tube is a relatively simple design. It is constructed of a 0.5 inch diameter transport tube that is operated at Standard Liters per Minute (SLM) from the ammonia storage tank to injection point. The tube protrudes into the exhaust flow, with the tube axis orthogonal to the flow, terminating at the pipe centre. The end of the tube is plugged. The re-agent flows out a radial orifice in the tube in the direction of the exhaust flow.

The effect of mixing for four different cases was studied. The first case was ammonia injection at the centre of the reactor section with the injecting orifice facing the direction of the flow. Just downstream of this injector is two 'D' shaped mixers that are at right angles to each other. In the second case, this mixer was removed with the injector orifice remaining at the centre. In the third case, the injector tube was cut at the wall of the reactor and the mixer was placed downstream of the injection location. In the fourth case, the mixer was removed and injection was the same as the third case. Results of all four cases were analyzed to compare the mixing uniformity.

It is clear from Figure 4.1 that the injector tube extends into the reactor section of the model and the injection orifice faces the direction of the exhaust gas flow.

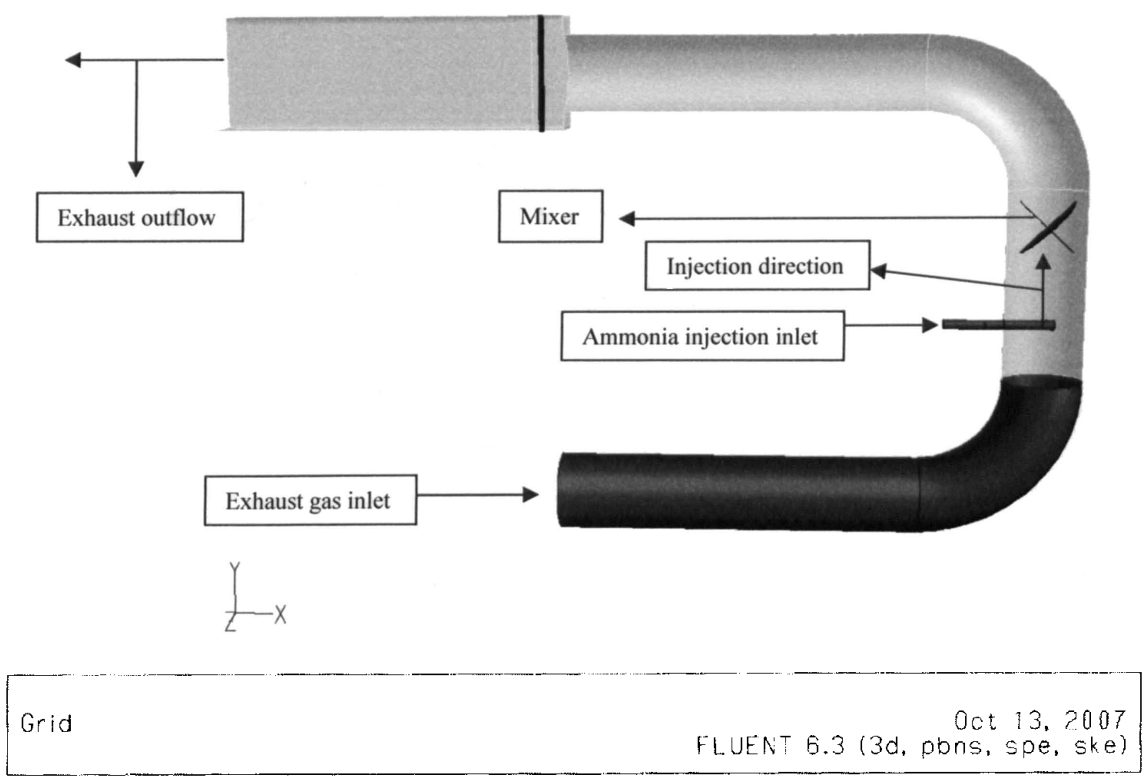

Figure 4.1: Central injection with downstream mixer

Downstream of this injector tube are a two 'D' shaped plates (mixer) welded to each other at right angles. A vertical cylinder, to model the exhaust gas flow around a sample probe, has been included in the extended square section. The mesh created was made very fine inside the ammonia injector tube and in the vicinity of the orifice through which ammonia is released. The meshes were mapped between the outer wall of the injector tube section inside the reactor and the inner wall of the reactor such that it grows coarser away from the injector tube. This way a uniform mesh with concentration around the injector tube could be obtained. Approximately, 240,000 cells were created from the mesh. A tetrahedral - hybrid element with a T-Grid type element was chosen for meshing the model. The boundary conditions for this case remained mostly similar to that of the 2-d case except that the outlet surface was changed from the circular pipe exit to the square pipe exit. The part of the injector tube that penetrates through the reactor, the mixer and the probe were called 'wall' in *Fluent* so these parts would be treated as an obstruction in the flow similar to the physical process. The rest of those surfaces inside the model were called as 'interior' so the flow could go through those surfaces.

Figure 4.2 depicts the model created in *Gambit* of case (b). In case (b), the mixer downstream of the injector tube was eliminated but the injection tube still injects at the centre of the reactor. However, the rest of the parameters such as the total number of mesh elements, the boundary conditions, the type of mesh and the mesh concentrations around different sections of the model were all kept same.

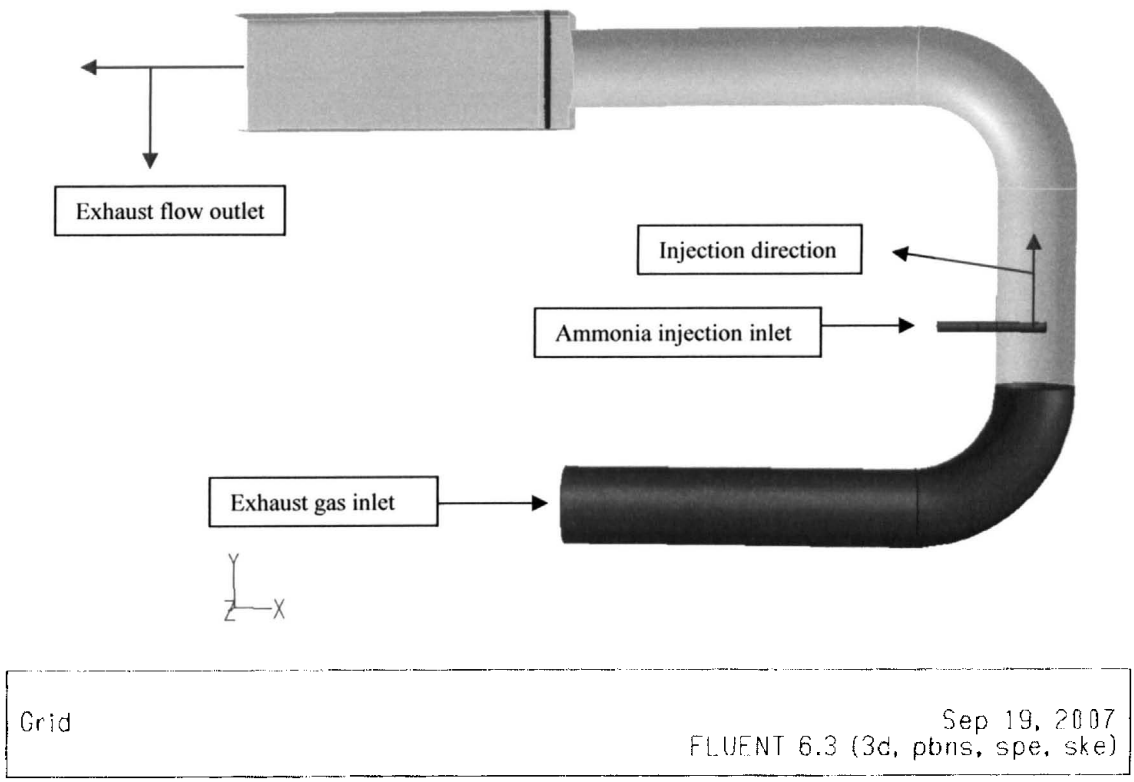

Figure 4.2: Central Injection without downstream mixer

In case (c), the injector tube was cut off at the point where it enters the reactor section so that it will inject ammonia at the wall rather than at the centre as in case (a) and (b). The two 'D' shaped mixers were utilized in this case to see how the flow and mixing would behave with ammonia injection at the wall. About 200,000 elements were created from the mesh. A tetrahedral - hybrid element with a T-Grid type element was chosen for meshing the model. The boundary conditions for this case remained similar to that of the 2-D case except that the outlet surface was changed from the circular pipe exit to the square pipe exit. The mixer and the probe were called 'wall' so the flow would go

around the tube. The injector section that penetrates through the reactor, in this case, is not present. Hence, the surface of intersection between the injector and the reactor was

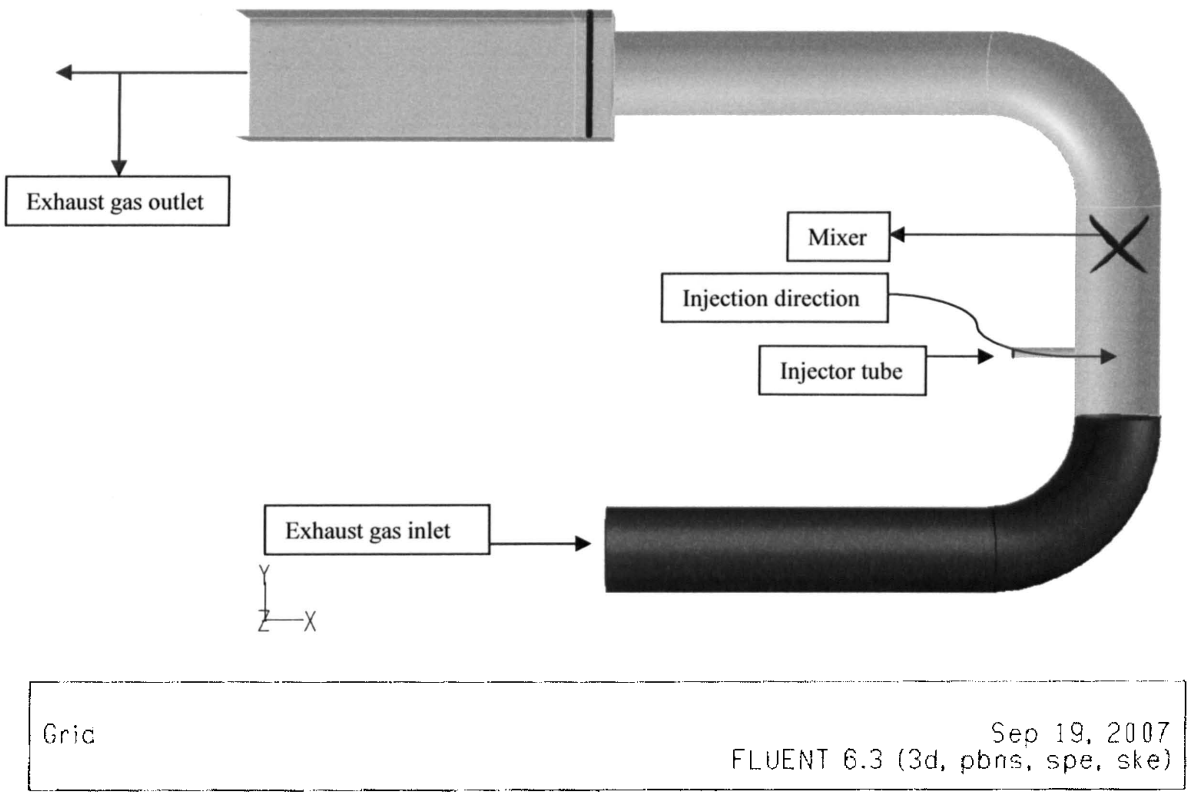

Figure 4.3: Wall Injection with downstream mixer

called 'interior' and ammonia was injected though this surface. The rest of the surfaces inside the model were called as 'interior' so the flow could go through those surfaces.

In case (d), the mixer downstream of the ammonia injection was removed with injection remaining at the wall. Similar boundary conditions were applied as in case (c), except that the mixer is removed. Parameters such as the total number of mesh elements, the boundary conditions, the type of mesh and the mesh concentrations around different sections of the model were kept same. Approximately 200,000 elements were created

using a Tetrahedral Hybrid element. A T-grid type mesh was used in creating the mesh. Like in cases (a), (b) and (c), a probe was modeled just outside the circular pipe exit, about one inch inside the square pipe, and upstream of the catalyst bricks.

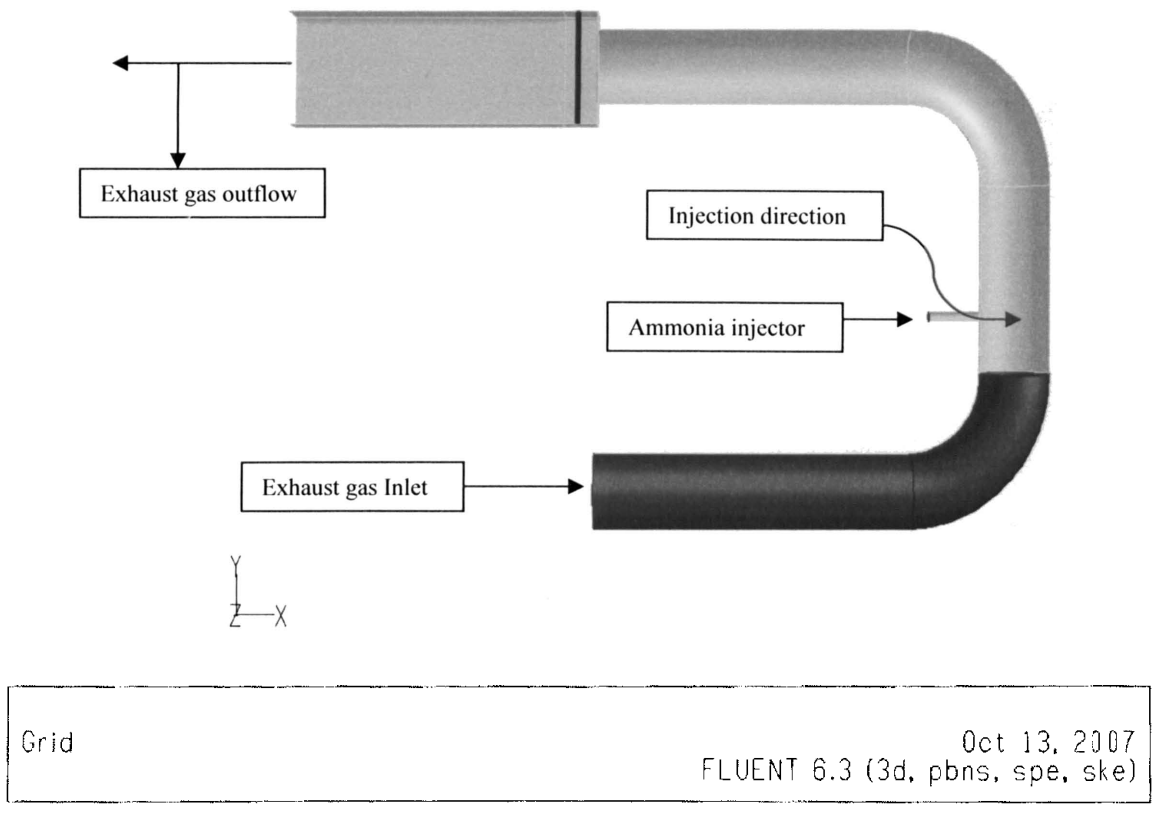

Figure 4.4: Wall Injection without downstream mixer

4.3 *FLUENT* Analysis:

In conducting *FLUENT* analysis, certain assumptions are necessary for the simplification of problem solving, while maintaining a consistency with the physical hardware. The exhaust gas composition was assumed to have Nitrogen (N_2), Oxygen (O_2), Carbon dioxide (CO_2) and Water (H_2O). Concentrations of the assumed gases in the

exhaust were extracted from the experimental data that was recorded using different catalysts in the SCR catalyst housing separately. In the 3-D model, the outlet boundary condition was changed from 'pressure outlet' to 'outflow' to reduce the iteration time. The 'outflow' option simply sets the outlet surface as outflow and does not change the way the solver iterates to obtain the solution. 'Pressure outlet' boundary condition requires the specification of a static (gauge) pressure at the outlet boundary. The rate of ammonia injection for the modeling was based upon experimental data. Experimentally, the ammonia injection rate depends on the exhaust flowrate, NO_x concentration and the desired NH_3/NO_x molar ratio (typically between 0.75 and 0.95).

Case (a): Central Injection with downstream mixer

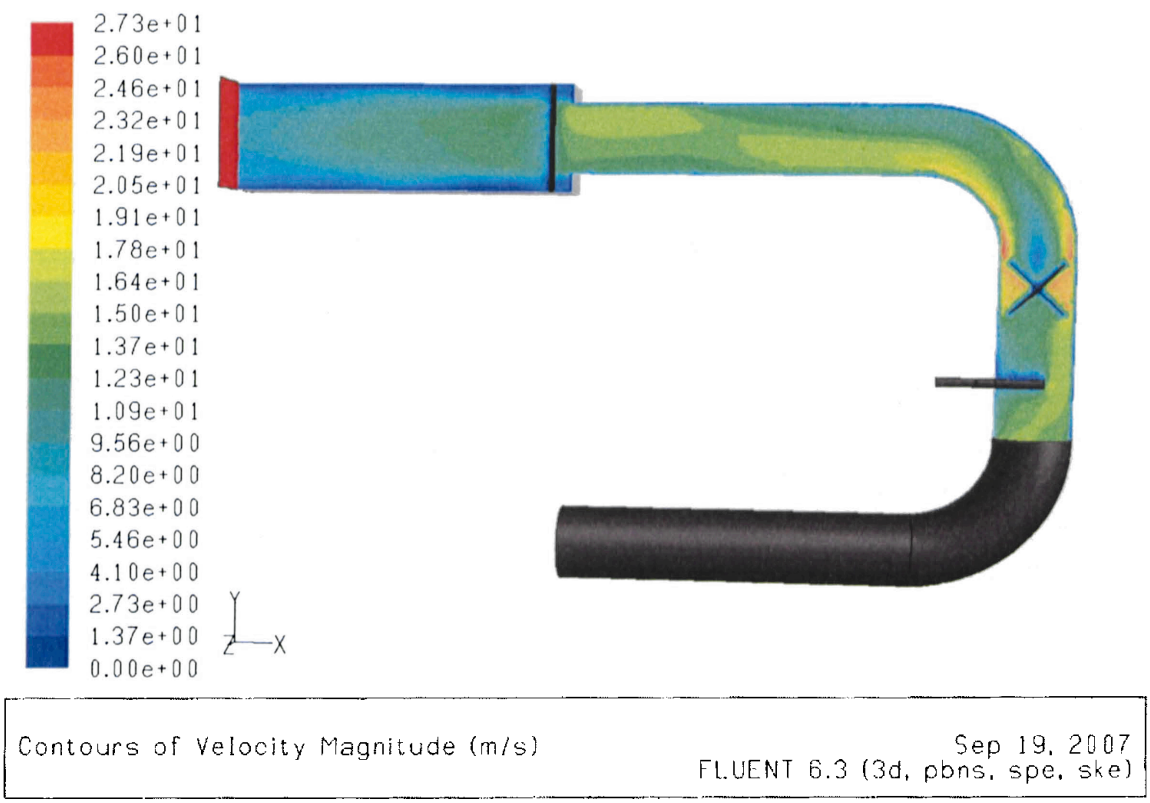

Figure 4.5: Velocity magnitude in the z=0 plane

Figure 4.5 depicts the contours of velocity magnitude through the model at the central plane, z=0. This view was selected so to show the flow pattern around the mixer and the probe in the square tube. Velocity reaches a maximum at the sides of the mixer where most of the flow is diverted. The flow from the inner wall is pushed off the wall as it traverses through the second bend. At the exit section of the circular pipe, which forms the inlet section for the square pipe, there is an expansion due to the increase in flow area and consequently, low velocity magnitudes are seen in the corners at the square pipe entry section. Inside the square pipe, velocity magnitude reduces in the negative X direction. The boundary layer develops down the square pipe.

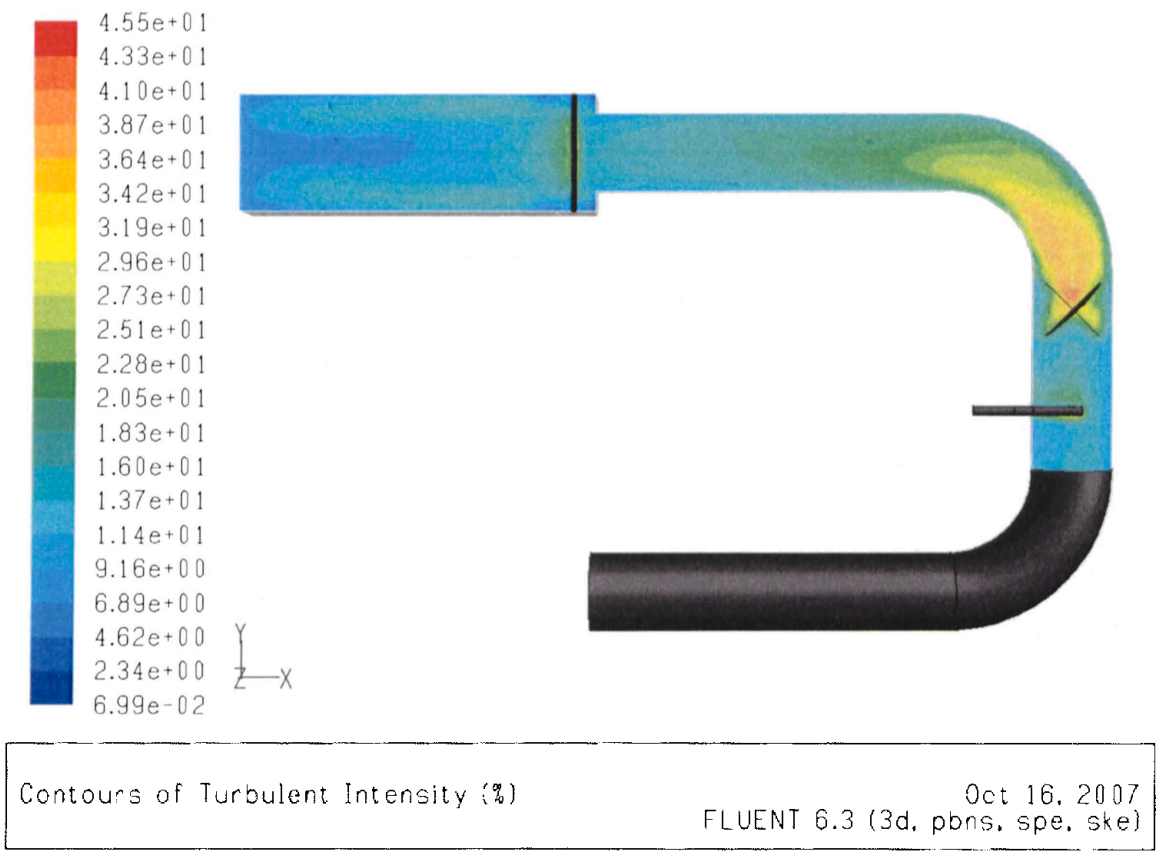

Figure 4.6: Turbulent intensity in the z=0 plane

The turbulence intensity is defined as the ratio of the root means square (RMS) of the turbulent velocity fluctuation to the mean velocity. The RMS velocity can be calculated from the turbulent energy. Typically a high turbulence case corresponds to turbulent intensity between 5 % and 20%. Downstream of the injector, the turbulent intensity is greater than 5% throughout the flow. Highest turbulent intensities are just downstream of the mixer ranging from 30% to 45%. This indicates that the location and shape of the mixer utilized in the study are effective. Just outside the circular pipe exit, where the traversing probe is stationed, the turbulent intensity ranged from 5% at the walls and peaked at the centre to about 16%. As seen in Figure 4.6, a jump in turbulence intensity from about 6% to 21% was observed behind the vertical probe.

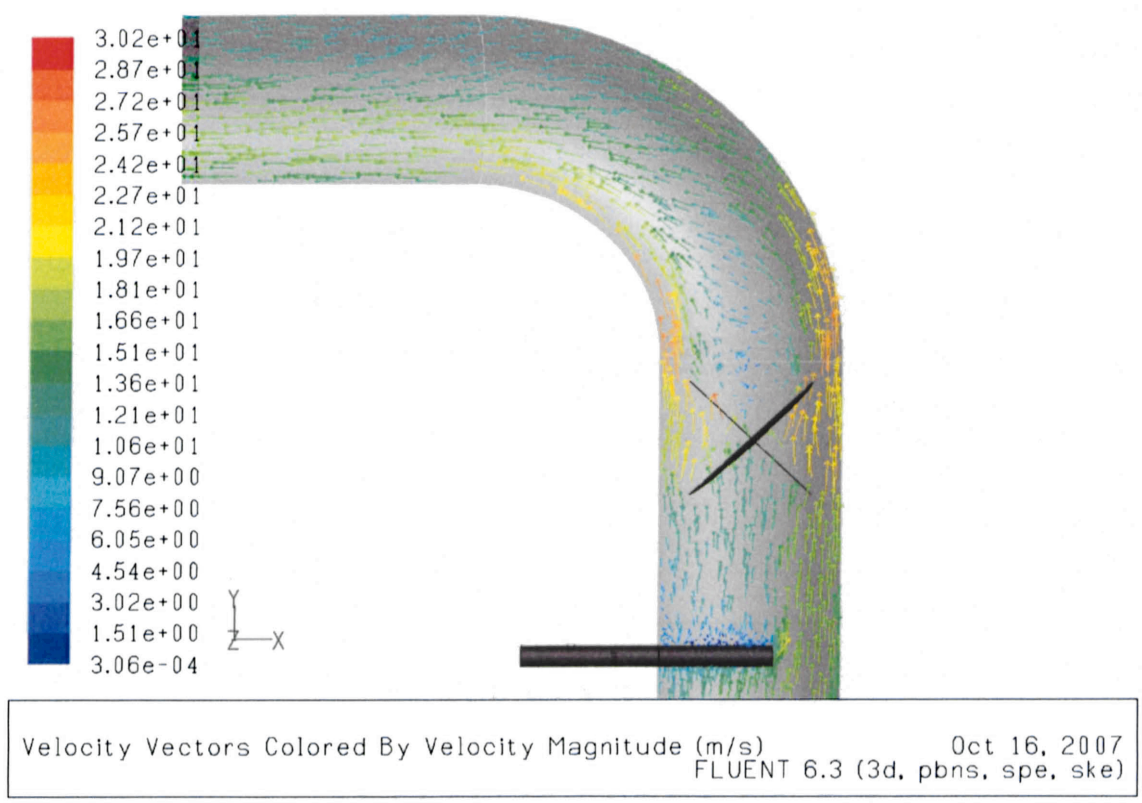

Figure 4.7: Velocity vectors in the z=0 plane

Figure 4.7 depicts the contours of the velocity vectors colored by velocity magnitude. In the z=0 plane, it was observed that the velocity vectors in the layers towards the outer wall were greater in velocity magnitude compared with those towards the inner wall. This was due to the location of the ammonia injector and also as a result of the centrifugal force that the flow undergoes after going through the first bend. The exhaust flow has to go around the injector tube and is then obstructed by the mixer downstream. This mixer forces the flow to go around it and induces turbulence. Localized eddies can be observed just downstream of the mixer, which causes turbulence to grow. Ammonia mass fractions were measured to be in the range of $10^{-4.2}$ to $10^{-4.3}$.

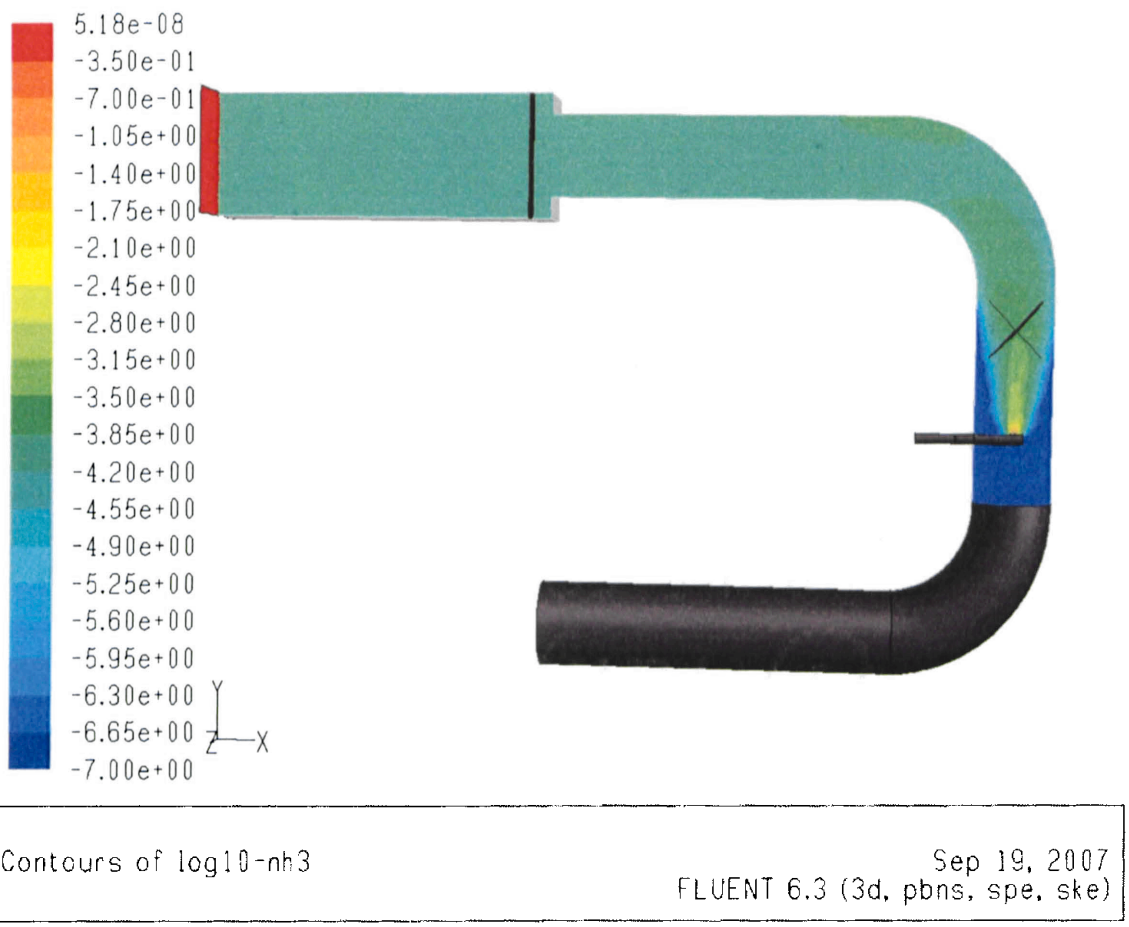

Figure 4.8: Logarithmic Mass fractions of NH_3 in z=0 plane

Logarithmic plots of NH_3 mass fractions are shown to avoid the plotting artifact (blank colorless space in the contour, if the values are out of range) of *FLUENT* when trying to plot the mass fractions ranging from 10^{-7} to 10^{-3}, which are the minimum and maximum mass fractions. Figure 4.8 shows effective mixing of ammonia. Ammonia mass fraction is relatively uniform after the flow interacts with the mixer. At the vertical probe, the mass fractions are in the $10^{-4.2}$ to $10^{-4.5}$ range.

Case (b): Central Injection without downstream mixer

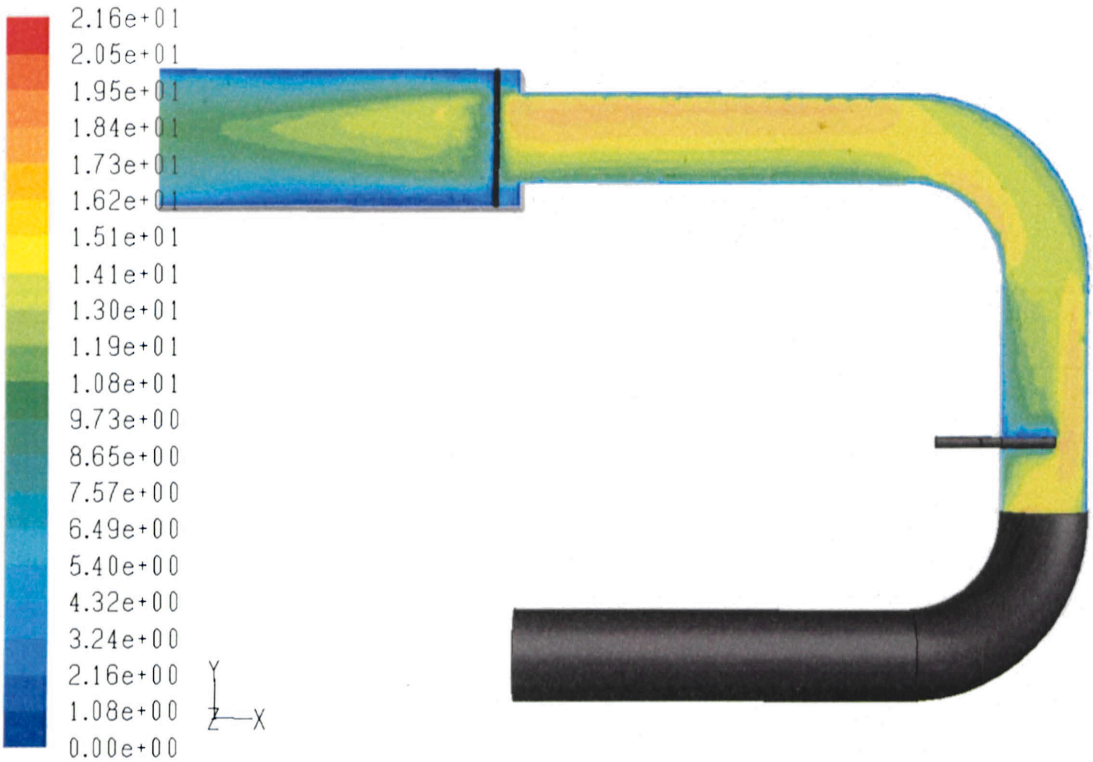

Figure 4.9: Velocity Magnitude in the z=0 plane

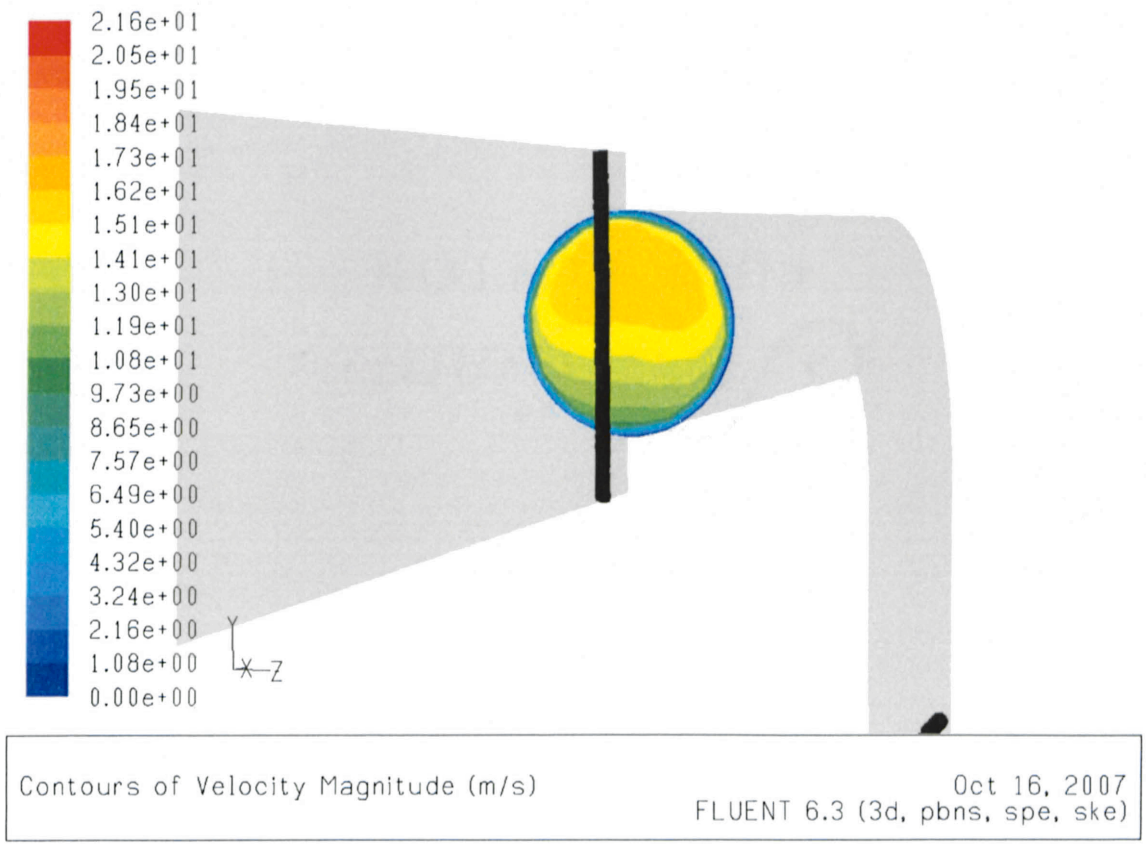

Figure 4.10: Velocity Contours at the exit section of the circular pipe

The effect of removing the mixer is illustrated in case (b), shown in Figures 4.9 to 4.12. Although the injection was at the centre of the reactor, the velocity contours look different from that of case (a). Exhaust gases flow in through the first bend at approximately 14.3 m/s and deviates around the injector tube and concentrate towards the outer walls. The centrifugal force causes the velocity to be greater in the upper layers after the second bend. Velocities range from 9 m/s to 17 m/s.

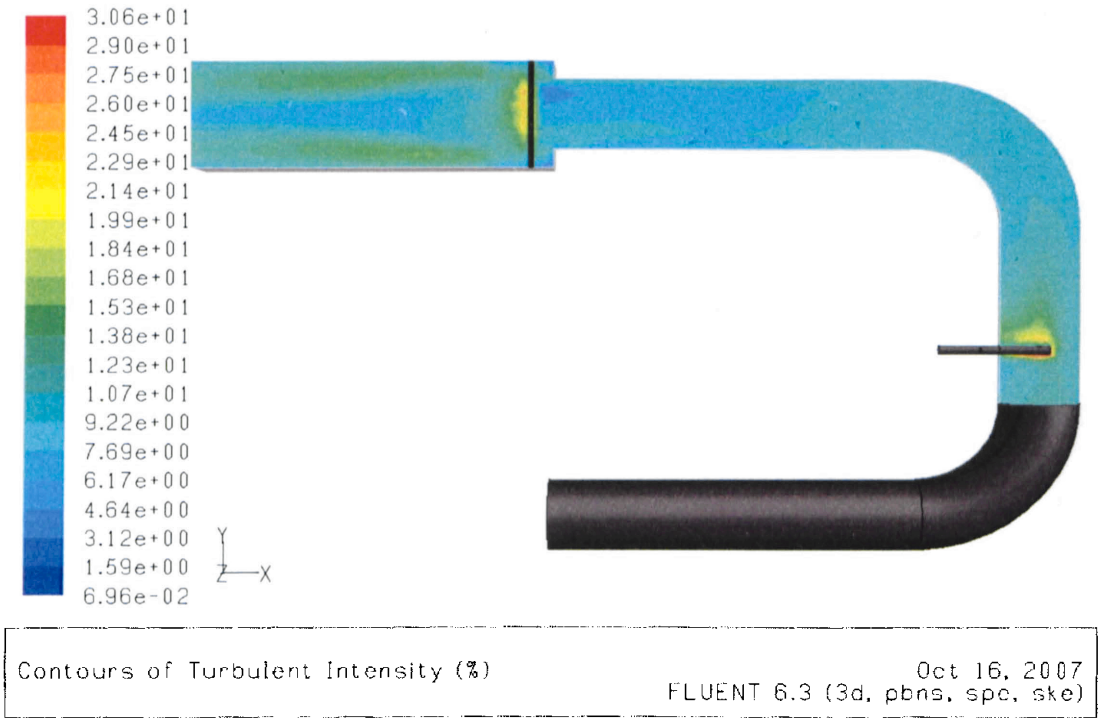

Figure 4.11: Turbulent Intensity in the z=0 plane

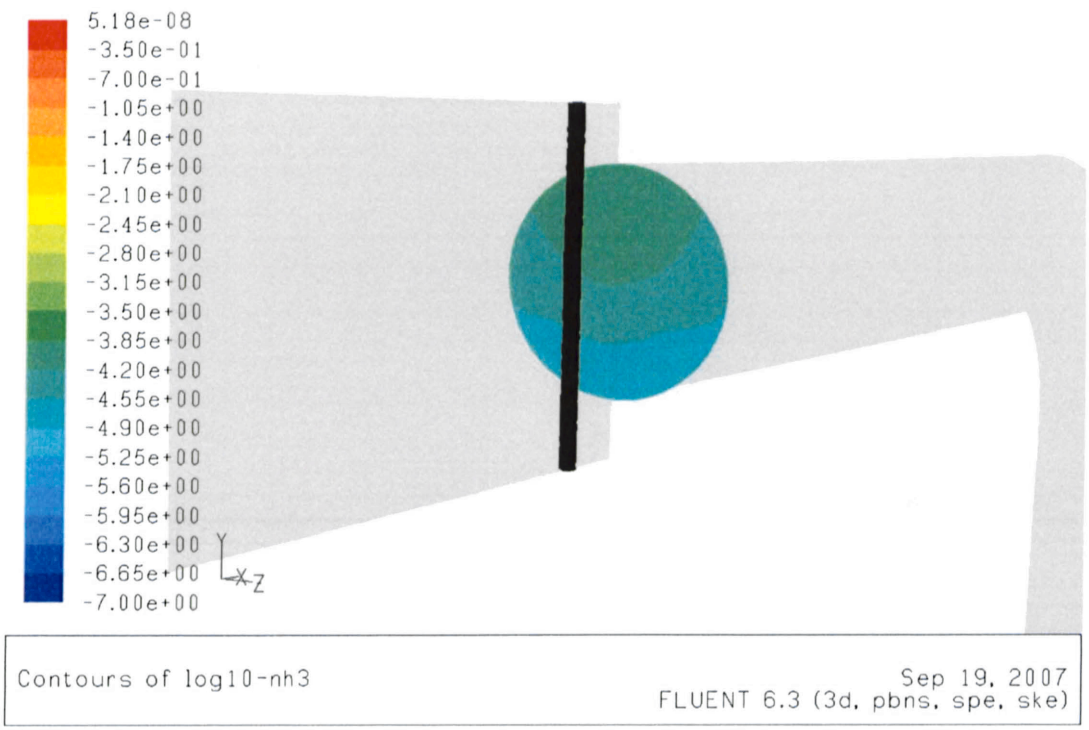

Figure 4.12: Logarithmic mass fractions of NH_3 at exit section of circular pipe

The Figures 4.11 shows contours of turbulent intensity in the z=0 plane. Figure 4.12 depicts contours of logarithmic contours of mass fractions on the surface of the exit section of the circular pipe. Figure 4.12 explains better the effect of the turbulence in the model. The turbulent intensities ranged from 2% to about 7% at the exit section, which suggests that low turbulence was computed. From Figure 4.12, it can be observed that ammonia is concentrated towards the top (outer wall) and gradually reduces towards the bottom. This is possible when there is poor mixing in the system. The flow is pushed outward at the second bend and so hence ammonia concentrates towards upper layers. Ammonia mass fractions were computed to be between $10^{-3.5}$ and $10^{-5.5}$.

Case (c): Wall Injection with downstream mixer

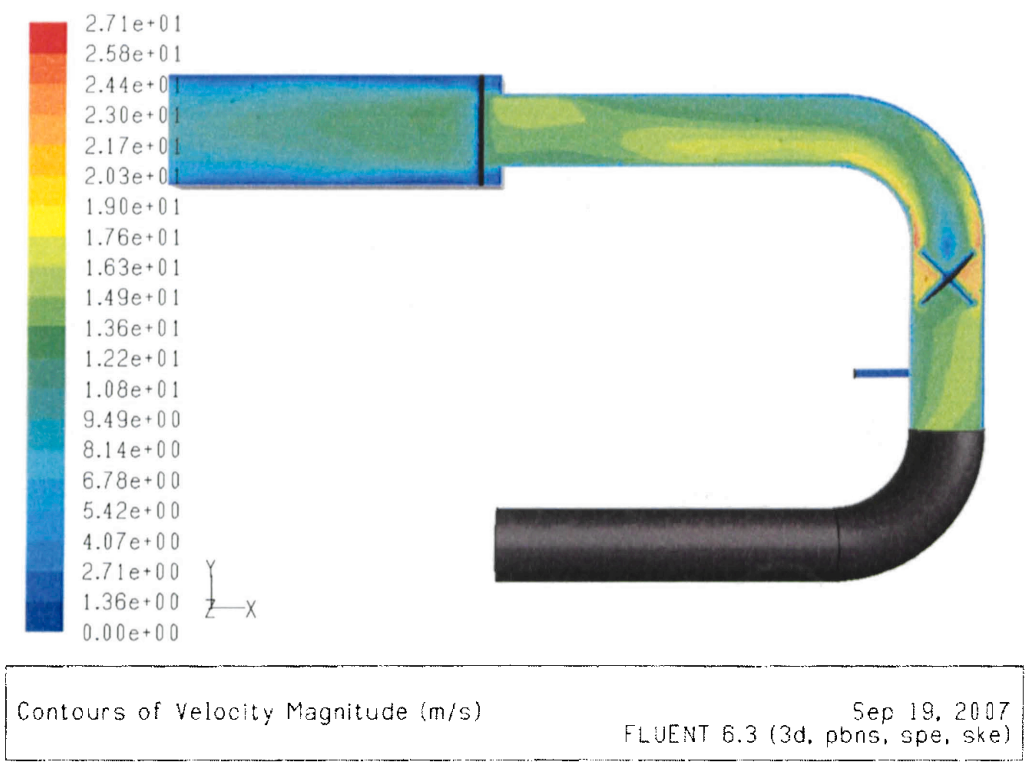

Figure 4.13: Velocity Magnitude in the z=0 plane

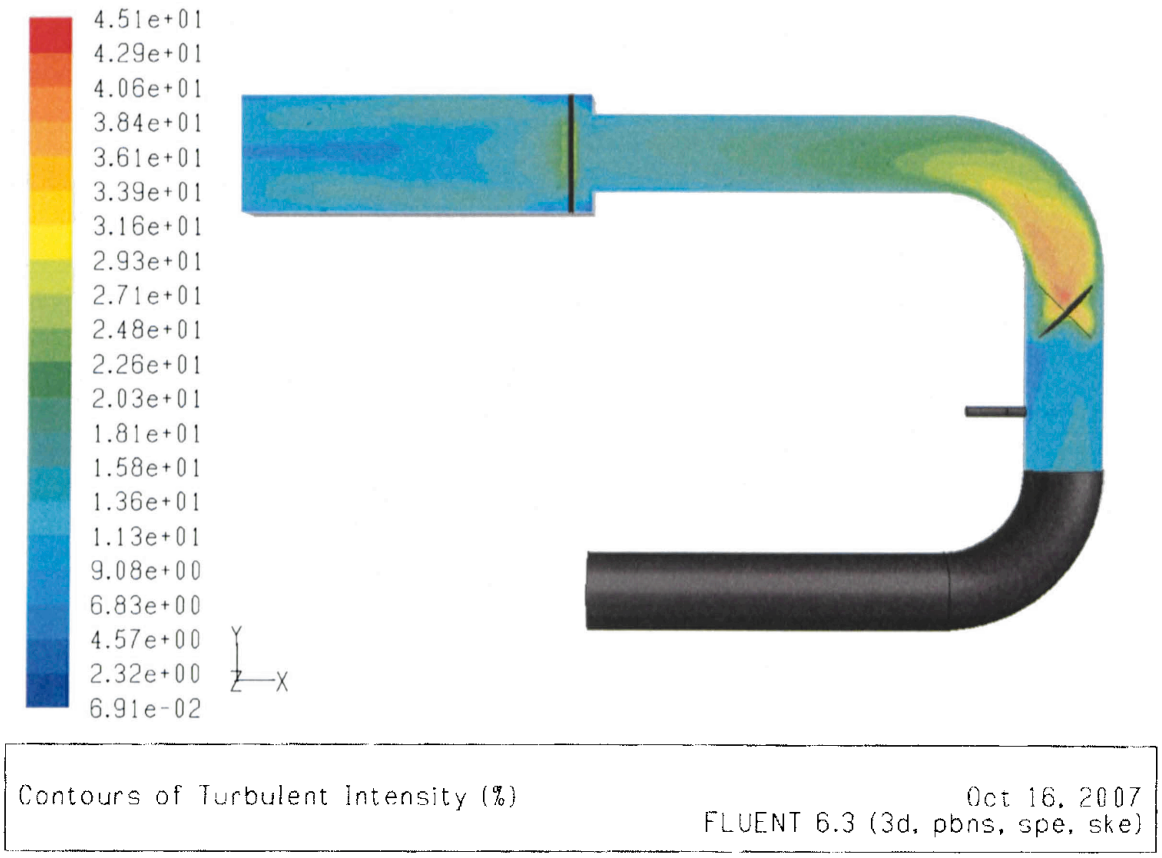

Figure 4.14: Turbulent Intensity in the z=0 plane

Figures 4.13 to 4.15 depict the case of re-agent injection orthogonal to the exhaust flow direction at the wall. In this case, the velocity magnitudes are approximately constant to the second significant number at the exit section of the circular pipe. The velocity was shown to be relatively uniform throughout the cross-section of the circular pipe exit ranging between 13.5 m/s and 14.5 m/s.

The turbulent intensity contours are shown in Figure 4.14 in the z=0 plane. The contours show that there is a significant amount of turbulence using a mixer downstream of the injector. The contour looks similar to case (a) with high turbulent intensities

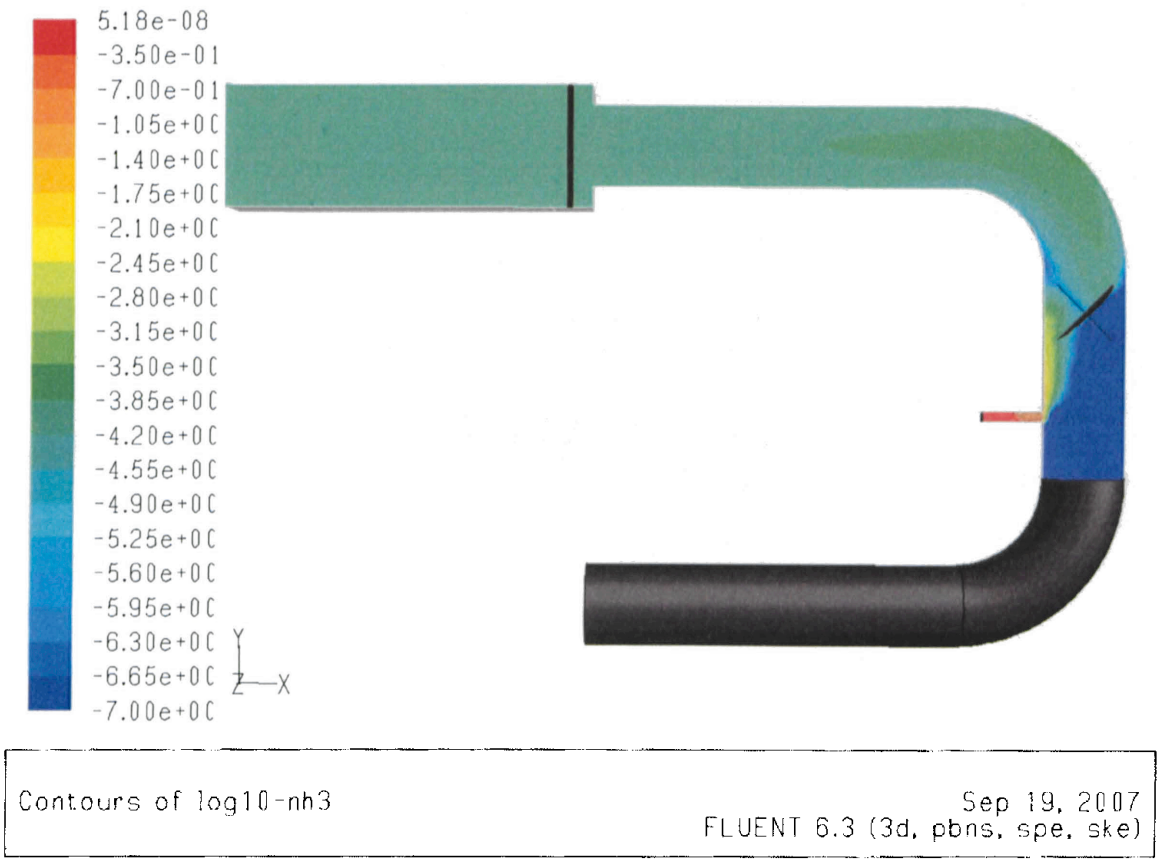

Figure 4.15: Logarithmic Mass fractions of NH_3 in z=0 plane

ranging in the order of 37% to 45%. This is high turbulence that can lead to uniform mixing. The contours suggest that the flow is similar to that of case (a).

Although the injector was terminated at the wall of the reactor, there appears to be adequate mixeding in the pipe. Almost immediately downstream of the mixer ammonia is relatively uniform with mass fractions of about $10^{-4.2}$. As ammonia is injected out of the injector at the wall, it has a tendency to stick to the inner wall owing to its very small local velocity in comparison with the high velocity of the exhaust gas. The presence of the mixer provides the needed obstruction to divert the flow across the cross section of the pipe and enhance mixing.

Case (d): Wall Injection without downstream mixer

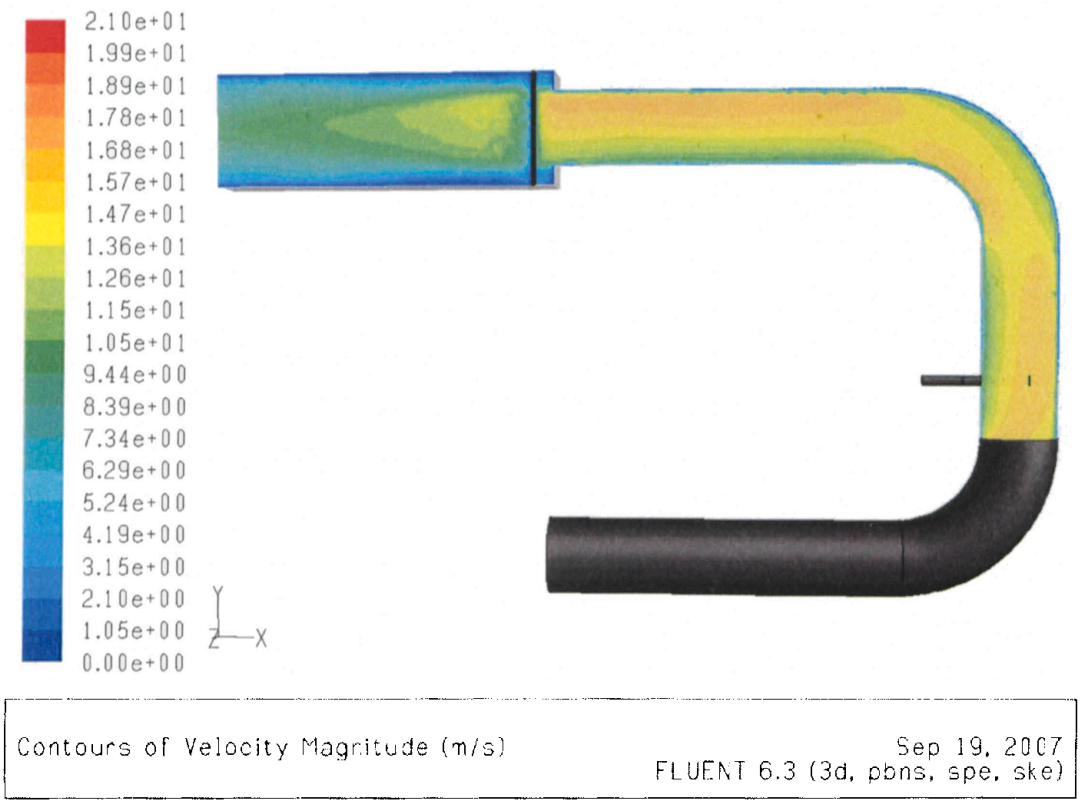

Figure 4.16: Velocity Magnitude in the z=0 plane

Figures 4.16 to 4.18 show the contours of velocity magnitude, turbulent intensity and mass fractions of ammonia after mixing with exhaust gas. Ammonia was injected similar to case (c). In the case of wall injection and no downstream mixer, maximum stratification can be observed in the velocity magnitude at the exit section of the circular pipe. The velocity magnitude increases outward from the inner wall from about 9 m/s to 17.5 m/s. The layers at the inner wall while making the second bend see a sudden increase in the velocity and are then further pushed outward due to the centrifugal effect. At the entry of the square pipe that there is an expansion in the flow and localized low velocity magnitude zones are formed at the corners.

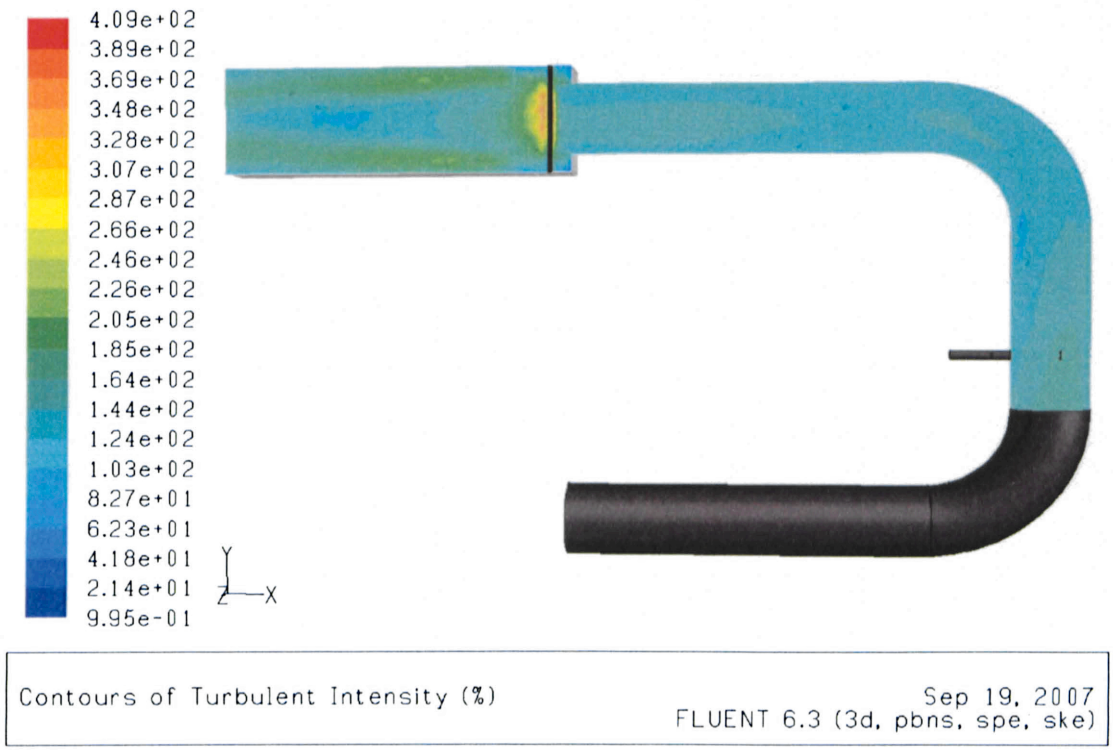

Figure 4.17: Turbulent Intensity in the z=0 plane

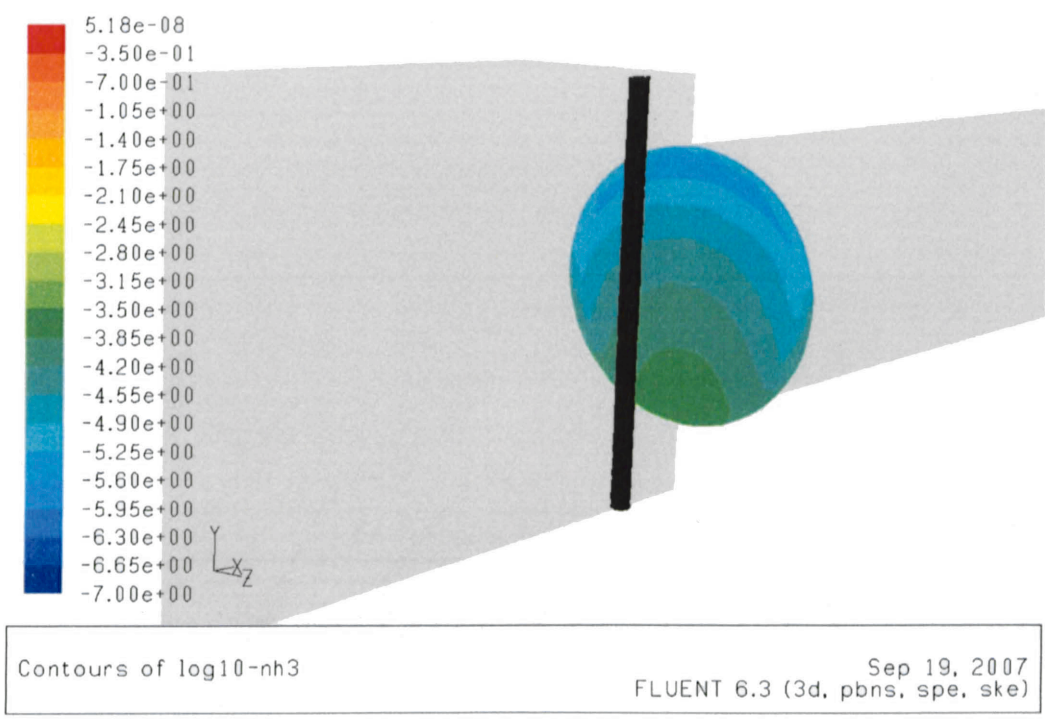

Figure 4.18: Logarithmic mass fractions at the exit section of the circular pipe

Owing to the fact that there is no downstream in-line mixer to instigate turbulence, no turbulence is observed. Turbulent intensity of approximately 40% is seen right behind the vertical probe. However, the intensity ranges from about 6% to 10% in the rest of the pipe. From Figure 4.18, it is clear that there is poor distribution of ammonia across the exit surface of the circular pipe. The trend is expected to be, more or less, the same after expanding into the square pipe where the measurements will be taken using a traversing probe. There is a variance in mass fraction between $10^{-5.6}$ to $10^{-3.5}$.

The four cases discussed demonstrate the importance of utilizing an in-line mixer downstream of the ammonia injector tube. Uniform concentrations are expected across the cross section of interest (just outside the circular pipe) when utilizing a mixer.

4.4 Comparison of mass fractions at the vertical probe

Figure 4.19 is a comparison between all the four 3-D cases discussed. The Y-axis is the position from the upper face to the lower face of the square pipe. The upper wall corresponds to the 27.5 inches and the lower to 21.5 inches. These values refer to the actual dimensions from the datum, which was set to the centre of 'exhaust gas inlet' face in Figures 4.1, 4.2, 4.3 and 4.4. The X axis shows mass fractions (log scale). The maximum variation in ammonia mass fraction is seen in wall injection without mixer (red trend) ranging from $10^{-5.6}$ to $10^{-3.6}$. The variation in mass fraction for wall injection with mixer (black trend) is in the range of $10^{-4.36}$ to $10^{-4.29}$, which matched very closely with the case of central injection with mixer (green trend). The mass fractions of ammonia in the case of central injection without mixer (blue trend) were in the range of $10^{-4.9}$ to $10^{-4.1}$.

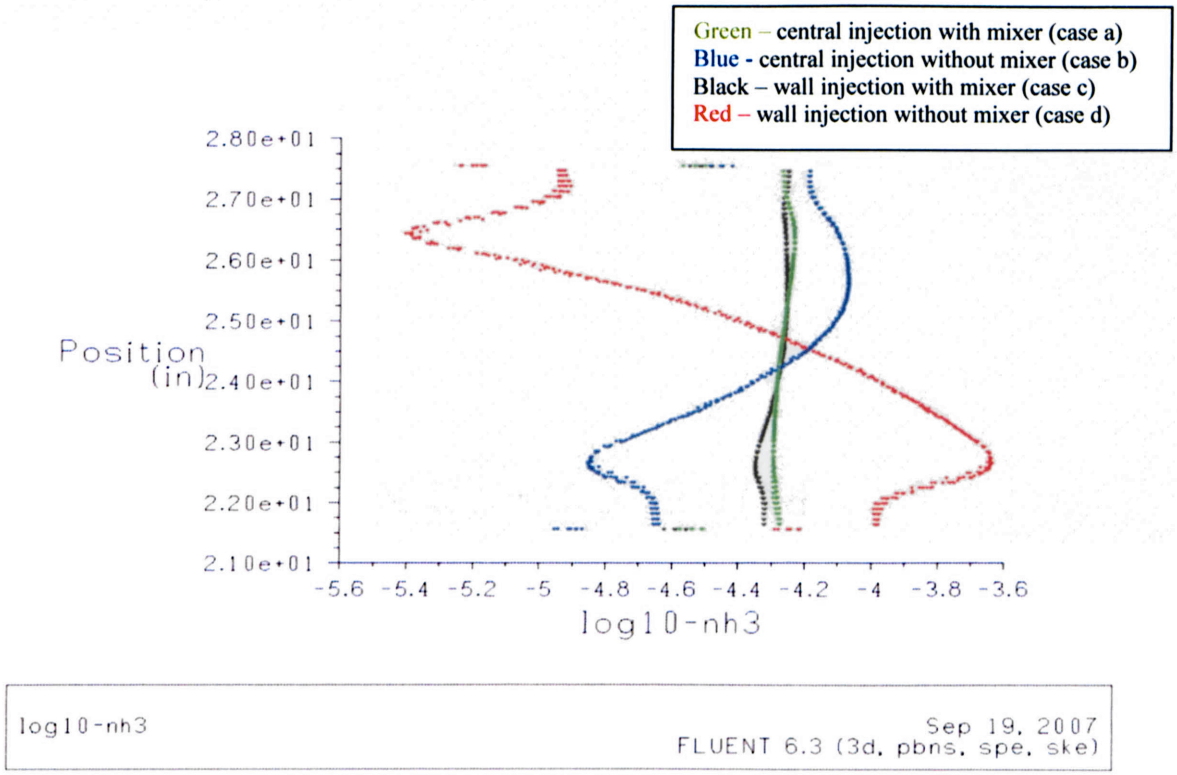

Figure 4.19: Comparison of mass fractions (log scale) between all four cases at the vertical probe section

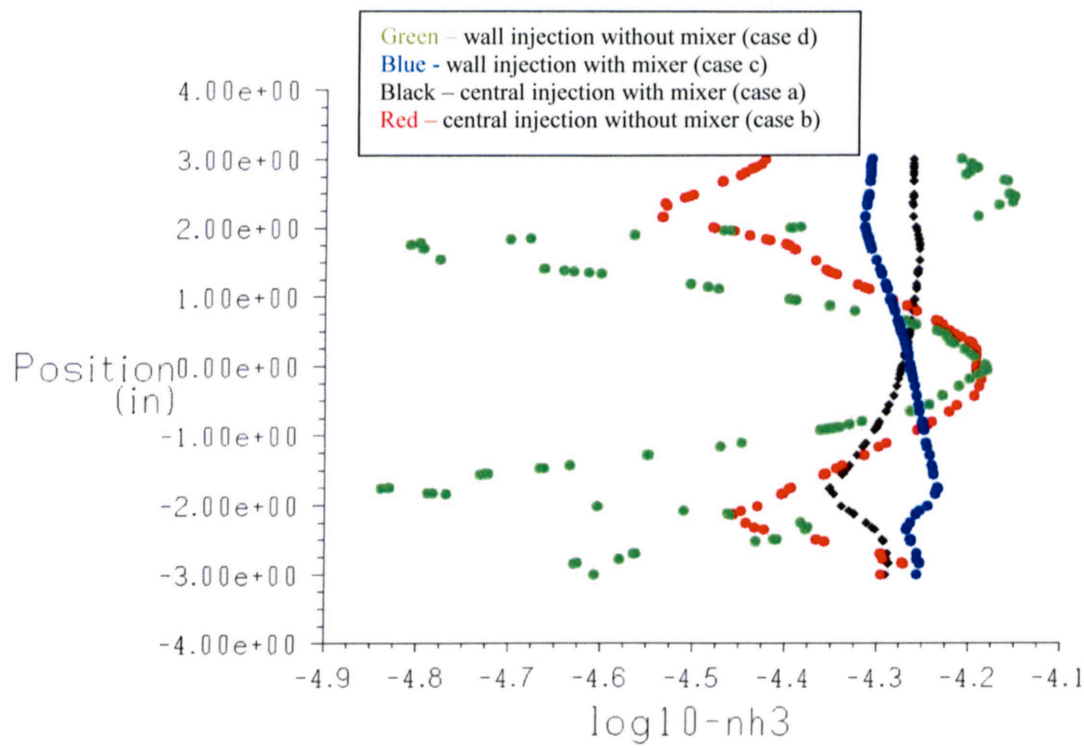

Figure 4.20: Comparison of mass fractions (log scale) between all four cases at the movable probe (horizontal)

Figure 4.20 shows the comparison of mass fractions (log scale) between all the four 3-D cases at the movable probe. The horizontal axis is $\log_{10}$ of mass fractions and the vertical axis is the distance into the square pipe (negative Z axis) from the wall. There is a difference in mass fraction distribution in the horizontal axis in all the four cases, which implies the mal-distribution present in the horizontal plane. The mixing at the probe for the horizontal axis is generally more uniform. However, the relative comparison between the four 3-D cases with the vertical plane is maintained. The cases of wall injection and central injection employing a downstream mixer (Blue and black trends) are relatively uniform. The ammonia mass fractions in case of central injection without a mixer (red trend) varied between $10^{-4.6}$ and $10^{-4.2}$. Mass fractions in case of wall injection without mixer (green trend) showed poorest mixing with mass fraction ranging between $10^{-4.9}$ and $10^{-4.15}$.

4.5 Degree of heterogeneity:

To describe the level of heterogeneity, or "mal-distribution", a degree of heterogeneity parameter (α) was introduced. The degree of heterogeneity is defined as

$$\alpha = \frac{\sqrt{\frac{1}{XY}\sum_{x,y}\left[X_f(x,y) - X_{f,mean}\right]^2}}{X_{f,mean}}$$

Where,

α = degree of heterogeneity

XY = number of measuring points, or pixels, in the measuring plane

$X_f(x,y)$ = ammonia mole fraction at measuring point (x,y)

Case	Degree of heterogeneity (α)
Central injection with mixer	0.065
Central injection without mixer	0.475
Wall injection with mixer	0.071
Wall injection without mixer	0.875

Table 4.1: Comparison of Degree of Heterogeneity between all four cases

$X_{f,mean}$ = mean ammonia mole fraction over measuring plane

Table 4.1 lists the degree of heterogeneity in all the four 3-D cases.

In the equation above for the degree of heterogeneity, the numerator is the spatial standard deviation of the ammonia mole fraction. The standard deviation is normalized by the spatial mean ammonia mole fraction in the denominator.

Highest degree of heterogeneity (alpha) was computed in case (d) - wall injection without mixer – with a degree of 0.875. Alpha was computed about 0.48 for case (b). Alpha was very small in cases (a) and (c), with values of 0.065 and 0.071.

Chapter 5: EXPERIMENTAL INVESTIGATION

5.1 Motivation:

A CFD solution is never perfectly accurate in replicating a physical problem. This may be due to the various assumptions taken in simulating the physical process. An experimental comparison is useful to assess the accuracy of the numerical solution. This comparison will identify any shortcomings of the numerical simulation and lead to the reasons for any discrepancies. Any numerical solution should be validated with experimental results. In this case, after a thorough design process, a traversing probe was built to sample ammonia concentration across the catalyst housing. This provides the data to compare with the CFD solution and additional insight into the flow scenario.

5.2 Traversing Probe:

A traversing probe was designed using Pro/E for the purpose of sampling the concentrations of NH_3 at successive locations of the catalyst housing cross section. Figures 5.1 and 5.2 (below) represent the traversing probe assembly connected to the catalyst housing and the traversing probe assembly, respectively. A rack and pinion gear mechanism was utilized to convert the rotary motion to translational motion. The aim was to be able to crank the rack and pinion mechanism along with a quarter inch steel sample tube at desired distances into the catalyst housing. For this purpose, the quarter inch sampling tube was welded to the gear rack that was end milled on the bottom face so as to accommodate the sampling tube in the groove. The steel tube was welded to the gear rack in the groove so that it moves along with the gear rack. Various guiding and supporting parts such as a central guide, a bend guide etc. were designed so as to have

maximum control over the lateral movement of the gear rack and to support the rack and pinion assembly to bend on its own weight. Holes - of size 0.5 inch - were made on opposite walls of the catalyst housing to which half coupling were welded. These ½ inch NPT (national pipe thread), couplings were welded. A two piece sealing assembly containing graphite gaskets, threads into the ½ inch NPT couplings.

A list of all components with their design details - used in the traversing probe - assembly is provided below.

1. **Square tube**: A 4 inch by 4 inch square tube 18 inches in length and a wall thickness of 0.125 inch was used to house the entire assembly. All the components such as the rack and pinion, guiding block plates and structural enhancement blocks were fitted into this tube. This square tube was bored with 0.5 inch holes on the longer sides in order to accommodate the hardened precision shaft so it can provide the necessary torque to set the gear rack into motion. Two sets of holes of 0.375 inch diameter were machined on the top and bottom faces to be able to fasten the centre guide and bend guide blocks. End grooves were machined at one end of the tube on the longer sides to provide ability to fasten the end plate with a hole for the probe on it.
2. **Rack and Pinion gears**: A gear rack of 12 pitch – 0.75 inch face width, 7 inch in length and 0.75 inch in overall height was machined with a lengthwise continuous groove that can accommodate the 0.25 inch stainless steel sample tube of wall thickness 0.049 inch. The steel finished mating spur gear was through bored. The dimensions were 12 pitch – 0.75 inch face width, 14 teeth, 1.167 inch pitch diameter and 0.5 inch bore.

3. **Hardened Precision shaft**: A 0.5 inch hardened precision shaft was connected on one end to the crank handle and aligned to mate with the spur gear.
4. **Set Screw Shaft Collars**: Set screw shaft collars of 0.5 inch bore. 1 inch outer diameter, 0.4375 inch width and 0.25 inch-20 screw size were used to hold the precision shaft tight on the outer sides of the square tube.
5. **Crank Handle**: A 4 inch long steel crank handle with 12.06 inch diameter solid hub was used to crank the rack and pinion mechanism.
6. **Centre Guide**: A 2 inch by 3.5 inch stainless steel vertical block with a hole of 0.3 inch diameter was machined and placed in between the coupling attached to the catalyst housing pipe and the gear rack. This hole was to guide the sampling tube through it and minimize the lateral movement of the probe. Threaded holes of size 0.375 inch-16 tap and depth 1 inch were machined on the top face to be able to bolt it to the square tube, thus, locking the movement of the centre guide.
7. **Bend Guide**: A 2 inch by 1.15 inch stainless steel block with threaded holes on the bottom end was machined. The threaded holes were of size 0.375 inch-16 and 1 inch deep. The purpose of the bend guide was to provide structural rigidity to the rack and pinion assembly so as to prevent bending of the probe, which may result in sluggish movement of the traversing probe.
8. **End Plate**: An end plate of thickness 0.375 inch was machined and fastened to the open end of the square tube. Two right angles threaded studs were welded to the end plate. A quarter inch hole that can accommodate the probe was also machined to provide additional support to the traversing probe.

9. Additionally, two steel plates of size 2 inch by 4 inch were welded to the either sides of the square tube with two holes of 0.375 inch diameter. These two holes were machined for the one side threaded studs welded on to the catalyst housing pipe on one side and the circular pipe on the other side. The whole traversing probe assembly was connected using these studs and was fastened using screws.
10. Graphite gasket sealing material was cut into circular shape with an inner hole of 0.24 inch diameter to provide a compression sealing with the probe. This machined sealing was placed inside the female coupling that is part of the traversing probe assembly.

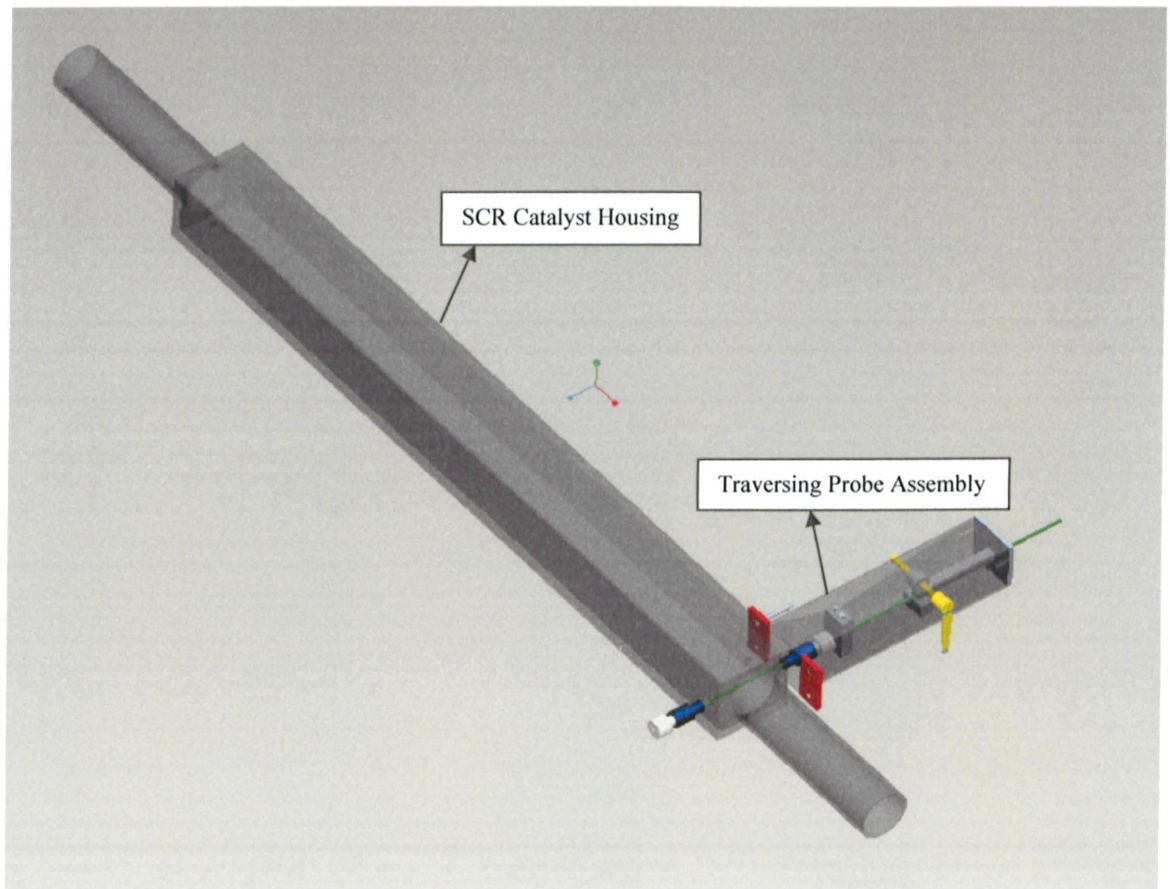

Figure 5.1: Traversing probe assembly fitted to the catalyst housing

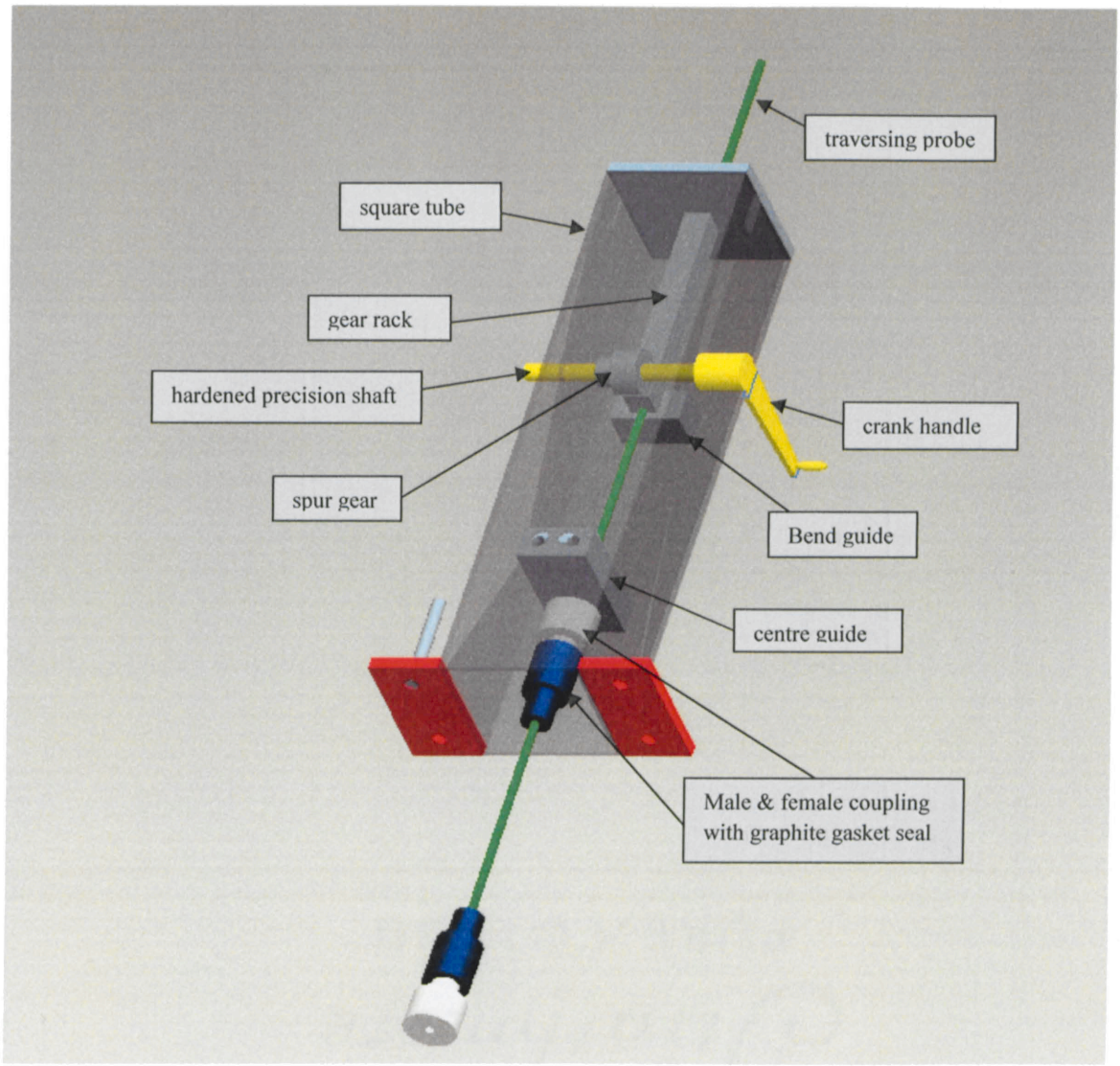

Figure 5.2: Traversing probe assembly

In Figure 5.2, the SCR catalyst housing is removed for clarity. The traversing probe consists of a 0.15" diameter hole facing the direction of exhaust gas flow. It is a single port utilized to sample the exhaust products at different locations in the cross section. One end of the probe is plugged and the other is connected to a heated sample line that carries exhaust gas to the gas analyzers. An FTIR analyzer and a 5-Gas Rack analyzer are utilized to analyze the gas.

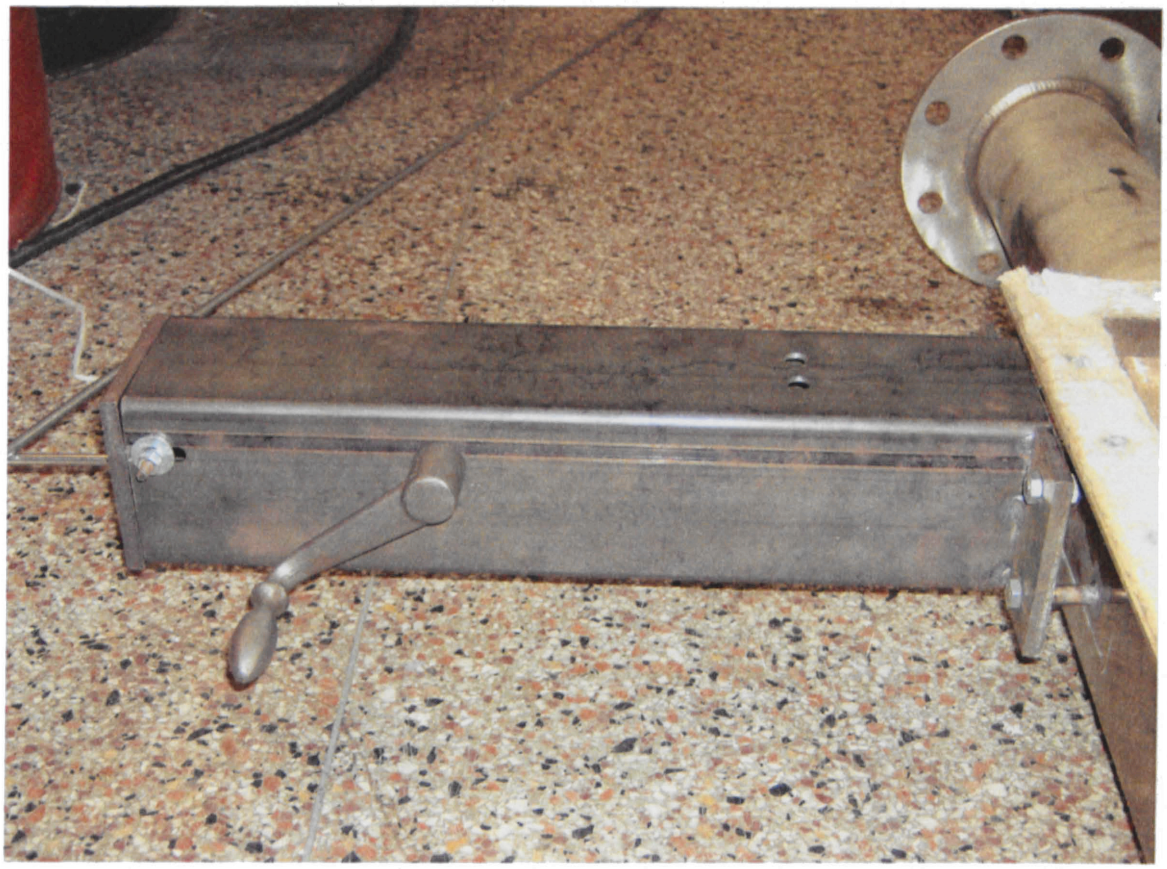

Figure 5.3: Traversing probe assembly connected to SCR catalyst housing (shown partly)

Figure 5.3 shows a picture of the completed traversing probe that is connected to the SCR catalyst housing. The complete traversing probe assembly is bolted to the SCR catalyst housing using one side threaded studs that were welded on to the housing.

5.3 Gas Analyzers:

The Rosemount 5-gas emissions bench measures CO, CO_2, Total Hydro Carbon (THC), NO_x and O_2 concentrations. A Peltier type condenser removes water from the exhaust sample before the gas enters the analyzers. Infrared radiation (IR) adsorption is

used by the analyzer to determine CO concentrations. IR detection is also used to measure CO_2 concentrations in the exhaust. THCs are detected using a flame ionization detector (FID) method. A regulated flow of sample gas passes through a flame sustained by regulated flows of fuel gas and air. Within the flame, the hydrocarbon sample stream undergoes a complex ionization that produces electrons and positive ions, which are collected by an electrode, causing a measurable current flow. The ionization current is proportional to the rate at which carbon atoms enter the burner and is therefore a measure of the concentration of hydrocarbons in the sample. The NGA 2000 CLD uses the chemiluminescence method for detection for NO_x. All NO_2 is reduced to NO over a catalyst. The NO is reacted with internally generated ozone (O_3) to form NO_2 in an electronically excited state. The excited molecule immediately reverts to the ground state emitting photons (red light), which are measured by a photodiode. The intensity of the chemiluminescence is directly proportional to the NO_x concentration. The determination of O_2 concentration is based on measurement of the magnetic susceptibility of the sample gas. O_2 is strongly paramagnetic, meaning its molecules have permanent magnetic moments even in the absence of an applied field, while other common gases are weakly diamagnetic.

Hazardous Air Pollutants (HAPs) are measured using FTIR analyzer. The primary HAPs of interest for natural gas engines are formaldehyde, acrolein and acetaldehyde. Ammonia and hydrogen cyanide are also measured. THC and NO_x speciation are performed with the FTIR. The most important aspects of the Magna 560 FTIR spectrometer include the mercury cadmium telluride (MCT) detector, germanium-on-potassium bromide (Ge-on-KBr) beam splitter, and an instrument resolution limit of

0.125 cm^{-1} (after apodization). The instrument uses a 10 meter gas cell, which has a volume of 2 liters and utilizes zinc selenide windows.

5.4 Results:

5.4.1 Comparison of experimental and CFD results in the best mixing case (central injection with downstream mixer)

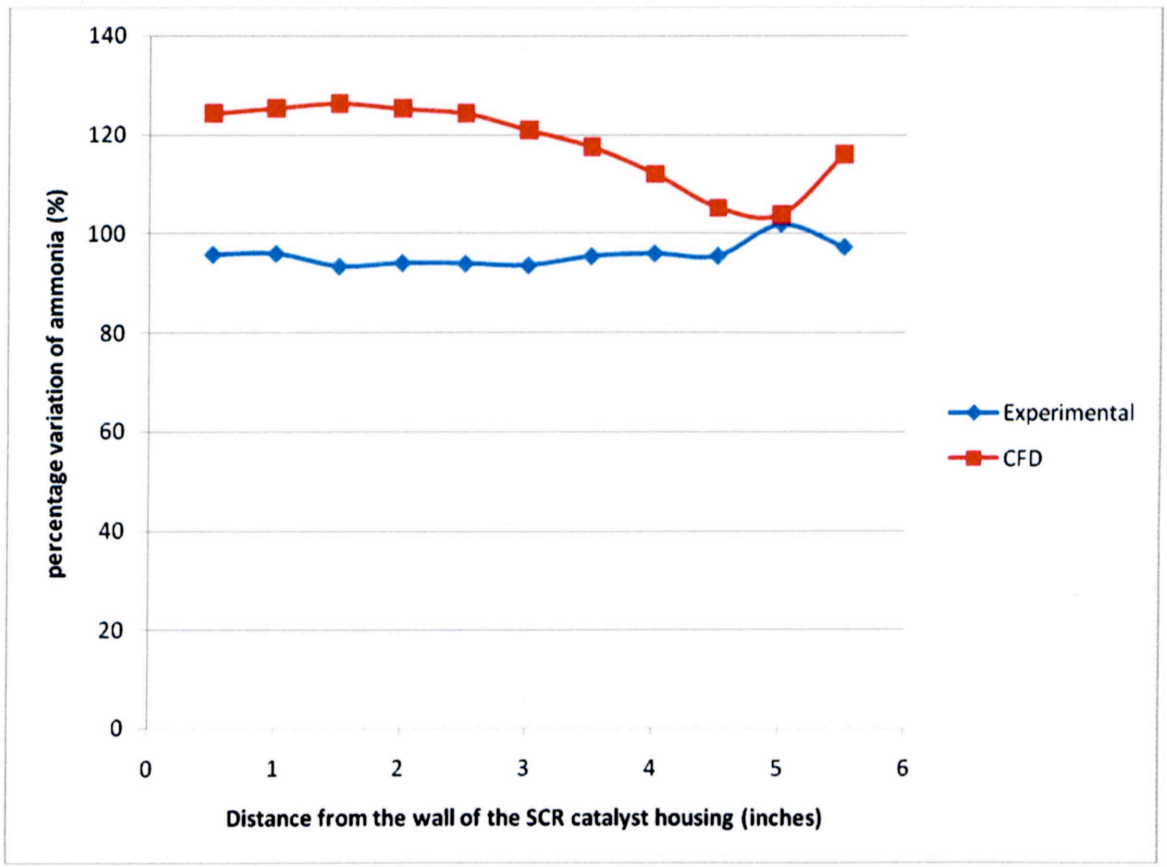

Figure 5.4: percentage variation of ammonia comparison between experimental & CFD using traversing probe in case of central injection and downstream mixer

Figure 5.4 depicts the variation in ammonia concentration using a traversing probe for ammonia measurements and the CFD solution. The graph is a comparison between the percentage variations of ammonia at each point of traversal with respect to

the average ammonia concentrations measured. The average ammonia concentration – in the experimental case - was found to be about 191 ppm (using an averaging stationary probe), whereas the CFD solution computed about 88 ppm. The maximum deviation observed in the experimental solution was about 12 % and the CFD suggests about 18 %. The two trends suggest uniform mixing at all the points in the path of traversal in the case of central injection and a downstream mixer. The offset could be due to secondary flows and the existence of the two additional probes just downstream of the bend, which will be discussed in the wall injection case (below).

5.4.2 Comparison of experimental and CFD results in the poorest mixing case (wall injection without downstream mixer)

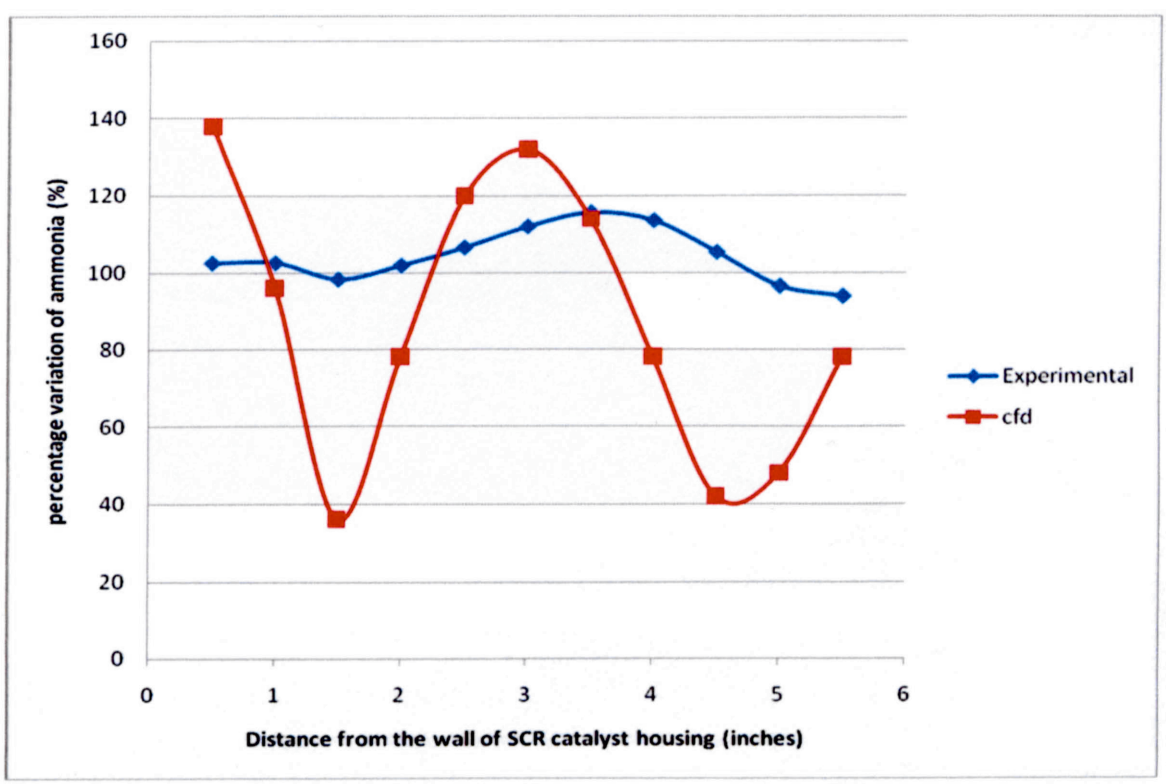

Figure 5.5: percentage variation of ammonia comparison between experimental & CFD using traversing probe in case of wall injection and no mixer

Figure 5.5 depicts the variation in ammonia concentration using a traversing probe for experimental values and the CFD solution. The graph is a comparison between the percentage variations of ammonia at each point of traversal with respect to the average ammonia concentration in the exhaust for the case of wall injection and no mixer. The average concentration in the experimental case was found to be close to 190 ppm (using an averaging stationary probe), whereas the average concentration in the CFD solution was computed to be about 91 ppm. This is due to the difference between mass flow rate of ammonia injected at the time of the experiment and the assumed value used for CFD computation. In comparison, the experimental concentrations ranged from 179 ppm to about 225 ppm. However, expressing ammonia concentrations in percentage normalize the trends in the two scenarios (CFD and experimental). As we move along each location of the traversing probe, the experimental trend (series in blue) rises and dips corresponding to the CFD solution, thus validating the CFD solution.

5.4.3 Possible reasons for CFD-Experimental Difference:

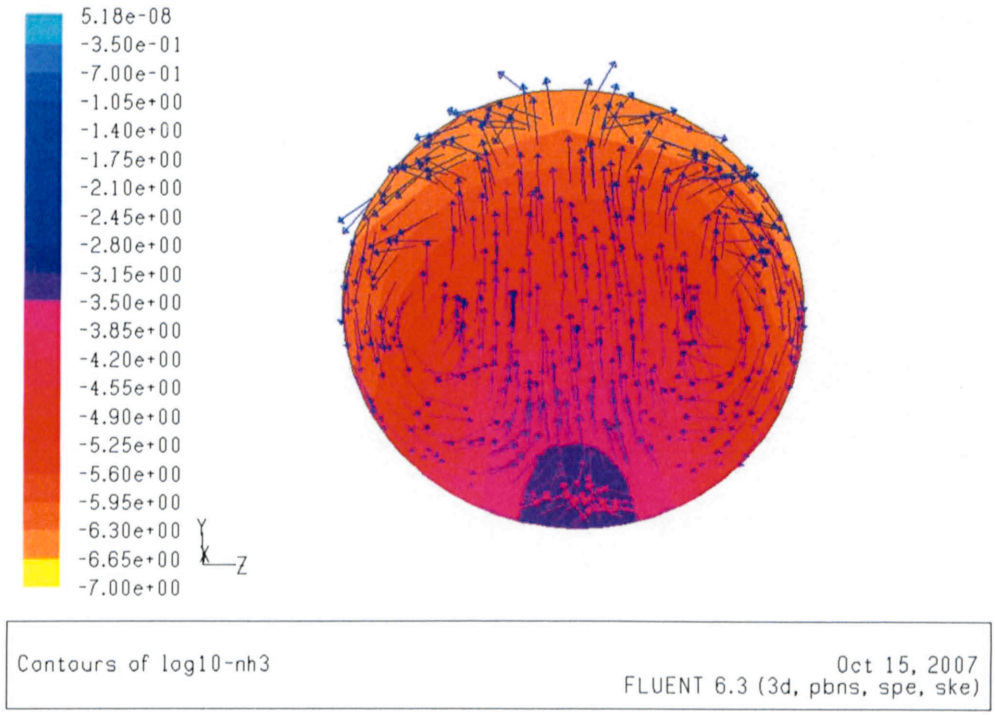

Figure 5.6: Logarithmic mass fractions of NH_3 overlaid with velocity vectors colored by logarithmic mass fractions of NH_3

Figure 5.6 depicts logarithmic contours of mass fractions of ammonia overlaid by flow vectors (colored by logarithmic mass fractions of ammonia) on a surface in the YZ plane downstream of the second bend and upstream of the circular exit section. The picture suggests the existence of secondary flow. Secondary flows can be understood as a small disturbance on a primary flow where the primary flow is the main flow. They occur when the flow turns a bend when a sheared flow, such as a boundary layer, is forced around a turn. Slower moving fluid follows a tighter radius of curvature, leading to a tangential flow across the passage. In order to maintain continuity, a vertical flow is formed. The presence of a slightly asymmetric secondary flow (see in Figure 5.6) explains the asymmetry in the concentration of ammonia at the traversing probe.

Another reason causing the variance in the CFD and experimental comparison is the presence of a concentration averaging probe of size 0.375 inch diameter all the way across and a thermocouple of about the same size just downstream of the second bend. Both these probes are present in the circular pipe and downstream of the mixer. Their locations seem to play an important because of their presence just downstream of the bend. To demonstrate how turbulence can vary in this situation, a 2-D model was created with two circular probes imitating the two probes was built and analyzed.

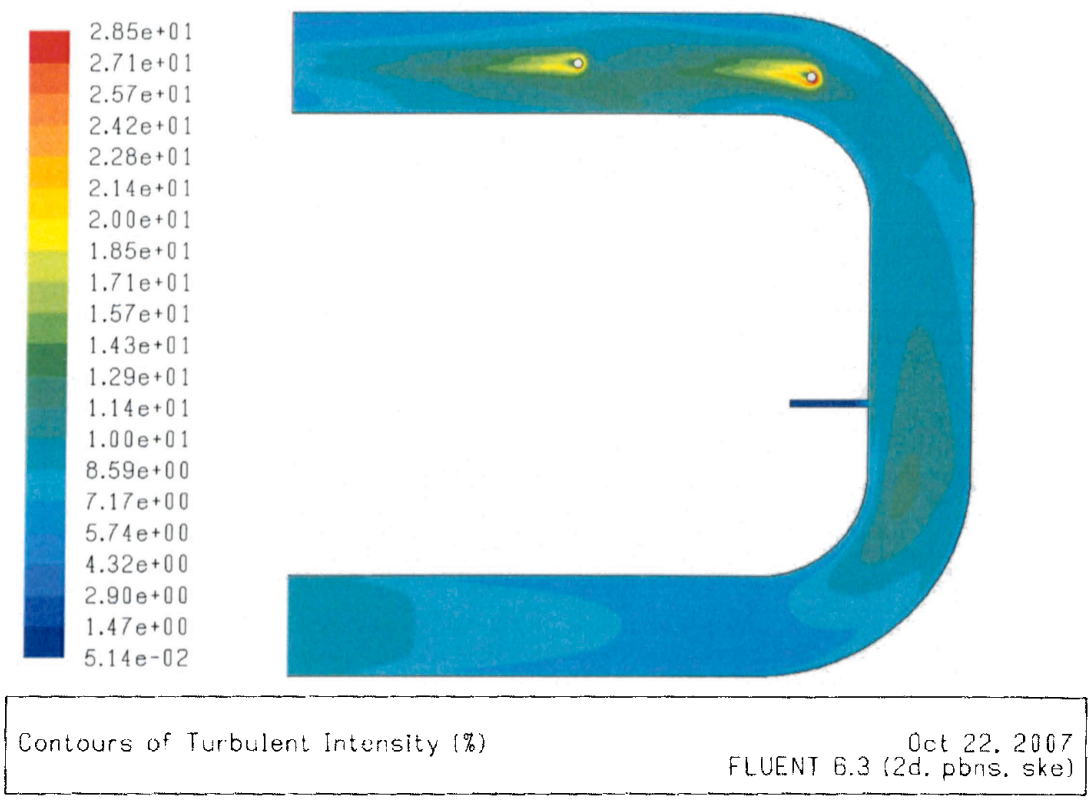

Figure 5.7: Turbulence intensity with two additional probes downstream of the second bend

Figure 5.7 shows the contours of turbulence intensity in this re-constructed case. The two probes are attached in the same orientation as the movable probe. Clearly, there is additional turbulence due to their presence. Maximum turbulent intensity was seen in the vicinities of the two probes. The turbulent intensities reached a maximum of about 29%. The turbulent intensities seen in case of wall injection without mixer (discussed in chapter 4) are seen to be in the range of 8%. This can be extrapolated in to a 3-D case using the same order or magnitude. A 3-D test run of this case would give a better picture of changes expected in turbulent intensities. This explains the asymmetry in the concentrations of ammonia across the traversing probe path.

Chapter 6: SUMMARY AND CONCLUSIONS

6.1 2-D Numerical Solution:

- Three different cases were modeled and analyzed.
- A model with no downstream mixer (case a), a model with an angled wall mixer downstream of the re-agent injection (case b) and a model with one inch central wall (orthogonal to flow) downstream of the re-agent injection (case c) were modeled for analysis.
- Ammonia injector tube was terminated at the wall to simulate the flow process.
- Flow data (pressures, temperatures etc) for *FLUENT* analysis was extracted from actual experimental data.
- The inclusion of a mixer (case b and c) showed a significant improvement in mixing of ammonia with the exhaust gas.
- Ammonia mass fractions ranged from $10^{-6.2}$ to $10^{-5.2}$ in case (a), $10^{-5.3}$ to 10^{-5} in case (b) and $10^{-5.6}$ to 10^{-5} in case (c) on a vertical plane that contains the traversing probe.

6.2 3-D Numerical Solution:

- Four different cases were modeled and analyzed.
- Two 'D' shaped metal plates were welded at right angles to each other to form a mixer that was used in the experiment.
- A model with the ammonia injector tube penetrating up to the centre of the pipe (central injection) with the injecting orifice facing the direction of flow

and a downstream mixer (case a), a model with central injection and no downstream mixer (case b), a model with ammonia injector tube terminating at the wall of the pipe (wall injection) injecting orthogonal to the direction of exhaust gas flow and a downstream mixer (case c) and a model with wall injection and no downstream mixer (case d) were modeled for analysis.

- Degree of heterogeneity (α) was calculated by normalizing the standard deviation of ammonia concentration with the spatial mean ammonia mole fraction in the plane of the traversing probe.
- Highest degree of heterogeneity was observed in case (d) and was calculated to be 0.875.
- Least degree of heterogeneity was observed in case (a) and was calculated to be 0.065
- The degree of heterogeneity in case (c) was computed to be 0.077.
- Mixing quality was best when re-agent was injected from the centre of the pipe with the orifice in the direction of exhaust gas flow.
- Turbulence was greatly increased in the pipe with a downstream mixer.

6.3 Experimental Investigation:

- A traversing probe was designed and built at the laboratory test centre to sample ammonia concentrations at different locations.
- CFD solutions and experimental data were compared as percentage variation of ammonia concentration at different locations.

- In case (a), where best mixing was computed by CFD, the maximum deviation observed in experimental data was about 12%, whereas CFD results show a deviation of 18%.
- In case (d), where poorest mixing was computed, maximum deviation observed in experimental data was about 35%; CFD computation yield a maximum deviation of 100%.
- The trends (CFD and experimental) in case (d) and case (a) show similarities in shape, which supports the validity of CFD solutions.
- The difference between experimental data and CFD results are likely due to,
    - Inconsistency between model analyzed and experimental hardware. The presence of an averaging sample probe and a thermocouple upstream of the traversing probe was ignored in the model. Additional turbulence is expected due to their presence, which was seen in a simple 2-D study.
    - For the sake of CFD simulation, ammonia injection was assumed at Standard Temperature Pressure (STP) and not Standard Liters per Minute (SLM).
    - Presence of secondary flow in the mixture after the second 90° bend is a possible reason for variation in experimental measurement of ammonia concentration at the traversing probe.

APPENDIX A:

TRAVERSING PROBE DESIGN DRAWING

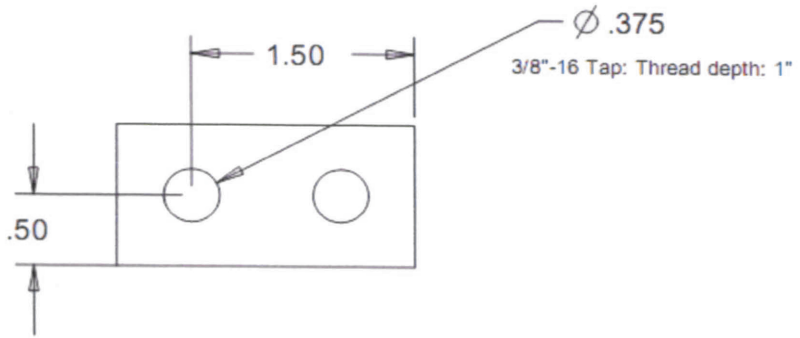

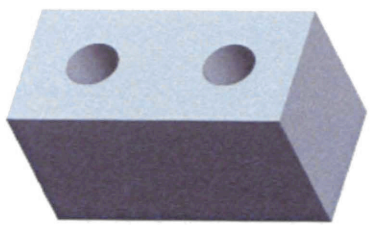

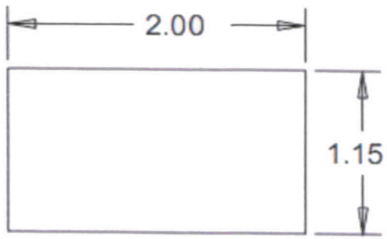

-X.X ±0.1
-X.XX ±0.01
-X.XXX ±0.005

PART NO	SCR-5	PART NAME	BEND GUIDE	QTY:	2
		Colorado State University		UNLESS OTHERWISE SPECIFIED DIMENSIONS ARE IN INCHES TOLERANCES ARE: FRACTIONS ± 1/32 DECIMALS ± .002 ANGLES ± 5°	
		Mechanical Engr. Dept. Fort Collins, Co 80521 (970) 491-6558	DRAWN BY: KIVATURI	MATERIAL:	CARB ST
SCALE:	1.000				
SHEET:	5/12	ALL PARTS ARE IN Inches		FINISH:	

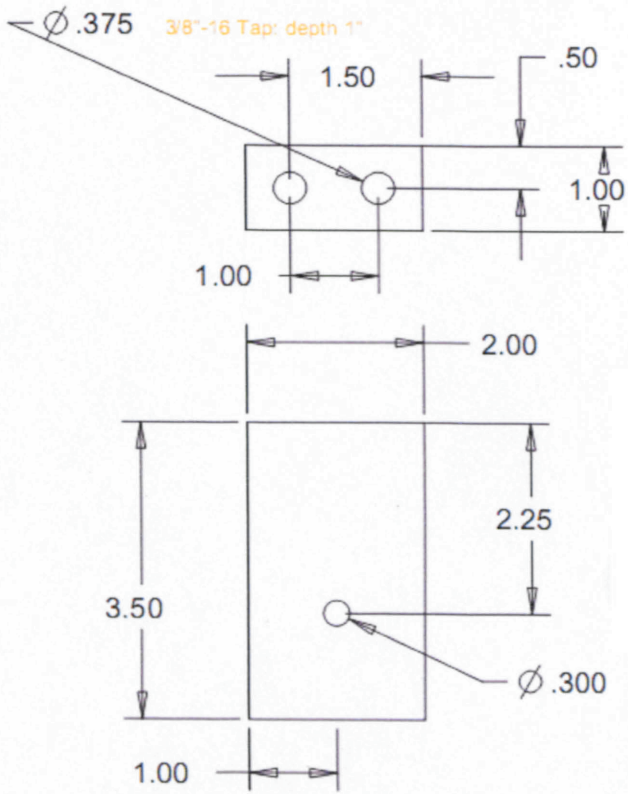

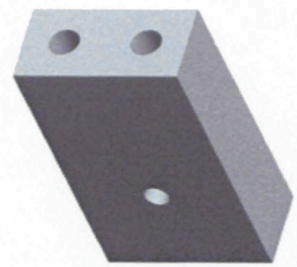

PART NO:	SCR-4	PART NAME:	CENTRE GUIDE	QTY:	2
		Colorado State University Mechanical Engr. Dept. Fort Collins, Co 80521 (970) 491-6558		UNLESS OTHERWISE SPECIFIED DIMENSIONS ARE IN INCHES TOLERANCES ARE: FRACTIONS: ± 1/32 DECIMALS: ± .002 ANGLES: ± 1°	
SCALE:	0.6	DRAWN BY:	KIVATURI	MATERIAL:	CARB ST
SHEET:	4/12	ALL DIMENSIONS ARE IN inches		FINISH:	

-X.X ±0.1
-X.XX ±0.01
-X.XXX ±0.005

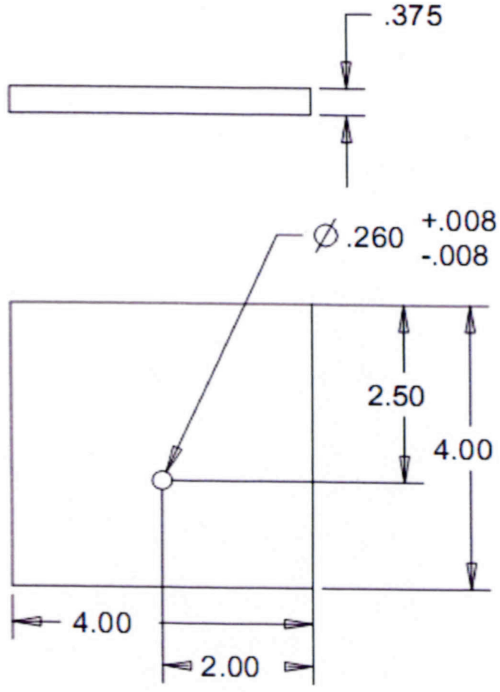

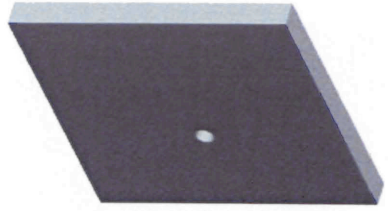

-X.X ±0.1
-X.XX ±0.01
-X.XXX ±0.005

PART NO:	SCR-3	PART NAME:	END PLATE	QTY:	2
		Colorado State University		UNLESS OTHERWISE SPECIFIED DIMENSIONS ARE IN INCHES TOLERANCES ARE: FRACTIONS: ± 1/32 DECIMALS: ± .002 ANGLES: ± 1 °	
		Mechanical Engr. Dept. Fort Collins, Co 80521 (970) 491-6558			
SCALE:	0.5	DRAWN BY:	KIVATURI	MATERIAL:	CARB ST
SHEET:	3/12	ALL DIMENSIONS ARE IN inches		FINISH:	

S.No	Component	Vendor	Part No.	Qty.
1	SCR-3	---------	---------	-----
2	Right Angled Stud	Mcmaster	96466A060	2

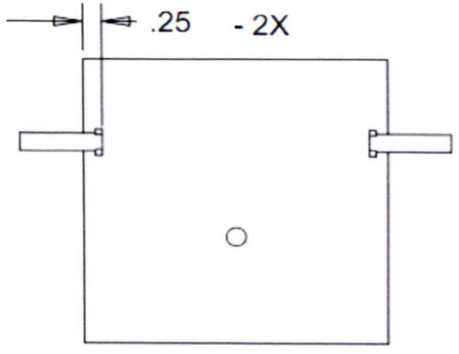

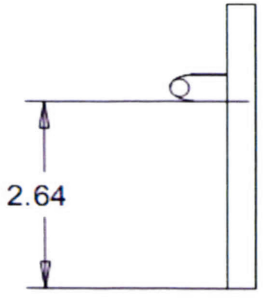

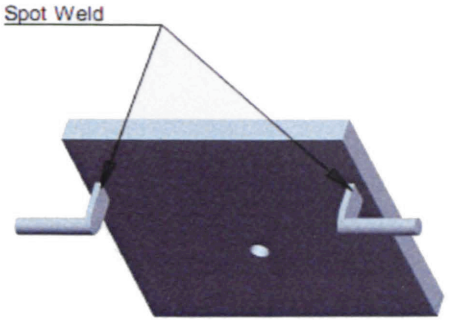

X.X ±0.1
X.XX ±0.01
X.XXX ±0.005

PART NO:	SCR-7	PART NAME:	ENDPLATE_STUD Assy	QTY:	2
		Colorado State University Mechanical Engr. Dept. Fort Collins, Co 80521 (970) 491-6558		UNLESS OTHERWISE SPECIFIED DIMENSIONS ARE IN INCHES TOLERANCES ARE: FRACTIONS ± 1/32 DECIMALS ± .002 ANGLES ± 5°	
SCALE:	0.5	DRAWN BY:	KIVATURI	MATERIAL:	SS
SHEET:	7/12	ALL DIMENSIONS ARE IN inches		FINISH:	

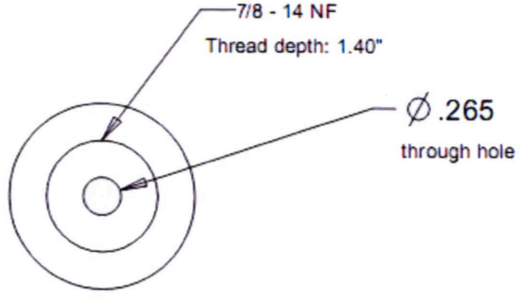

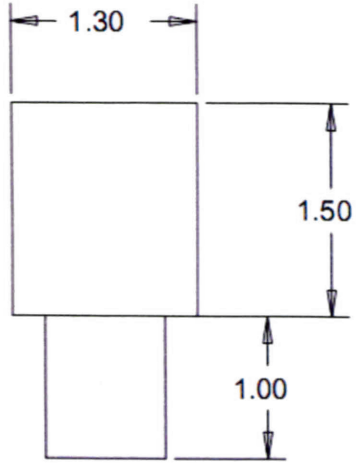

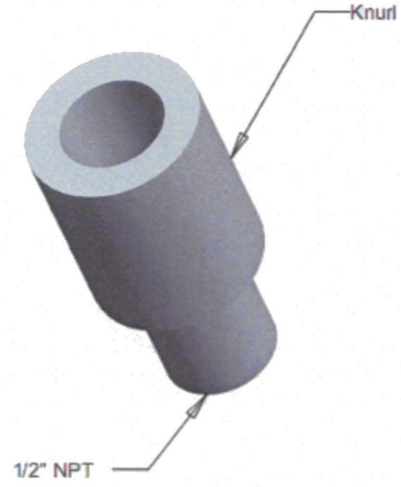

X.X ±0.1
X.XX ±0.01
X.XXX ±0.005

PART NO	SCR-10	PART NAME	Female	QTY:	3
		Colorado State University		UNLESS OTHERWISE SPECIFIED DIMENSIONS ARE IN INCHES TOLERANCES ARE: FRACTIONS ± 1/32 DECIMALS ± .002 ANGLES ± 5 °	
		Mechanical Engr. Dept. Fort Collins, Co 80521 (970) 491-6558			
SCALE:	1.000	DRAWN BY	KIVATURI	MATERIAL:	CARB ST
SHEET:	10	ALL DIMENSIONS ARE IN inches		FINISH:	

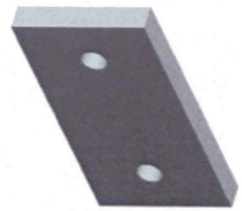

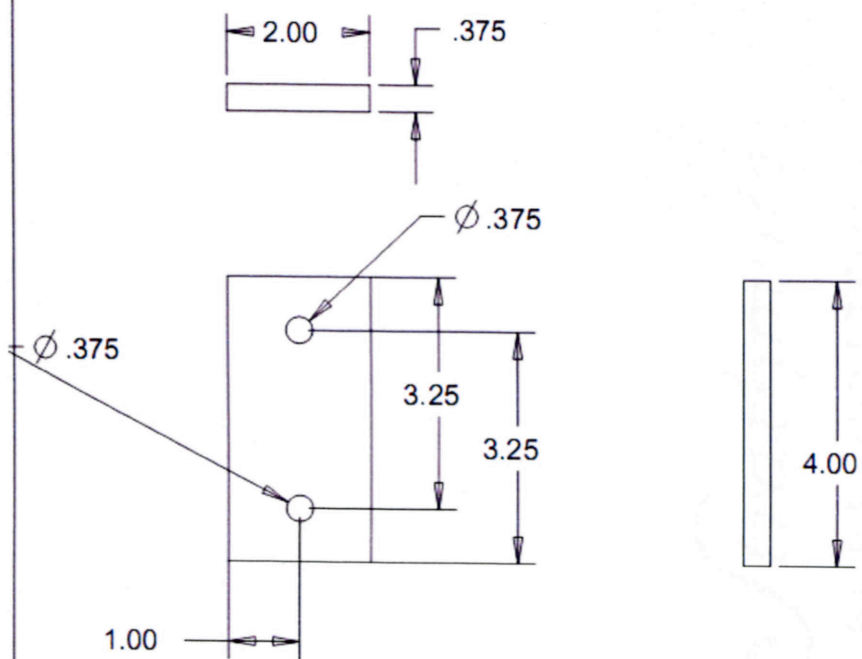

PART NO	SCR-2	PART NAME	FRONT PLATE	QTY:	6
		Colorado State University		UNLESS OTHERWISE SPECIFIED DIMENSIONS ARE IN INCHES TOLERANCES ARE: FRACTIONS ± 1/32 DECIMALS ± .02 ANGLES ± 5 °	
		Mechanical Engr. Dept. Fort Collins, Co 80521 (970) 491-6558			
SCALE:	0.5	DRAWN BY	KIVATURI	MATERIAL:	CARB ST
SHEET:	2/12	ALL DIMENSIONS ARE IN inches		FINISH:	

-X.X ±0.1
-X.XX ±0.01
-X.XXX ±0.005

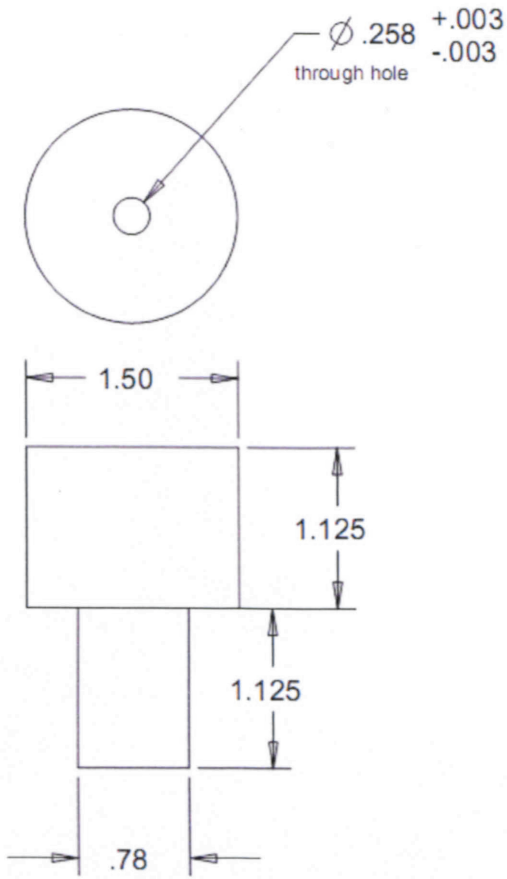

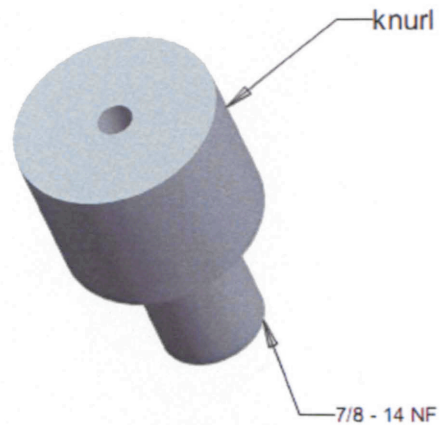

X.X ±0.1
X.XX ±0.01
X.XXX ±0.005

PART NO:	SCR-9	PART NAME:	Male_Cap	QTY:	3
		Colorado State University		UNLESS OTHERWISE SPECIFIED DIMENSIONS ARE IN INCHES TOLERANCES ARE: FRACTIONS: ± 1/32 DECIMALS: ± .002 ANGLES: ± 5 °	
		Mechanical Engr. Dept. Fort Collins, Co 80521 (970) 491-6558			
SCALE:	1.000	DRAWN BY:	KIVATURI	MATERIAL:	CARB_ST
SHEET:	9/12	ALL DIMENSIONS ARE IN inches		FINISH:	

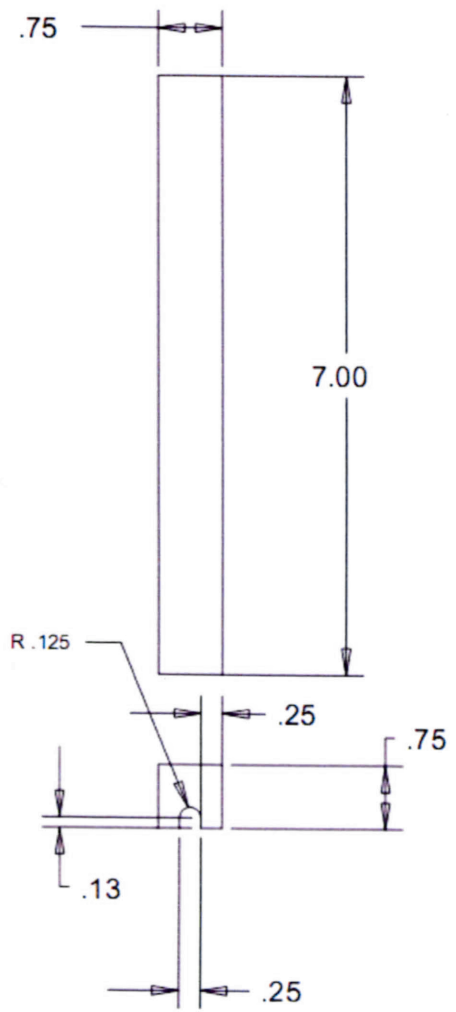

X.X ±0.1
X.XX ±0.01
X.XXX ±0.005

PART NO:	SCR-12	PART NAME:	Gear Rack	QTY:	1
		Colorado State University		UNLESS OTHERWISE SPECIFIED DIMENSIONS ARE IN INCHES TOLERANCES ARE: FRACTIONS ± 1/32 DECIMALS ± .002 ANGLES ± 5°	
		Mechanical Engr. Dept. Fort Collins, Co 80521 (970) 491-6558			
SCALE:	0.6		DRAWN BY: KIVATURI	MATERIAL:	SS
SHEET:	12/12	ALL DIMENSIONS ARE IN inches		FINISH:	

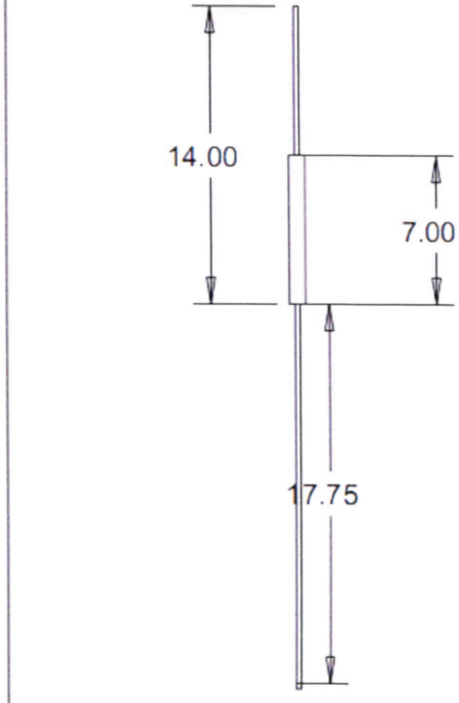

SEE DETAIL B

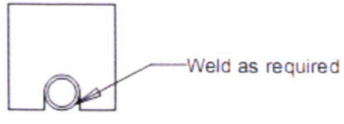

DETAIL B
SCALE 1.000

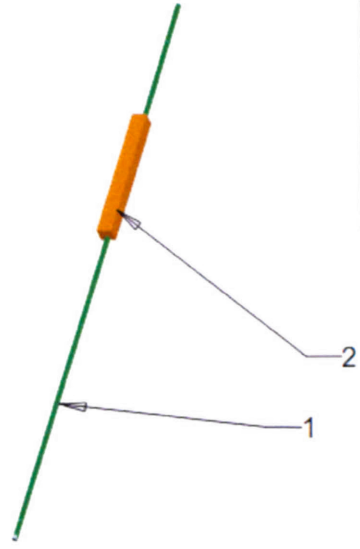

S.No	VENDOR	PART No.
1	CSU	----
2	MCMaster	6295K16

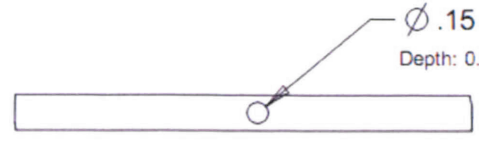

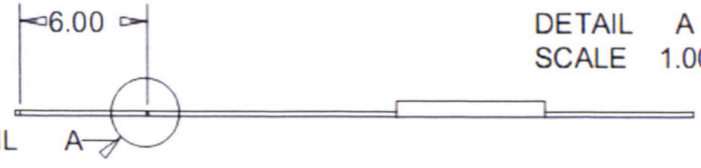

SEE DETAIL A

DETAIL A
SCALE 1.000

X.X ±0.1
X.XX ±0.01
X.XXX ±0.005

PART NO.	SCR-6	PART NAME	Rack_Tube_Assy	QTY.	1
		Colorado State University		UNLESS OTHERWISE SPECIFIED DIMENSIONS ARE IN INCHES TOLERANCES ARE: FRACTIONS ± 1/32 DECIMALS ± .002 ANGLES ± 5°	
		Mechanical Engr. Dept. Fort Collins, Co 80521 (970) 491-6558			
SCALE:	0.15	DRAWN BY	KIYATURI	MATERIAL	CARB ST
SHEET	8/12	ALL DIMENSIONS ARE IN inches		FINISH:	

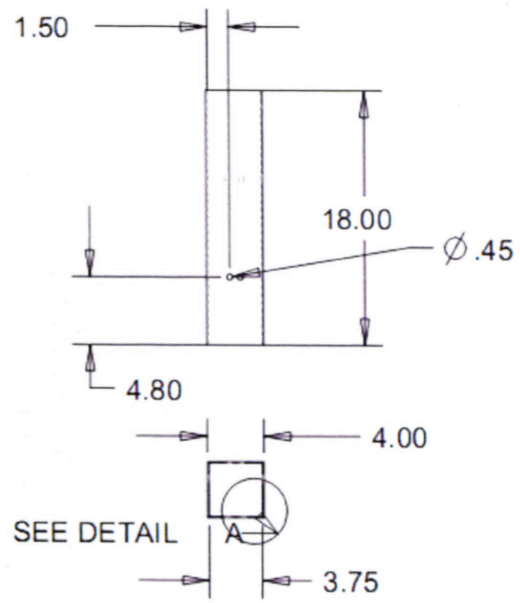

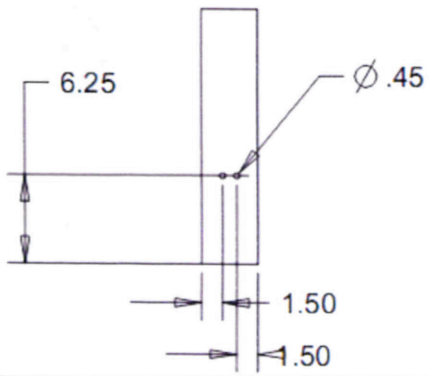

DETAIL A
SCALE 0.160

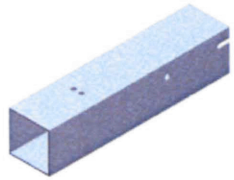

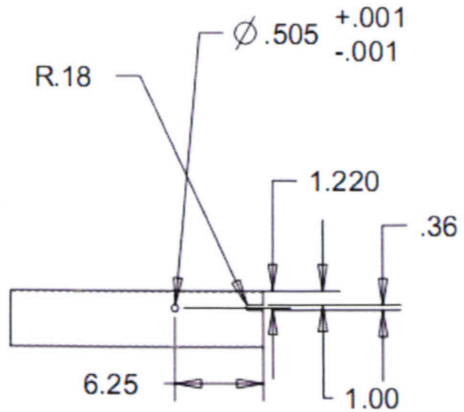

-X.X ±0.1
-X.XX ±0.01
-X.XXX ±0.005

PART NO	SCR-1	PART NAME	SQUARE TUBE	QTY:	2
		Colorado State University		UNLESS OTHERWISE SPECIFIED DIMENSIONS ARE IN INCHES TOLERANCES ARE: FRACTIONS ± 1/32 DECIMALS ± .002 ANGLES ± 5°	
		Mechanical Engr. Dept. Fort Collins, Co 80521 (970) 491-6558			
SCALE:	0.1	DRAWN BY	KIVATURI	MATERIAL:	CARB ST
SHEET:	1/12	ALL DIMENSIONS ARE IN inches		FINISH:	

S.No	Component
1	SCR-1
2	SCR-2

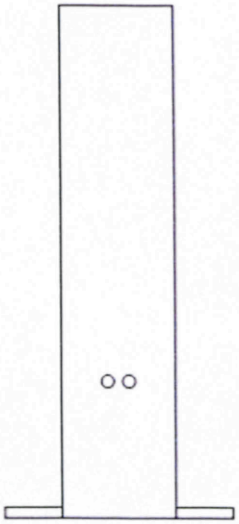

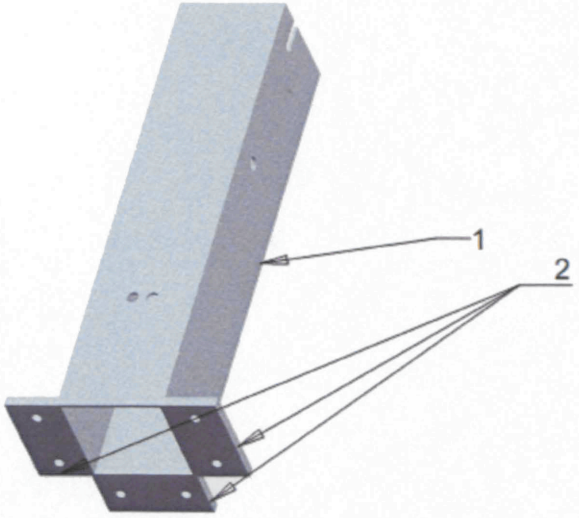

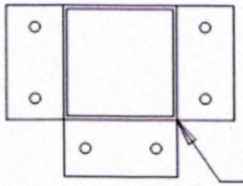

spot weld 3X

X.X ±0.1
X.XX ±0.01
X.XXX ±0.005

PART NO:	SCR-6	PART NAME:	TUBE_FRONT_PLATE Assy	QTY:	2
		Colorado State University		UNLESS OTHERWISE SPECIFIED DIMENSIONS ARE IN INCHES TOLERANCES ARE: FRACTIONS ± 1/32 DECIMALS ± .02 ANGLES ± 5°	
		Mechanical Engr. Dept. Fort Collins, Co 80521 (970) 491-6558			
SCALE:	0.2	DRAWN BY:	KIVATURI	MATERIAL:	CARB ST
SHEET:	6/12	ALL DIMENSIONS ARE IN Inches		FINISH:	

S.No	Component	Vendor	Part No.
1	Housing	CSU	----
2	Fitting	McMaster	4464K224

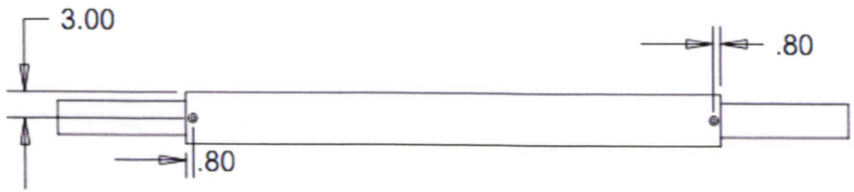

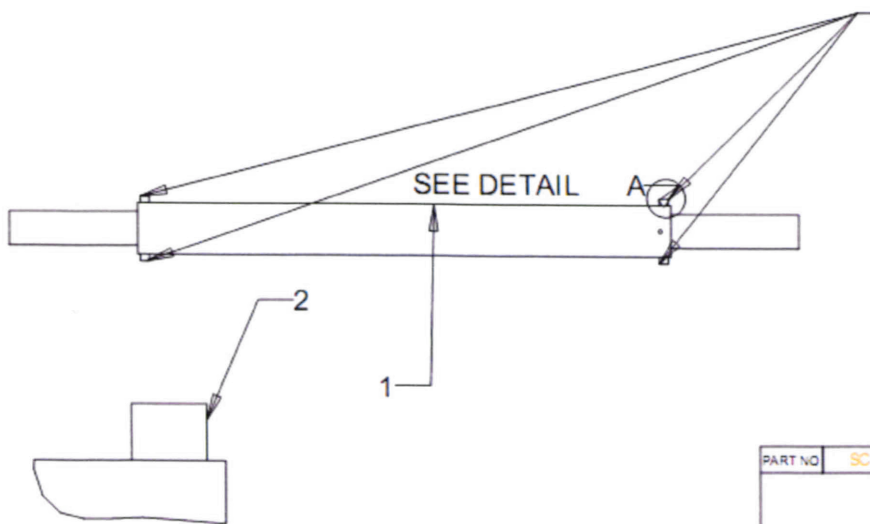

DETAIL A
SCALE 0.500

-X.X	±0.1
-X.XX	±0.01
-X.XXX	±0.005

PART NO:	SCR-11	PART NAME:	Housing Assy	QTY: 1
		Colorado State University Mechanical Engr. Dept. Fort Collins, Co 80521 (970) 491-6558		UNLESS OTHERWISE SPECIFIED DIMENSIONS ARE IN INCHES TOLERANCES ARE: FRACTIONS ± 1/32 DECIMALS ± .002 ANGLES ± 5°
SCALE:	0.06	DRAWN BY:	KIVATURI	MATERIAL: SS
SHEET:	11/12	ALL DIMENSIONS ARE IN inches		FINISH:

S.No	Component	Vendor	Part No.
1	Housing	CSU	----
2	Fitting	McMaster	4464K224

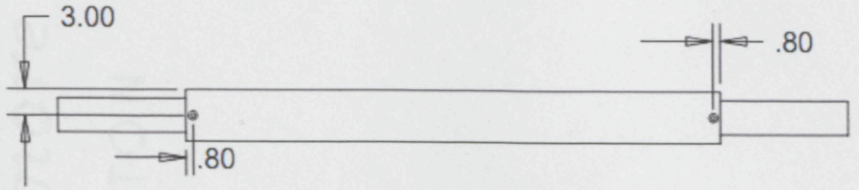

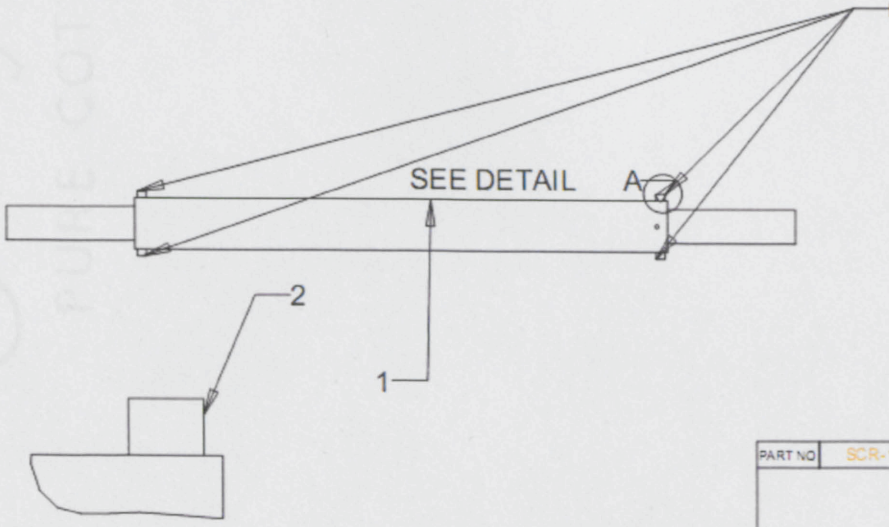

DETAIL A
SCALE 0.500

-X.X	±0.1
-X.XX	±0.01
-X.XXX	±0.005

PART NO:	SCR-11	PART NAME:	Housing Assy	QTY:	1
		Colorado State University		UNLESS OTHERWISE SPECIFIED DIMENSIONS ARE IN INCHES TOLERANCES ARE: FRACTIONS: ± 1/32 DECIMALS: ± .002 ANGLES: ± 5 °	
		Mechanical Engr. Dept. Fort Collins, Co 80521 (970) 491-6558			
SCALE:	0.06	DRAWN BY:	KIVATURI	MATERIAL:	SS
SHEET:	11/12	ALL DIMENSIONS ARE IN inches		FINISH:	.